

UNIVERSIDAD ADOLFO IBAÑEZ FACULTAD DE INGENIERIA Y CIENCIAS DOCTORADO EN INGENIERIA DE SISTEMAS COMPLEJOS

Equilibrium and Non-Equilibrium in a Reversible and Conservative Cellular Automaton

Felipe Andrés Urbina Parada

Advisor : Professor Sergio Rica

 ${\bf Commission} \ : \ {\bf Professor} \ {\bf Pierre} \ {\bf Coullet}$

Professor Alejandro Maass Professor Marco Montalva Professor Enrique Tirapegui

Facultad de Ingeniería y Ciencias Universidad Adolfo Ibáñez

Agradecimientos

Abstract

The main goal of this thesis, relies the dynamics of a reversible and conservative cellular automaton Q2R model. Q2R is a automaton that runs on a two-dimensional grid of finite size and is reversible in a physical sense, that is, not only is the automaton rule invertible, but the backward rule reads exactly the same as the forward one. This model is a dynamical variation of the Ising model for ferromagnetism that possesses quite a rich and complex dynamics.

As expected, the Q2R automaton only possesses fixed points and periodic orbits and it has been shown that possesses an energy like quantity, and, at least an extra conserved quantity. Although, the dynamics includes only fixed points and periodic orbits, numerical simulations show that the system exhibits a ferromagnetic phase transition in the large system size limit for a well defined critical energy.

In the present work, we characterize the configuration space, that is composed of a huge number of cycles with exponentially long periods. More precisely, we quantify the probability distribution functions of states in terms of the aforementioned invariants. We show that the dynamics of the system in the phase space appears to be, depending on the energy, a random walk or a Levy flight.

The main contribution of the present thesis is the application of a coarse-graining approach that allows to write a coarse-grained master equation, which characterizes equilibrium and non equilibrium statistical properties, for the Q2R model. Following Nicolis and collaborators, a coarse-graining approach is applied to the time series of the total magnetization, leading to a consistent master equation that governs the macroscopic irreversible dynamics of the Q2R automata. The methodology is replicated for various lattice sizes. In the case of small systems, we show that the master equation leads to a tractable probability transfer matrix of moderate size, which provides a master equation for a coarse-grained probability distribution. The method is validated and some explicit examples are discussed.

Contents

\mathbf{A}_{i}	Agradecimientos			i
A	bstra	\mathbf{ct}		ii
In	trodi	uction		1
1	Aro	und of	the Ising model	5
	1.1	Ising-b	oased models	5
		1.1.1	Generalities	6
		1.1.2	The time-dependent Glauber-Ising Model	7
		1.1.3	The Q2R cellular automata	8
		1.1.4	Schelling model for Social segregation.	9
		1.1.5	Bootstrap percolation	10
		1.1.6	Recapitulation	11
	1.2	Ising p	patterns, transitions, and dynamical behavior	12
		1.2.1	Glauber and Decision-Choice model dynamics	12
		1.2.2	Schelling dynamics	14
		1.2.3	Bootstrap percolation	15
2	The	Q2R	Cellular Automaton	29
	2.1	The Q	2R model	29
		2.1.1	The rule	29
		2.1.2	Energy Conservation	31
		2.1.3	Staggered Invariants	32
		2.1.4	The Magnetization	33
		2.1.5	Mean Field Approximation	33
	2.2	Dynan	nics of the Q2R model	34
		2.2.1	Initial conditions	34
		2.2.2	One-dimensional Systems	34
		2.2.3	Two-dimensional Systems	35
		2.2.4	Ferromagnetic and Paramagnetic Behaviors	36
		2.2.5	Phase Transition	37

vi *CONTENTS*

		2.2.6	Exact results from the Ising model in statistical mechanics	40
3			Space characterization	43
	3.1		alities	43
	3.2		phase space calculation for very small lattices	44
		3.2.1	Phase space 2 × 2	44
		3.2.2	Exact Phase Space for the $N = 4 \times 4$ case	44
	3.3		rolution of states in configuration space	46
		3.3.1	Sensitivity to initial conditions	46
		3.3.2	Levy flight structure	48
		3.3.3	Configuration space for a system 256×256	50
4	Coa	rse-Gr	aining and Master Equation	53
	4.1	Genera	al Scope	53
		4.1.1	General formalism	53
		4.1.2	Explicit calculation for the transition probability matrix \hat{W}	57
		4.1.3	The Chapman-Kolmogorov condition and time reversal symmetry	57
	4.2	Specifi	c computation of the transition probability matrix in various situation	ns. 59
		4.2.1	Robustness of the methodology	59
		4.2.2	Exact calculation for various lattices	62
		4.2.3	The Chapman-Kolmogorov conditions.	64
	4.3	Slow n	nodes and transport coefficients	67
		4.3.1	Pomeau's reversal symmetry relation	69
	4.4	Appen	dix	69
		4.4.1	Exact calculation for the 4×4 lattice	69
		4.4.2	The Chapmann-Kolmogorov condition	71
5	Con	clusior	1S	73
Ri	hlion	raphy		75
וכו	DIIUg	Japiny		10
\mathbf{A}_{I}	ppen	dices		79
A	Arti	icle		79
В	Arti	icle		91
\mathbf{C}	Arti	icle		109

Introduction

The Ising model, introduced in the early 1920's by Lenz [1] and Ising [2] as a thermodynamical model for describing ferromagnetic transitions, has evolved as one of the most prolific theories in the twenty century, opening a huge number of new areas of knowledge. The importance of the Ising model raises in its universality and robustness, indeed despite its simplicity, this model has been the starting point for the emergence of various subfields in physical (and social) sciences, namely, phase transitions, renormalisation group theory, spin-glasses, lattice field theories, among others [3].

A cellular automata approach to the two-dimensional Ising model is provided by the Q2R model, first introduced by Vichniac in the mid-80's [4], where "Q" means the number of neighbors (quatre in french), "2" indicates a two-step dynamics, and "R" is for reversibility. This model exhibits several important features of physical systems: a deterministic rule, reversibility and is formally not ergodic, because it only possesses finite periodic orbits. It is crucial to notice that since the evolution of the dynamics involves only discrete steps, with boolean values 0 and 1, there is no any numerical or round errors associated to finite approximations.

The study of the dynamics and properties of the Q2R model has a long history. The first work was done by Vichniac [4] and Pomeau [5], who showed that the energy E is conserved. Then, Herrmann [6] implemented the Q2R algorithm to study the two-dimensional Ising model in the frame of the micro-canonical ensemble. In this work, Herrmann used the concept of magnetization and represented its magnitude as a function of the initial energy, displaying the first pattern picture for the phase transition of the Q2R model. Later, Herrmann, Carmesin and Stauffer [7] studied numerically the probability to reach an "infinitely" long period for some energy values. Moreover, if the energy is large enough, this probability tends to one. On the other hand, Takesue [8] studied the Q2R model from the point view of reversibility, using statistical mechanics. His studies concerned explicitly all class of rules for the one dimensional case, the Q2R being only a special case. However, the Q2R (90R in his terminology), is the analogue of an ideal gas of particles with speeds +1 or -1, which is a system that cannot reach equilibrium in practice, but, it is ergodic only in thermodynamical equilibrium. Ultimately the Q2R model was studied numerically for the irreversible behavior and the existence of a spontaneous transition

2 CONTENTS

from a non-coherent state to a coherent state [9].

In order to quantify the behavior of the Q2R cellular automata, we have deeply described spin dynamics in phase space, through the study of a macroscopic observable, called Magnetization (M), defined as the sum of all the states at each time step. Previously, it has been stressed that on two-dimensional lattices, the system exhibits a phase transition when the value of the energy is close to the critical energy of the Ising model, $E_c/N = -\sqrt{2}$. Also, in the literature [9] it has been observed numerically two different behaviors of the system, defined in term of M, and as function of energy: ferromagnetic, paramagnetic and metastable.

The goal of this thesis, consists in the development of a detailed description of the above mentioned behaviors based on the concepts of statistical methods, using more extensive numerical tools (*OpenMP* libraries in C++ language) than previous approaches. To fullfil the requirements for this goal, several methods of Statistical Mechanics have been used, for instance, Phase diagrams, Coarse-graining, probability distribution functions (PDF), among others [10, 11].

The main contribution of this thesis is the application, by of following [12, 13], a coarse-graining approach that allows us to write a coarse-grained master equation, which characterizes equilibrium and non-equilibrium statistical properties, for the Q2R automata. We can see that this coarse-graining technique is a powerful tool, which reduces the information for the whole system to a tractable probability transfer matrix which simplifies the original master equation.

A second contribution focused on the appearance of orbits, that is, trajectories defined by the same initial and final configurations, with different periods at the same energy level. In order to quantify these orbits, we defined an observable, called Hamming or Manhattan distance, between the states at time steps t and t+1. Thus, we have shown how the system presents two types of behaviors: random walks and Lévy flights.

This thesis is organized as follows. The first chapter 1 discusses different models with common features arising in a class of Ising-based models. In the second chapter 2, the fundamental properties of the Q2R model are presented: the dynamics in one and two dimensions, the behavior of the system when the energy is near the critical value E_c , and the corresponding phase transition. The third chapter 3, we present the phase space characterization. Finally, the chapter 4 presents a coarse-graining.

4 CONTENTS

Chapter 1

Around of the Ising model

1.1 Ising-based models

In this chapter, we shall discuss four distinct applications of Ising-based models with applications to both statistical mechanics and social sciences. The first one is devoted to the Glauber-Ising time dependent model with applications to decision-choice theory in economics and social sciences. In the sixties Glauber [14], introduced an stochastic time dependent rule to mimic the statistical properties of the original Ising problem. Glauber's dynamics has been considered in the context of social sciences by Brock and Durlauf [15, 16], and, more recently, by Bouchaud [17].

The second topic is Q2R automata model introduced in the 80's by Vichniac [4]. The Q2R¹ possess time reversal symmetry, which is at the core of any fundamental theory in physics. Moreover, the temporal evolution of this automata conserves a quantity which is closely related to the energy of the Ising model [5]. We are interested in this model because is a natural starting point for studying the statistical and typical irreversible behavior of reversible systems. As shown in Ref. [9], this system evolves in an irreversible manner in time towards an "statistical attractor", moreover the macroscopic observable, the temporal average of the global magnetization, depends on the value of the initial energy following a law which is exactly the one obtained theoretically by Onsager [18] and Yang [?], more than 60 years ago. Moreover, in Ref. [19] it is shown how this model exhibits the same features of Hamiltonian systems with many degrees of freedom, that is, a sensibility to initial conditions, positive Lyapunov exponents, among others.

The second model that we shall discuss in this article concerns the Schelling model of social segregation, introduced in the early seventies by Thomas C. Schelling [20, 21, 22]. This model became one of the paradigm of an individual-based model in social science.

¹Q by four, *quatre*, in french, 2 by two steps automata rule as explicitly written below, and R by reversible.

Schelling's main contribution is that shows on the formation of a large scale pattern of segregation as a consequence of purely microscopic rules. More recently, it has been shown that the Ising energy, which is a good measure of segregation, acts as a Lyapunov potential of the system is driven, under particular conditions, by a strictly decreasing energy principle [23].

Finally, we shall discuss a model for dissemination's disease known as Bootstrap percolation, first introduced in the late seventies by Chalupa, Leath and Reich [24]. In this model a healthy individual may be infected if the majority of its neighbors are infected. On the other hand an infected individual never recovers, so it remains infected forever. This model has been used as a model for disease's propagation. One of the most important questions arising is the determination of the critical number of infected individuals to contamine the whole population.

1.1.1 Generalities

The lattice and the neighborhood

All models discussed below, display similar features, the system consisting of a lattice with $N \gg 1$ nodes, in which each node, k, may take a binary value $x_k(t) = \pm 1$ at a given time. Each node k on the lattice interacts, in general, with all other individuals, with an interaction coefficient J_{ik} (i denotes an arbitrary node). But in particular, a node, k, may interact only with a finite neighborhood denoted by V_k . The number of neighbors for site k, $|V_k|$, is the total number of non zero J_{ik} for each node. In Fig. 1.1 we show, as an example, four possible lattice configurations.

The "energy" and the "magnetization".

We define the macroscopic observables of the system, by analogy with the original Ising model of ferromagnetism, as follows:

$$E[\{x\}] = -\frac{1}{2} \sum_{i,k} J_{ik} x_i(t) x_k(t) , \qquad (1.1)$$

$$M[\{x\}] = \sum_{k=1}^{N} x_k(t). \tag{1.2}$$

These quantities will be the pertinent observables, and we shall use them to classify the distinct cases that we will be described in the next sections.

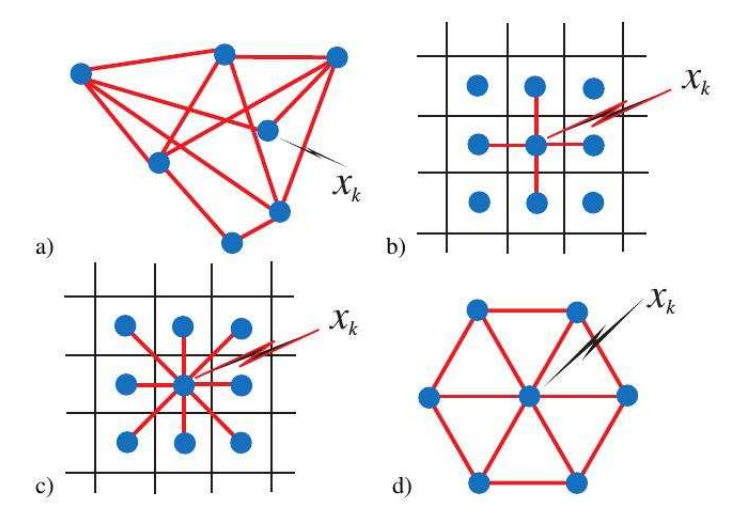


Figure 1.1: Examples of lattices and neighborhoods. We illustrate explicitly: a) an arbitrary network with a random number of neighborhoods; and three periodic regular lattices in two space dimensions: b) a square lattice with a von-Neuman neighborhood of 4 individuals (the original lattice of the Ising model with the nearest neighborhood); c), a square lattice with a Moore neighborhood of 8 individuals, and d) a hexagonal lattice with 6 neighborhoods.

1.1.2 The time-dependent Glauber-Ising Model

Glauber [14], in the sixties, introduced a dynamical model for the study of the Ising model. The rule governing Glauber's model is the following:

Let, the local magnetization at the site k and at a time t, be:

$$U_k(t) = B + \sum_{i} J_{ik} x_i(t),$$
 (1.3)

with B being an external magnetic field. Then, the spin's value at the next time step, t+1, will be

$$x_k(t+1) = \operatorname{sgn}(U_k(t)), \tag{1.4}$$

that is $x_k(t+1) = +1$ if $U_k(t) \ge 0$ and $x_k(t+1) = -1$ if $U_k(t) < 0$. We call (1.4) the deterministic rule. In probability language, if $U_k(t) \ge 0$, then $x_k(t+1)$ would be +1 with probability 1, and it would be -1 with probability 0. This rule is updated in parallel fashion.

Next, this deterministic rule may be modified by a probabilistic rule, in the following way:

$$x_k(t+1) = \begin{cases} +1 & \text{with probability} \quad p = \frac{1}{1+e^{-\beta U_k(t)}} \\ -1 & \text{with probability} \quad p = \frac{1}{1+e^{\beta U_k(t)}} \end{cases}$$

$$(1.5)$$

Notice that in the limit $\beta \to \infty$ one recovers the deterministic behavior (1.4), while in the limit $\beta \to 0$ one reaches a completely random (binomial) dynamics regardless of the value of U, that is $x_k(t+1)$ would be +1 with probability 1/2.

The Glauber rule is indeed a Markov chain which manifests, in a perfect way, the statistical properties of the Ising phase transition for the case of Von-Neuman neighbourhoods, and it also agrees with the mean field approximation for the case of a large number of neighbours. Finally, nowadays the Glauber dynamics is the starting point for numerical simulations of spin glasses systems with random values for the J_{ik} coefficients.

Random Decision-Choice Model

Let us consider now a random choice model [15, 16, 17] in the context of social sciences. An individual takes a choice based on a combination of decision quantities, namely an individual "decision parameter" f_k , a "global decision" or "public information" parameter F(t) (which could be included in the previous individual decision parameter) and a "social pressure" $\sum_i J_{ik} x_i(t)$.

Next take the so called "perceive overall incentive agent function", by Bouchaud [17].,

$$U_k(t) = f_k + F(t) + \sum_{i} J_{ik} x_i(t), \qquad (1.6)$$

and follow the Glauber deterministic dynamics (1.4) or more generally the Glauber random dynamics (1.5).

Due to both, the Ising-like feature as the Glauber Dynamics evolution rule, a phase transition is known to appear. This transition favors the decision into one or another of the two options of the binary variable.

1.1.3 The Q2R cellular automata

The Q2R rule considers the following two-step rule which is updated in parallel [4] this two-step rule may be naturally re-written as a one-step rule with the aid of an auxiliary

dynamical variable [5].:

$$x_k(t+1) = x_k(t-1) \times \begin{cases} +1 & \text{if } \sum_i J_{ik} x_i(t) \neq 0 \\ -1 & \text{if } \sum_i J_{ik} x_i(t) = 0 \end{cases}$$
 (1.7)

Naturally, it is possible to add, without any difficulty, an external magnetic field B. However, some caution should be taken into account: the model works if $U_k(t) = B + \sum_i J_{ik}x_i(t)$, may vanish, therefore, B and the J_{ik} factors should be integers. For instance in the case of a finite neighborhood, $B + |V_k|$ should be an even number.

The rule (1.7) is explicitly invariant under a time reversal transformation $t + 1 \leftrightarrow t - 1$. Moreover, as shown by Pomeau [5], the following quantity, that we may call an energy, despite not being exactly the energy of the Ising model.

$$E[\{x_k(t), x_i(t-1)\}] = -\frac{1}{2} \sum_{i,k} J_{ik} x_k(t) x_i(t-1),$$
(1.8)

is preserved under the dynamics defined by the Q2R rule (1.7). Moreover, the energy is bounded by $-2N \le E \le 2N$.

1.1.4 Schelling model for Social segregation.

Schelling model, is also characterized by a binary variable x_k which may take values +1 and -1. We shall say that an individual x_k at the node k is "happy" at his site, if and only if, there are less than θ_k neighbors at an opposite state. θ_k is a tolerance parameter that depends in principle on the node and, it may take all possibles integer values, such that $0 < \theta_k < |V_k|$ (we exclude the cases $\theta_k = 0$ and $\theta_k = |V_k|$ from our analysis).

The satisfaction criterion reads the criteria (1.9) may be unified in a single criteria [23] (multiplying both sides of the two inequalities by x_k):

an individual
$$x_k$$
 is unhappy at the node k if , and only if, $x_k \sum_{i \in V_k} x_i \leq |V_k| - 2\theta_k$,

which is a kind of energy density instead of the threshold criteria found in Glauber dynamics (1.4).

An individual x_k is unhappy at the node k if and only if:

$$\sum_{i \in V_k} x_i = \begin{cases} |V_k| - 2n_k(-1) \le |V_k| - 2\theta_k, & \text{if } x_k = +1\\ 2n_k(-1) - |V_k| \ge 2\theta_k - |V_k|, & \text{if } x_k = -1. \end{cases}$$
(1.9)

Here $n_k(+1)$ is the number of neighbors of x_k that are in the state +1; and, $n_k(-1)$ the number of neighbors of x_k in the state -1, naturally $n_k(+1) + n_k(-1) = |V_k|$.

Having labeled all different un-happy individuals, one takes randomly two of them in opposite states (one +1, and one -1) and exchanges them. Even when this is not exactly the original Schelling's rule, the present *Schelling's protocol* is a simpler one. In any case, it can be modified in a straightforward way to include for example vacancies [25, 26], different probabilities of exchange [25], multiple states variables [27], etc.

If k and l are these random nodes, then the evolution rules:

$$x_k(t) \to x_k(t+1) = -x_k(t), \quad x_l(t) \to x_l(t+1) = -x_l(t)$$

and for all other nodes $i \neq k \& l$ remain unchanged $x_i(t) \to x_i(t+1) = x_i(t)$.

The protocol is iterated in time forever or until the instant when one state does not have any unhappy individuals to be exchanged.

Notice, that Schelling criteria (1.9) is deterministic, however the exchange is a random process, therefore two initial configurations will not display the same behavior in detail, but they will evolve to the same statistical attractor [28].

Schelling's protocol, defined above, has a remarkable property: if $\theta_k > \frac{|V_k|}{2}$ then any exchange $k \leftrightarrow l$, will always decrease the energy

$$E[\{x\}] = -\frac{1}{2} \sum_{k} \sum_{i \in V_k} x_i(t) x_k(t). \tag{1.10}$$

The energy (1.10) follows from (2.5), whenever $J_{ik} = 1$ for neighbors and $J_{ik} = 0$ otherwise.

For a proof, we refer to Ref. [23]. We shall only add the following remark: if $\theta_k > \frac{|V_k|}{2}$, then the evolution necessarily stops in finite time. This is because the energy (1.10) is bounded from below by $E_0 = -\frac{1}{2} \sum_{k=1}^{N} |V_k|$ and because the energy (2.5) decreases strictly. On the other hand, for $\theta_k < \frac{|V_k|}{2}$, the energy may increase or decrease after an exchange indistinctly.

1.1.5 Bootstrap percolation

We shall consider the problem of bootstrap percolation for a given lattice [24]. As in the previous models, each node k interacts with $|V_k|$ neighbors, the neighborhood defined by the set V_k . As before the state, x_k may take values +1 and -1 depending on if it

is "infected" or not. At a given "time" the state $x_k(t)$ evolves into $x_k(t+1)$ under the following parallel rule: if a site is not infected, and if the *majority* of its neighbors are infected, then the site becomes infected [29]. On the other hand, if the site is already infected it keeps its infected state.

Summarizing, the evolution rule, which is updated in parallel, may be written in the following general way:

if
$$x_k(t) = -1$$
 and $\sum_{i \in V_k} x_i(t) > 0$, then $x_k(t+1) = +1$, (1.11)

otherwise, if $x_k(t) = 1$ then $x_k(t+1) = 1$.

From the dynamics it follows directly that the energy (1.10) decreases in time, $E(t+1) \leq E(t)$, as well as the magnetization increases in time: $M(t+1) \geq M(t)$. As in the case of the Schelling model, because the energy is a strictly decreasing functional, and because it is bounded from below in a finite network, then the dynamics always stops in finite time.

Finally, let us comment that a problem that has increased in interest in recent times deals with the question of how the total infection depends on the initial configuration which is randomly distributed and such that a site will be at the state $x_k = +1$ with a probability p [30].

Naturally, if initially $p \approx 1/2$, then every site has in average the same number of $x_k = +1$ states and $x_k = -1$ in its neighborhood, then the system would percolate almost in one step. However, as p decreases, one can define a probability, P(p), which is the probability that the system would percolate at the end of the evolution process. Though P(p) count be determined explicitly at the end this probability can be numerically determined.

1.1.6 Recapitulation

The afore mentioned models have in common a threshold criteria (1.4), (2.3), (1.9), and (1.11) the subsequent dynamics follows different rules. Therefore one should expect distinct properties.

The Glauber Dynamics does not preserve neither the energy or magnetization, however the Q2R dynamics does preserve only the energy but does not preserve the magnetization. The Schelling model does preserve only the magnetization, but if $\theta_k > |V_k|/2$ the system's energy is strictly a decreasing function. Finally, in the infection model of section 1.1.5, the energy strictly decreases whereas the magnetization is an increasing function of time.

properties.				
Dynamics	Evolution Criteria	Energy	Magnetisation	
Glauber	$sgn(B + \sum_{i} J_{ik} x_i(t))$	Not Conserved	Not Conserved	
Q2R	$\sum_{i} J_{ik} x_i(t) = 0$	Conserved	Not Conserved	
Schelling	$\operatorname{sgn}(x_k(t)) \sum_{i \in V_k} x_i(t) \le V_k - 2\theta_k$	Not Conserved ^a	$\operatorname{Conserved}$	
Bootstran	$\nabla x_{\cdot}(t) > 0$	$\Delta E < 0$	$\Delta M > 0$	

Table 1.1: Recapitulation of the four above mentioned models, and its main conservation properties.

1.2 Ising patterns, transitions, and dynamical behavior

In this section, we shall roughly describe the essential phenomenology of the Ising-like models and rules described in the previous section, whether they are governed (or not) by the rules of conservation of magnetization energy.

1.2.1 Glauber and Decision-Choice model dynamics

The time dependent Glauber-Ising model shows a very rich phenomenology. As such, the model's behavior has been explored using mean field approximation (the Curie-Weiss law) as well as by direct simulations of the rule (1.5). Here our macroscopic observable is the total magnetization per site, namely M(t)/N and were M(t) is defined in equation (1.2).

In what it follows, we will only show results for the direct simulation of the Glauber-Ising model (1.4) and we shall use the terminology of social sciences (1.14). In Figure 1.2 we show three distinct states characterized by different values of the parameter of "irrationality" β , In statistical physics, β is the inverse of the thermodynamical temperature, $\beta \sim 1/T$. and a null value for the public information parameter F(t).

^a If $\theta_k > |V_k|/2$ then $\Delta E < 0$.

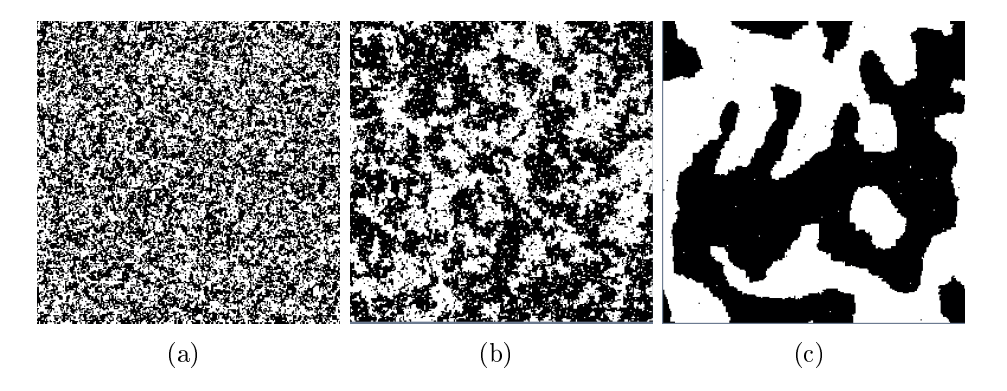


Figure 1.2: Snapshots of the patterns for the Glauber-Ising model. The simulation is for a $N=256\times256$ periodic lattice with von Neuman neighborhood. Moreover we take $f_k=0$ and F=0. The parameter of "irrationality" and the magnetization averages are, respectively: a) corresponds to a paramagnetic phase for $\beta=0.53$ and $\langle M\rangle/N=0.0006$; b) a critical phase for $\beta=0.82$ and $\langle M\rangle/N=0.02$; and c) corresponds to a ferromagnetic phase $\beta=1.8$, and $\langle M\rangle/N=0.39$.

In Fig. 1.3 we show two different bifurcation diagrams for the mean magnetization $\langle M \rangle/N$ versus the irrationality parameter β , for non-zero or null value for the public information parameter F(t). Each point, was calculated for a total of approximately 2×10^4 time steps. We can readily observe the appearance of a bifurcation for the case F=0 and β greater than $\beta_c\approx 0.8$.

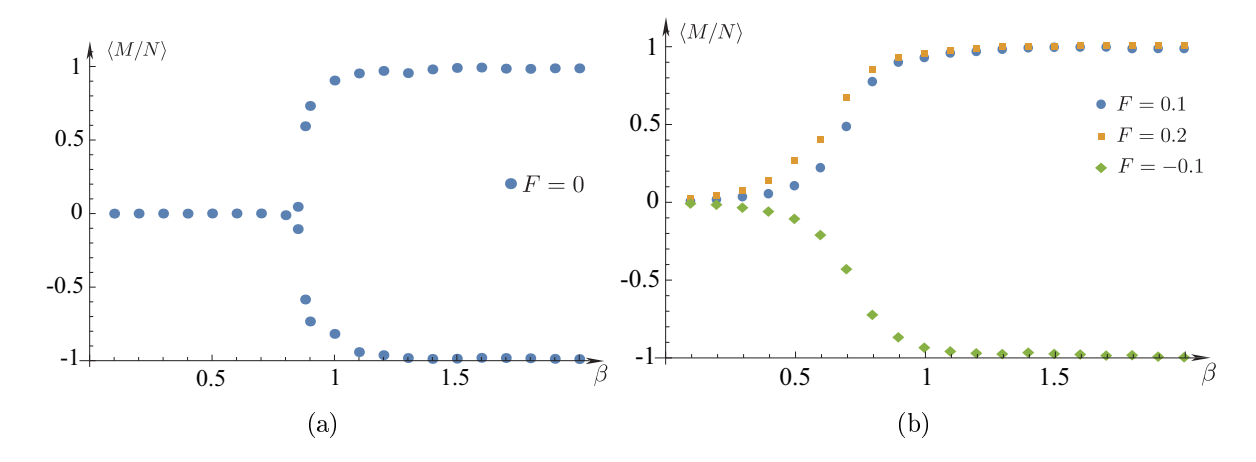


Figure 1.3: Average magnetization $\langle M \rangle$ versus β . The averages are taken from long time simulations of approximately 20000 time steps. In both cases the random external field is settled to zero $f_k = 0$. a) Case of F = 0; and , b) Cases of $F = \pm 0.1$ and F = 0.2.

Therefore, the time dependent Glauber-Ising model displays a transition from a para-

magnetic to a ferromagnetic phase for $\beta_c \approx 0.8$ which is in agreement with the critical threshold value of the Ising model [31], $\beta_c = \log(1 + \sqrt{2}) \approx 0.881...$

1.2.2 Schelling dynamics

We shall characterize the dynamics of Schelling model for the particular case in which the system is a two dimensional periodic lattice, and each site possess the same neighborhood consisting in the |V| closest individuals. We shall consider also that the parameter θ_k is uniform, that is, $\theta_k = \theta$.

Fig. 1.4 displays an example of typical patterns arising in the Schelling's model. As it can be observed, the dynamics depends critically on the value of the tolerance parameter θ , defined above. More precisely, if θ is larger or smaller than $\theta_{c_1} = |V|/4$, $\theta_c = |V|/2$, and $\theta_{c_2} = 3|V|/4$.

The initial state was chosen randomly with a binomial distribution, that is $x_k(t=0)$ was +1 with probability 1/2 and -1 with the same probability. Hence, the total magnetization is $M(t=0) \approx 0$, and it is kept fixed during the evolution.

The simulations shown in Fig. 1.4, corresponds to a Schelling rule with a vicinity of |V| = 20 elements. Clearly three different cases can be distinguished, and at least three transition points, namely $\theta_{c_1} = |V|/4$, $\theta_c = |V|/2$, and $\theta_{c_2} = 3|V|/4$.

For $1 < \theta \le |V|/4$ (see Fig. 1.4-a) one observes a non-segregated pattern, the states $x_k = \pm 1$ are swapping, more or less randomly in the system, without a formation of any kind of large scale structure. In a coarse graining scale, for instance, the scale of the vicinity, the coarse-grained magnetization, namely, $m = \frac{1}{|V|} \sum_{i \in V_k} x_i(t)$ is zero everywhere, as well as the energy notice that, as already said, the total magnetization is constant in the Schelling model. Therefore we cannot match the Schelling transitions observed here with the phase transition for the cases of the Glauber-Ising and the Q2R models. In this situation, it is tempting to make an analogy with the Ising paramagnetic phase.

For $|V|/4 < \theta \le |V|/2$, one observes how a segregation pattern arises (see Fig. 1.4-b & c). More important the coarse-grained magnetization is locally non-zero, and the pattern presents domain walls, which are characteristic of a ferromagnetic phase in the Ising-like terminology.

For $|V|/2 < \theta \le 3|V|/4$, one observes also segregation (see Fig. 1.4-e), but the dynamics stops in a finite time. The final state is a quenched disordered phase for which one may conjecture an analogy with a "spin glass" phase, and the appearance of a kind of quasi long-range order.

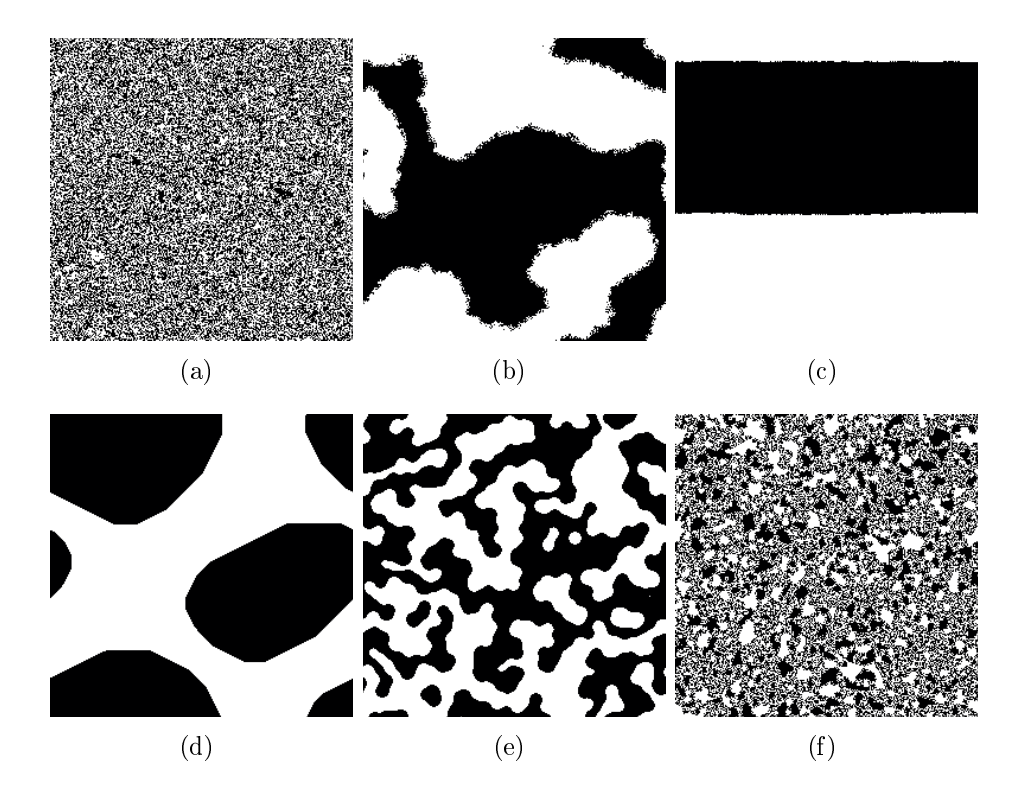


Figure 1.4: Schelling's patterns for various satisfaction parameter θ in a square periodic lattice of N=256 nodes. The vicinity is uniform and contains |V|=20 elements. a) $\theta=5$; b) $\theta=6$; c) $\theta=9$; d) $\theta=10$ (eventually this case the two spots observed merges into a single one, this coalescence dynamics, however, it happens after a longtime); e) $\theta=11$ and f) $\theta=15$, are two cases whenever the energy is a strictly decreasing function so the dynamics stops in finite time, in the former case this happens after a time so segregation is possible, however in the later case the dynamics stops shortly after the Schelling algorithm started. For $\theta=15$ we say that this is a frustrated dynamics, because the system cannot reach the ground state energy because the dynamics stops after one of the population is completely happy.

The case $\theta = 3|V|/4$ in (see Fig. 1.4-f) it is interesting because, although the are some islands of segregation, the system also recovers its original heterogeneity, with almost a null coarse-grained magnetization m.

1.2.3 Bootstrap percolation

The spin dynamics for the case of Bootstrap percolation of Section 1.1.5 is always characterized by an energy decreasing principle, moreover because a +1 spin never flips to a -1, the magnetization is mandated to increase up to a constant value because of the impossi-

bility to infect more individuals, or simply because the system has been fully percolated by the +1 spin states.

As said in Sec. 1.1.5, we shall consider a random initial state with a fraction p of the spins at the state $x_k = +1$ (that is, a fraction p of the population would be infected).

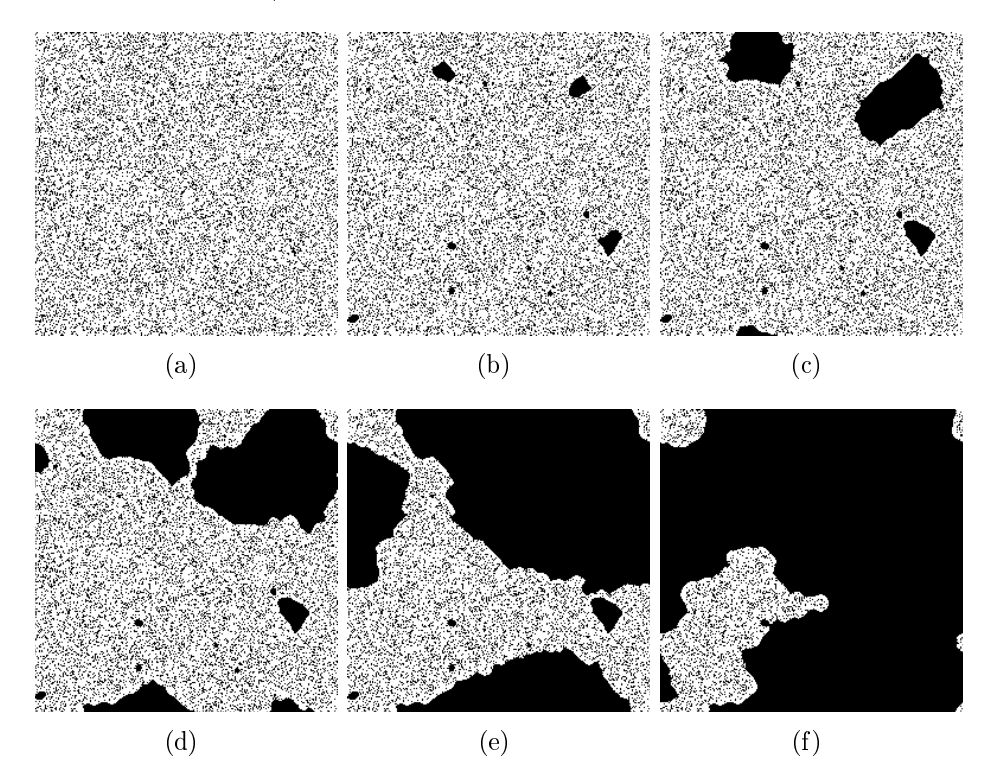


Figure 1.5: Bootstrap percolation's patterns at six different time steps. The network is a square periodic lattice of $N=256^2$ sites with a uniform vicinity of |V|=24 sites. a) display the initial random state with an initial fraction 0.2 of $x_k=+1$ (that is, a given site is +1 with probability 0.2, and -1 with probability 0.8); In b) one observes the nucleation of bubbles, which eventually would propagate the +1 state over the random phase; In c) one observes that some infected bubbles have not reach the critical size and they do not propagate; however, in d) big bubbles invade the system transforming the interface in a front propagation over the whole system e) and f).

It is observed, that for a moderately large value of p, say $p \approx 1/2$, the system becomes unstable very fast, percolating the $x_k = +1$ state everywhere almost instantaneously.

However, as one decreases p, the system presents a well defined scenario. Fig. 1.5 shows the typical evolution of a percolation pattern in time. More precisely, the system nucleates bubbles of infected states ($x_k = +1$) and two scenarios are possible, either these

bubbles continues to grow or they stop (compare Fig. 1.5 b & c). In analogy with the instability of a first order phase transition, it should exist a critical radius of nucleation that depends explicitly on p.

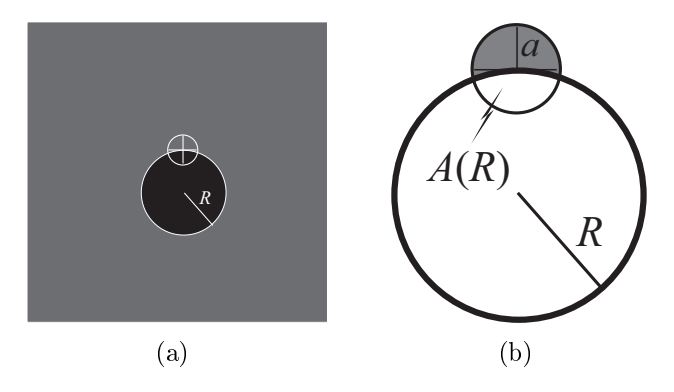


Figure 1.6: a) Scheme for the mean field estimation of the critical radius of infection. The gray region represents the random initial data with a fraction p of +1. b) Details of the geometry for the calculation of A(R).

This critical radius of nucleation maybe estimated in the limit of large vicinity, in other words, in the range of validity of the mean field approximation. Let be p the fraction of infected sites initially distributed randomly in the system and a the radius of the vicinity $(\pi a^2 = |V|)$. We shall add an infection bubble with a radius R (see Fig. 1.6-a). A $x_k = -1$ state in the boundary of the infected circle will become infected if $\sum_k x_k(t) = (2p-1)(\pi a^2 - A(R)) + A(R) > 0$, where A(R) is the surface of the portion of the circle inside the infection bubble (see Fig. 1.6-b). Therefore, the bubble will infect neighbors and will propagate into the system, if

$$\frac{A(R)}{\pi a^2} > \frac{1 - 2p}{2(1 - p)}. (1.12)$$

The surface A(R) follows from a direct geometrical calculation. In the large R/a limit, one gets

$$\frac{A(R)}{\pi a^2} \approx \frac{1}{2} - \frac{a}{3\pi R} - \frac{2a^2}{9\pi^2 R^2} + \mathcal{O}(R^{-3}),\tag{1.13}$$

therefore, one concludes that the critical radius of nucleation scales as

$$\frac{R_c}{a} \approx \frac{2(1-p)}{3\pi p}.$$

Figure 1.7 shows a numerical study of the nucleation radius, for various vicinity sizes, |V|, as a function of p. Moreover the figure also presents the mean field estimation by

an explicit geometrical calculation of the surface A(R) and using the critical condition (1.12). One sees that the mean field approach matches perfectly with the data in the large |V| limit.

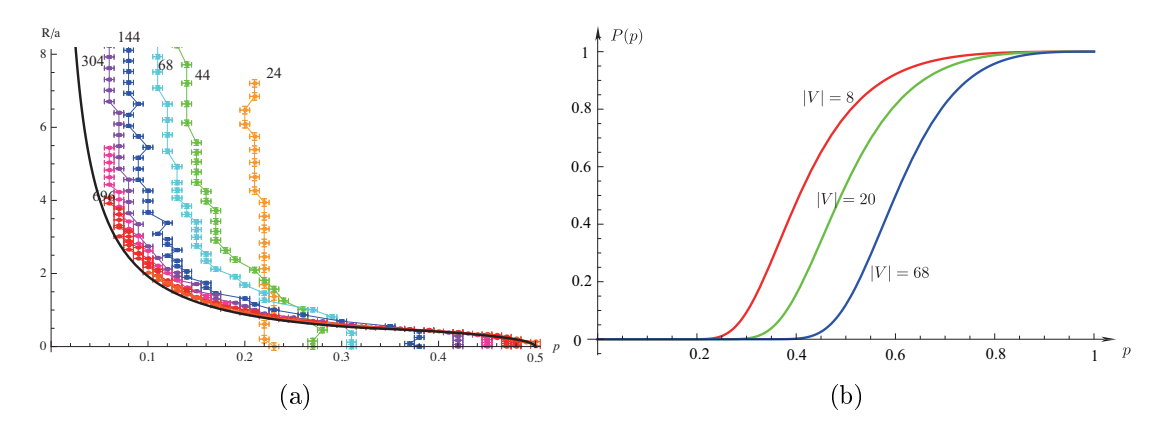


Figure 1.7: a) Critical radius of nucleation R/a as a function of p. As expected as $p \to 1/2$ the critical radius is zero, while as $p \to 0$ the critical radius diverges. The points correspond to the numerical simulations for different values of the vicinity size: $|V| = \{24, 44, 68, 144, 304, 696\}$ as indicated in the figure. b) Estimation of the lower bound of the probability P(p) of having a critical nucleation bubble of infected states, for |V| = 8, |V| = 20 and |V| = 68 One notices that this probability takes-off around a precise value of p.

However, a question remains open: what is the probability to obtain, *ab-initio* a bubble with a radius larger than R_c ? This probability seems to be very small, because it is proportional to the probability to obtain πR_c^2 sates +1 all together, that is

$$P_{\text{bubble}} \approx p^{\pi R_c^2} = p^{|V|(R_c/a)^2} \sim p^{|V|\frac{4(1-p)^2}{9\pi^2 p^2}},$$
 (1.14)

with R_c/a the function of p plotted in Fig. 1.7. Although, this probability P(p) is quite small, it is a lower bound for the problem of Bootstrap percolation. If, initially, a bubble has a radius greater than $R_c(p)$, then the system percolates, and the nucleation bubble may not initially exist, but it may be built solely by the evolution, this provides a better estimation of the probability P(p) of percolation.

Chapter 2

The Q2R Cellular Automaton

2.1 The Q2R model

2.1.1 The rule

The Q2R cellular automaton [4] is a network with $N \gg 1$ nodes, in which each node k represents a spin with a discrete value $(x_k = -1 \text{ or } x_k = +1)$. The spins interact with a neighbor V, moreover, the interactions can depend of the range of interaction (one-dimensional case), as display in Figure 2.1(a). For the following, we shall restrict the Q2R model, already introduced in section 1.1.3 in a two-dimensional lattice, for the case of Von Neumann neighborhood, therefore, with the four closest neighbors (see Figure 2.1(b)).

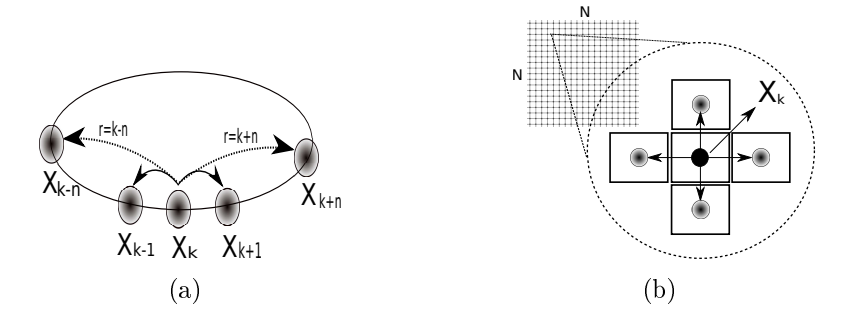


Figure 2.1: Figure (a) and (b) represent the interactions scheme for one and two-dimensional cases. Figure (a) shows a chain with a r ratio-interaction, and Figure (b) a square lattice of size $N \times N$, with a von-Neuman neighborhood. In both cases, periodic boundary conditions are employed.

This automaton is driven by the following two step-rule [4]:

$$x_k^{t+1} = x_k^{t-1} \phi\left(\sum_{i \in V_k} x_i^t\right),$$
 (2.1)

where the function ϕ is such that

$$\phi(s) = \begin{cases} +1 & \text{if} \quad s \neq 0 \\ -1 & \text{if} \quad s = 0. \end{cases}$$
 (2.2)

This two-step rule may be naturally re-written as a one-step rule with the aid of an auxiliary dynamical variable:

$$y_k^{t+1} = x_k^t,$$

which when substituted into equation (2.1), becomes

$$x_k^{t+1} = y_k^t \phi \left(\sum_{i \in V_k} x_i^t \right). \tag{2.3}$$

Note that the reversibility of the model corresponds to the equivalence of the inverse function $\phi\left(\sum_{i\in V_k}x_i^t\right)=1/\phi\left(\sum_{i\in V_k}x_i^t\right)$, because from conditions of the equation (2.2), one can show that the equation (2.3) is equivalent

$$\phi\left(\sum_{i\in V_k} x_i^t\right) x_k^{t+1} = y_k^t. \tag{2.4}$$

Example

In the following, we will present a simple example of the evolution of a Q2R model. Let be a lattice of size $N=5\times 5$ as displays Figure 2.2. For simplicity, in the lattice there are two colors: the red circles (\bullet) correspond to states with values $x_k=+1$, and the black circles (\bullet), are states with values $x_k=-1$. Also, we examine a case where the initial configuration at time t=0 is the same at t+1 time, i.e., $x^{t=0}=y^{t=0}$, as show the Figures 2.2(a,b).

First select a spin in the initial configuration $x^{t=0}$, as shown in Figure 2.2(a). We enclosed the particular spin with a square, then, we select the neighborhood which corresponds to the initial configuration $y^{t=0}$, but for the state $x_k^{t=0} = +1$. Now, if we perform a sum over neighbors, this is $\phi\left(\sum_{i \in V_k} x_i^t = 0\right) = -1$, using equation (2.3), the state

2.1. THE Q2R MODEL

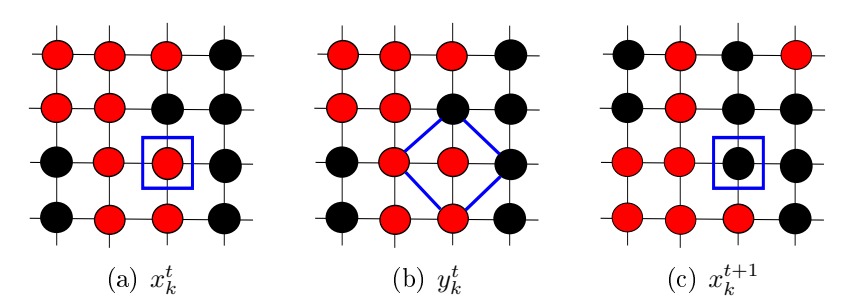


Figure 2.2: A system of size $N=4\times 4$, is present as an example for the dynamic of the Q2R model. The states are; the symbol (\bullet) for a state $x_k=1$, and the symbol (\bullet) for a state $x_k=-1$ respectively.

changes from $x_k = +1$ to $x_k = -1$ at each time-step (all states are updated in parallel fashion). Figure 2.2(c) represents the evolution of the system, where the initial energy E = -4 and initial magnetization M(t = 0) = 2. The final magnetization from x^t to x^{t+1} will be M(t = 1) = 0. In this case, the dynamics of the system conserves the energy and the magnetization fluctuates during the evolution process.

2.1.2 Energy Conservation

Pomeau [5] showed that the following quantity, which we call energy,

$$E[\left\{x^{t}, y^{t}\right\}] = -\frac{1}{2} \sum_{\langle i, k \rangle} x_{k}^{t} y_{i}^{t}, \qquad (2.5)$$

21

is preserved under the dynamics defined by the Q2R rule (2.3). The summation on equation (2.5) $\sum_{\langle i,k\rangle}$ is over all states k together with their neighbors, i. This form is equivalent to $\sum_{\langle i,k\rangle} \equiv \sum_i \sum_{k\in V_i} \equiv \sum_k \sum_{i\in V_k}$.

In the following, we prove the energy conservation between the time t and t+1. To do that, let as compute the energy difference among the time t and t+1.

$$\Delta E = E[\{x^{t+1}, y^{t+1}\}] - E[\{x^t, y^t\}]$$
(2.6)

$$= -\frac{1}{2} \sum_{\langle i,j \rangle} x_i^{t+1} y_j^{t+1} + \frac{1}{2} \sum_{\langle j,i \rangle} x_j^t y_i^t.$$
 (2.7)

Because $y_k^{t+1} = x_k^t$ and $x_k^{t+1} = x_k^{t-1} \phi\left(\sum_{i \in V_k} x_i^t\right)$, one gets that

$$\Delta E = -\frac{1}{2} \sum_{\langle i,j \rangle} \left[y_i^t \phi \left(\sum_{k \in V_i} x_k^t \right) x_j^t - x_j^t y_i^t \right]$$
 (2.8)

$$\Delta E = -\frac{1}{2} \sum_{\langle i,j \rangle} x_j^t y_i^t \left[\phi \left(\sum_{k \in V_i} x_k^t \right) - 1 \right] \equiv 0$$
 (2.9)

We can see that the last equality by term is zero, because, if $\sum_{k \in V_i} x_k^t \neq 0$ then, the bracket is zero. On the other hand, if $\sum_{k \in V_i} x_k^t = 0$ the bracket does not vanish, but the term in front $\sum_{\langle i,j \rangle} x_j^t = 0$ of the bracket cancels out terms. Besides, the energy is bounded by $-2N \leq E \leq 2N$.

2.1.3 Staggered Invariants

As already suggested by [7], there exists a large number of period orbits, therefore it is believed that Q2R possesses a large number of other invariants.

An example of additional conserved quantities, are the "staggered invariants" [32]. Indeed, for a square periodic lattice of even size L ($N=L^2$), the full lattice may be divided into two sub-lattices as follows: Let us denote k_x and k_y , the indices of the full-square, then, we define the W sub-lattice by all points such that k_x+k_y is an even number, while the B-lattice is characterized by the condition k_x+k_y being an odd number. (In other words, these sub-lattices represent the white and black fields in the chessboard.) Then, we define:

$$E^{W}[\{x^{t}, y^{t}\}] = -\frac{1}{2} \sum_{k_{x} + k_{y} \text{ even}} x_{k}^{t} \sum_{i \in V_{k}} y_{i}^{t},$$

$$E^{B}[\{x^{t}, y^{t}\}] = -\frac{1}{2} \sum_{k_{x} + k_{y} \text{ odd}} x_{k}^{t} \sum_{i \in V_{k}} y_{i}^{t}.$$

The conserved energy (2.5) may be re-written as $E[\{x^t, y^t\}] = E^W[\{x^t, y^t\}] + E^B[\{x^t, y^t\}]$. Further,

$$J[\{x^t, y^t\}] = (-1)^t (E^W[\{x^t, y^t\}] - E^B[\{x^t, y^t\}]), \qquad (2.10)$$

is also an invariant, i.e.,

$$J[\{x^t, y^t\}] = J[\{x^{t=0}, y^{t=0}\}].$$

This extra invariant, splits the sub-space of constant E into a sub-set of constant E and constant J. The role of this staggered invariant in the macroscopic behavior will be investigated in the future.

23

2.1.4 The Magnetization

Another useful and important macroscopic observable is the magnetization M(t), that is, the sum of the states of the lattice for each time-step, e.g.,

$$M(t) = M[\{x^t\}] = \sum_{k} x_k^t.$$
 (2.11)

This quantity M(t) is bounded as $-N \leq M(t) \leq N$. Consequently, we can estimate the standard deviation of Magnetization, considering the place where the average does not change during time T, i.e.,

$$\langle M \rangle = \frac{1}{T} \sum_{t=t_0}^{t=t_0+T} M(t), \qquad (2.12)$$

$$\sigma(M) = \sqrt{\langle M^2 \rangle - \langle M \rangle^2}.$$
 (2.13)

The parameters t_0 and T are the initial and final times, respectively. Finally, the magnetization is not conserved by the dynamics, however, this global variable can be identified as the right order parameter [33].

2.1.5 Mean Field Approximation

To understand the global interaction of the system, we can reduce it using mean field theory. Then, assuming that we are in a permanent regime, $M(t) \approx M(t+1) \approx \langle M \rangle$. From the equation of energy (2.5) and considering a Von Neuman neighborhood, it is possible to approximate the sum

$$\sum y_i^t \simeq 4 \frac{\langle M \rangle}{N},$$

therefore one obtains taht the energy may be approximated in the mean field limit by

$$E = -\frac{1}{2} \sum_{\langle i,k \rangle} x_k^t y_i^t \simeq -2 \frac{\langle M \rangle^2}{N} = -2m^2 N.$$
 (2.14)

Where

$$m \equiv \frac{1}{N} \langle M \rangle$$

is the average magnetization per site a quantity that belongs to $m \in [-1, 1]$.

Finally, the magnetization as a function of the energy is

$$m = \pm \sqrt{-\frac{E}{2N}}. (2.15)$$

In next Section 2.2.2, we shall show that in the limit of large neighbors the mean field approximation becomes accurate.

2.2 Dynamics of the Q2R model

2.2.1 Initial conditions

We have explored the evolution of the Q2R model in the long-time run and with different initial random conditions of type,

$$x_k^{t=0} = y_k^{t=0} = B_k(p),$$

where $B_k(p)$ is:

$$B_k(p) = \begin{cases} +1 & \text{with probability } p \\ -1 & \text{with probability } 1-p \end{cases}$$
 (2.16)

Here, $B_k(p)$ is a probability function that can take boolean values with respect to p; if p = 0 then the system will have only +1 states as initial condition, however, if the probability is p = 1/2 the initial condition will exhibit an uniform distribution of states, i.e., an homogeneous distribution of +1 and -1 values into the lattice. The index k represents independent realizations over lattice sites. We have studied all possible pair of initial conditions: $\{x_k^{t=0} = y_k^{t=0}\}$ as given by equation (2.16).

First, we shall provide a brief overview of the dynamical behaviors and statistical properties in the case of one dimensional lattices. Then we proceed with two dimensional lattices.

2.2.2 One-dimensional Systems

In this section we shall study the one-dimensional case. Take a chain of L=256 sites. Let be r the interation range, i.e., the site k interactions with all sites $\{k-r, k-1, k+1, \ldots, k+r\}$. In the present study we have considered the cases $r=2^n$, where n may take different values $n=\{0,1,2,3,4,5,6,7\}$, being r=1, r=128 the shortest and longest range respectively.

Figure 2.3 shows the evolution of M(t)/N two different dynamics related to the interaction range for the evolution in Magnetization. We have taken the case where the range is r=2 and the initial energy E/N=-0.382, as shown in Figure 2.3(a). Here, the magnetization fluctuates as $\Delta M/N=[0.4,-0.4]$, and its average is $\langle M \rangle/N=-0.01$.

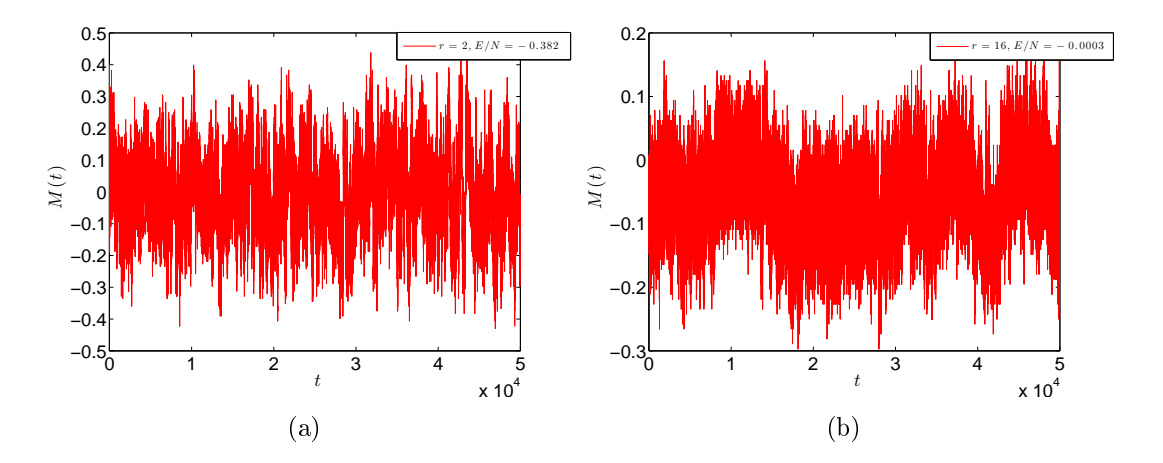


Figure 2.3: The plot corresponds to the dynamics of magnetization versus time. In (a), the system possesses an initial energy E/N=-0.382 and a interaction range, r=2. On the other hand, (b) exhibits a case where the interaction range is r=16 and the initial energy is E/N=-0.0003. In both cases the time evolution was $t=4\times 10^4$

On the other hand, in the case where the interaction range is r = 16, (see Figure 2.3(b)), the magnetization fluctuates as $\Delta M/N = [-0.3, 0.2]$, but its average is zero.

It is important to remark the following fact: The dynamics depends on an interaction range as well as the energy. Figure 2.4 plot the phase diagram for the average magnetization per site $\langle M \rangle/N$, as a function of the re-scaled energy (E/rN). This function has been normalized, with the purpouse of checking convergence for all curves to the value $E/rN \approx 0$. Notice that in the mean field approximation equation (2.15) becomes $m = \sqrt{-E/rN}$.

If the system takes the value r=4 (the curve is represented with the symbol +), $\langle M \rangle$ converges to an energy close to $E/rN \approx -0.2$. However, when we take as interaction range r=128, the curve converges to the value E/rN=0. In the latter case, we have a full interacting system. Moreover, when the latter condition of full interaction is satisfied, $m=\sqrt{-E/rN}$ is equivalent to the one obtained by applying mean field theory.

Therefore, the one-dimensional case manifests a dynamics, where the interaction does not show phase transition. This is coherent with the aim of the Q2R model, that is, a model equivalent to the one-dimensional Ising model.

2.2.3 Two-dimensional Systems

Now, we consider the case of a two dimensional periodic lattice of size $N = 256 \times 256$. Moreover, we will develop extensive numerical simulations in the long-time run, with the idea of generating the evolution of states as a function of the initial energy. Also, as it was shown in a previous article [9], the Q2R cellular automata exhibits an important feature,

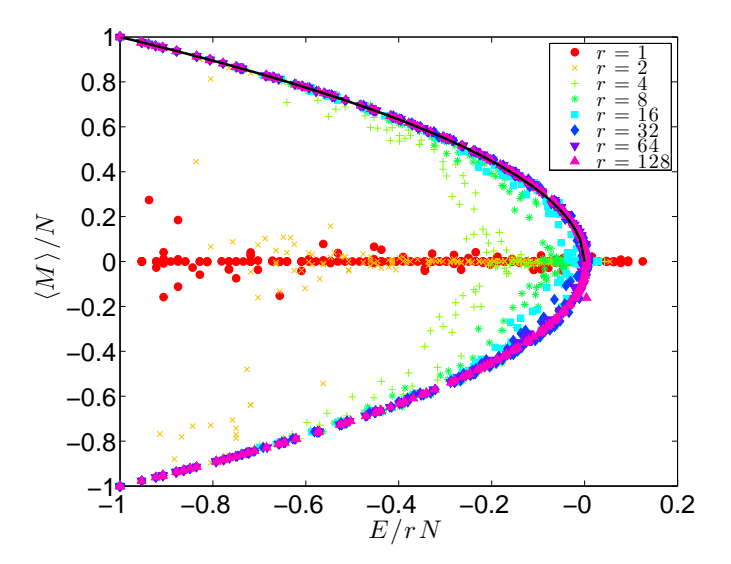


Figure 2.4: The average magnetization $\langle M \rangle/N$ as a function of E/rN. Here, we have presented eight different interaction range, from r=1 to r=128. The continuous line represents the result obtained by calculating using calculation of mean field, $m=\sqrt{-E/rN}$.

namely the existence of a phase transitions, for given a specific energy, as it occurs in the two-dimensional Ising model.

2.2.4 Ferromagnetic and Paramagnetic Behaviors

We have observed in the first place that with energies lower than a critical energy $E \ll E_c$ (which is equal to $E_c/N = -\sqrt{2}$), the system will exhibit a dynamics called ferromagnetic behavior. This behavior corresponds to a case where all the spins have a preferred orientation, which may be +1 or -1. To be more specific, if we take an energy equal to E/N = -1.62, we can observe (Figure 2.5(a)) the behavior of magnetization as function of time. This magnetization exhibits a fluctuating set of values in the range $\Delta M/N = [0.870, 0.895]$.

For this energy, the center of distribution is located close to the average $\langle M \rangle \approx 0.88$. However, in the accompanying (in Figure 2.5(b)) we can see the distribution function, in semi-log scale, showing that the distribution is not Gaussian.

On the other hand, when $E \gg E_c$, the system acquires a paramagnetic behavior. This type of behavior corresponds to a homogeneous distribution of spins, i.e., there is no preference spin orientation. In Figure 2.6(a), we show the evolution of the magnetization when the initial energy is E/N = -0.07. This, is different to the paramagnetic case,

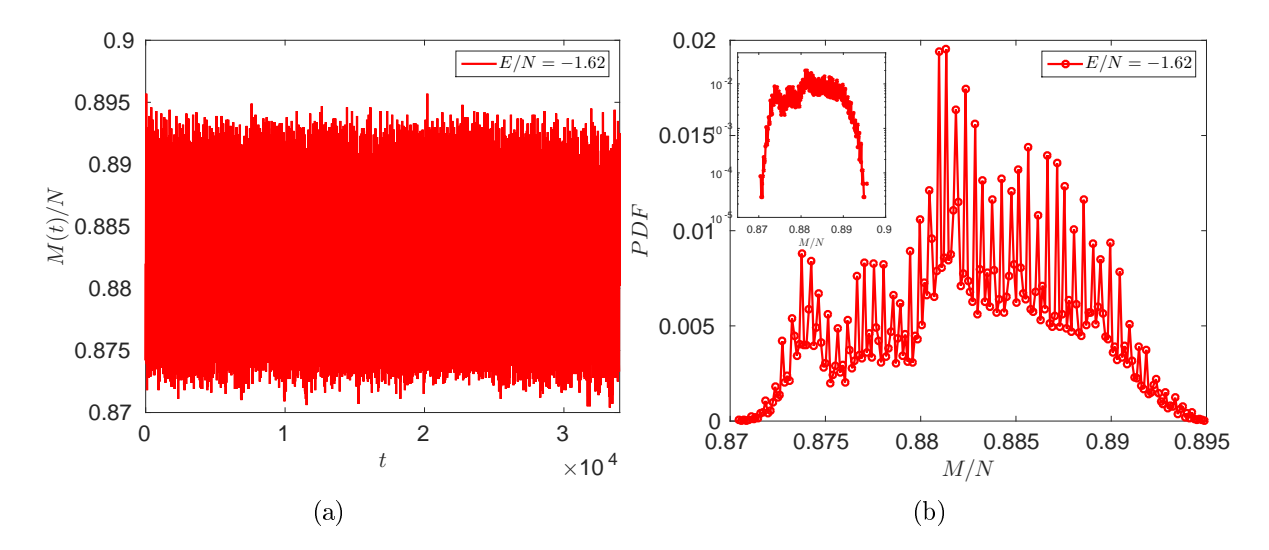


Figure 2.5: (a) Represents the dynamics of the magnetization versus time, for a system with an energy E/N = -1.62. In this case, the system exhibit a ferromagnetic behavior. (b) Represents the probability density distribution of the magnetization. The inset plot the PDF in log scale.

because the dynamics fluctuates around zero: $\Delta M/N = [-0.015, 0.015]$, being a behavior without large fluctuations. Moreover, Figure 2.6(b) represents the evolution of the pdf of $\langle M \rangle/N$, which exhibits an average equals to $\langle M \rangle/N = 0$. In such case, the system exhibits a similar number of spins +1 and -1. Also, in this case, the histogram shows a well defined Gaussian distribution.

2.2.5 Phase Transition

The Q2R model exhibits a phase transition for a critical energy, E_c . This value is close to the critical energy of the Ising model $E_c/N = -\sqrt{2}$ [31, 34].

As we can observe in Figure 2.7(a), we can distinguish three different regimes, when starting with on initial energy E/N=-1.416. The first one, shows a fluctuation for M(t)/N around the value $\langle M \rangle/N=0.55$. Analogously, for the second and third regimes, the corresponding fluctuations are around $\langle M \rangle/N=0$ and $\langle M \rangle/N=-0.55$ respectively. Finally, the fluctuation will return around zero.

We can see a spontaneous change in the behavior of the magnetization from higher to lower values. However, with an initial condition such that M < 0 (and $E \approx Ec$), the system will evolve from negative to positive values of $\langle M \rangle / N$.

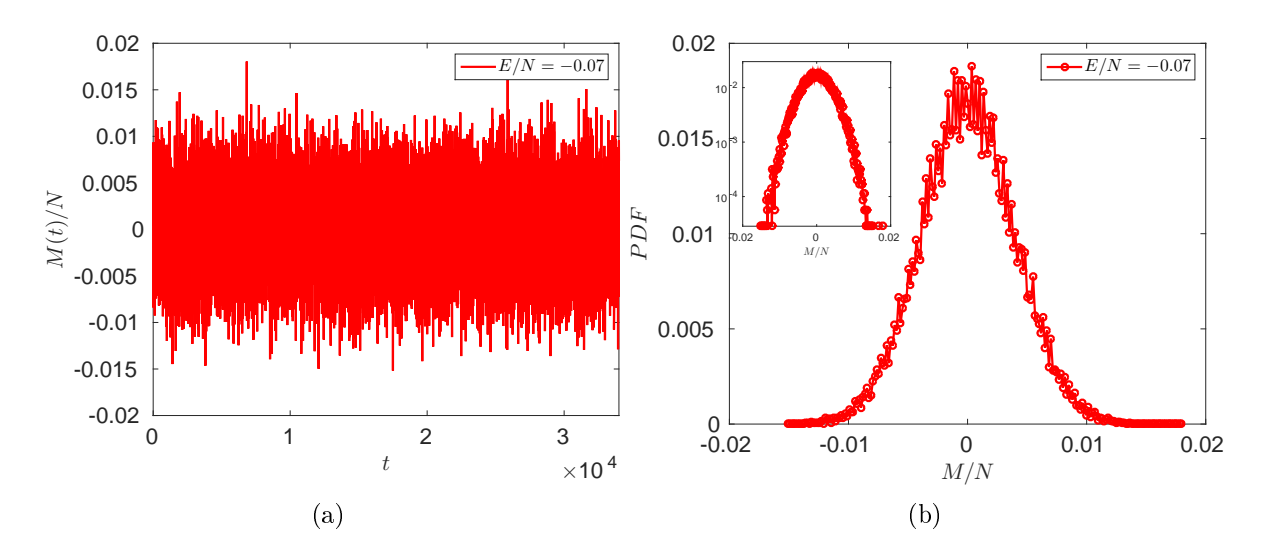


Figure 2.6: (a) Represents the dynamics of the magnetization versus time, for a system with an energy E/N = -0.07. In this case, the system exhibits a paramagnetic behavior. (b) Represents the PDF of magnetization. The inset show the PDF in log scale.

In this context, the distribution for the case of an energy E/N = -1.416 (Figure 2.7(b)), the pdf of magnetization shows the existence of three values where the distribution is concentrated, and which corresponds to the evolution of the magnetization, $\langle M \rangle / N = 0.55$, $\langle M \rangle / N = 0$ and $\langle M \rangle / N = -0.55$ respectively. Also, there is a higher concentration around the average $\langle M \rangle / N = 0$, because the system will remain a longer time in those regions, before jumping to a different magnetization value.

However, this shows that if the system is taking values different from the critical energy, there will be convergence to a paramagnetic or ferromagnetic behavior, as was previously shown. On the other hand, it is interesting how the Q2R cellular automata develops a very defined representation of a change of state similar to that the one which generates the classic Ising model [2].

Consequently, from the evolution of the magnetization, it is possible to make a statistical description for the average of magnetization $\langle M \rangle$ (see Eq. 2.12), as well as, for the standard deviation $\sigma(M(t))$ (see Eq. 2.13), versus the initial energy E/N. Then, the phase diagram of Figure 2.8(a) shows three specific behaviors, according to a given energy. In this context, starting from the lowest energy E/N = -2 (Ferromagnetic state) the curve begins to fall (or to rise) gently until it reaches a critical energy E_c , where, the system exhibits a metastable behavior mean phase transition. Then, the curve converges quickly to a zero value respect to the average magnetization (Paramagnetic state). Moreover, Figure 2.8(b) displays the standard deviation versus the Energy. Here, we can see

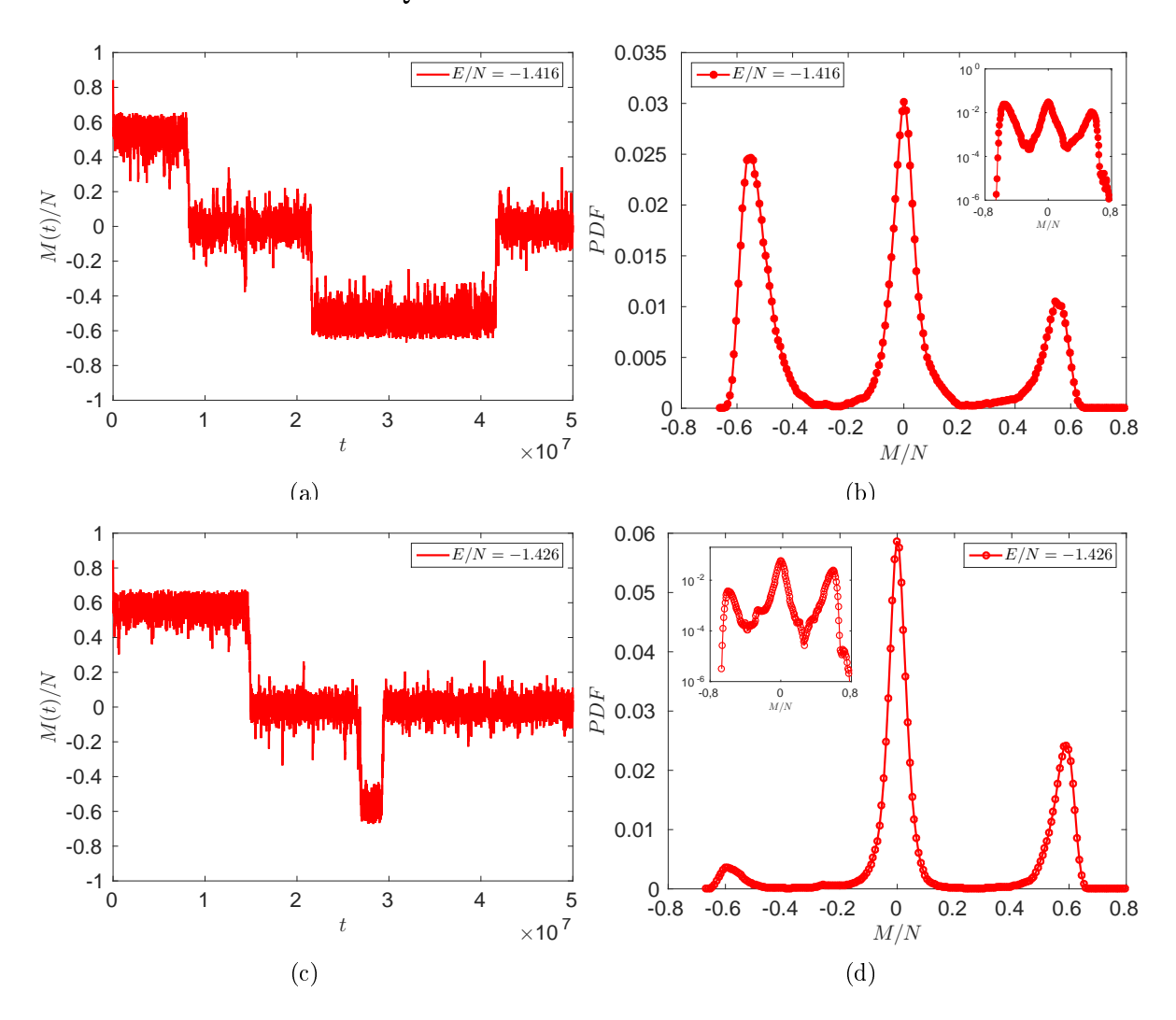


Figure 2.7: Plots (a) and (c) show the evolution of the magnetization for the case where their initial energies are E/N=-1.416 and E/N=-1.426 respectively. We can see that the magnetization jumps between states. In both cases, Figure (b) and (d) display the pdf for the respective magnetizations.

how the system exhibits a greater fluctuations around the critical energy E_c/N value.

During this research, we have observed in Q2R model a behavior which depends on the specific region of energy considered. Moreover, our analysis has alway been performed from a macroscopic point of view in terms of the observable of interest (Magnetization). However, as seen from a microscopic point of view, states can evolve into very specific patterns.

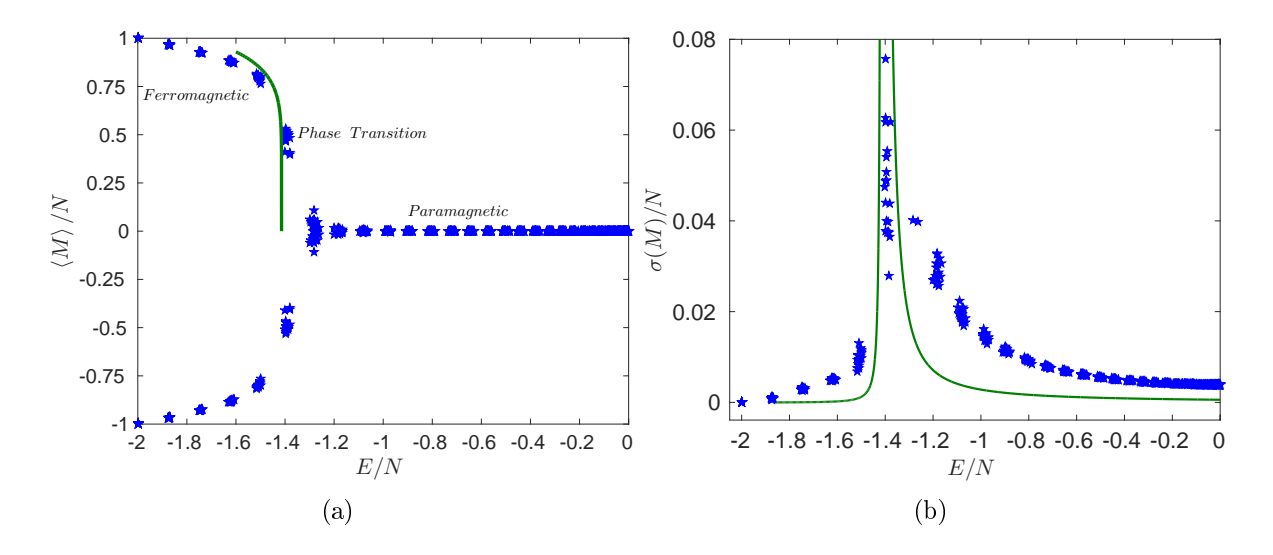


Figure 2.8: Phase diagram of average magnetization $\langle M \rangle / N$ versus the Energy E/N. One can see, regions where the system shows a ferromagnetic and paramagnetic behavior, for a given initial Energy, as well as, the critical regime. Figure (b) represents the standard deviation of magnetization versus the energy. Clearly, we can see that the system exhibit a maximum value when the energies are close to the critical energy $E/N = -\sqrt{2}$. The continuous line represents the well known statistical mechanics calculation for the Ising model $M/N \approx 2^{5/16} (\sqrt{2} + E/N)^{1/8}$ (see below).

When the dynamics shows ferromagnetic behavior, there will be a preferred spin orientation, as can be seen in Figure 2.9(a). The lattice only exhibits a small number of -1 spins and a big number of +1 spins. Clearly, this shows that during the evolution some states may change. However, when the initial energy gives rise to a paramagnetic pattern, in the lattice there will be an equal amount +1 and -1 states which are randomly distributed (Figure 2.9(b)).

Near the transition the dynamics, i.e., $E \approx E_c$, the patterns display patches, with +1 and -1 states. Here, the patches are spins concentration which can keep a state on a finite time, and then change to another state (see Figure 2.9(c)). Also, there will be zones where the average magnetization is zero, because the spins are into a chessboard-like pattern.

2.2.6 Exact results from the Ising model in statistical mechanics

Finally, to illustrate the connection with the Ising model. One can get a relation between the average energy and the average magnetization from the aid of the well-know formulas by Onsager [31] and Yang [34]. Similarly, we can obtain a relation between the magneti-

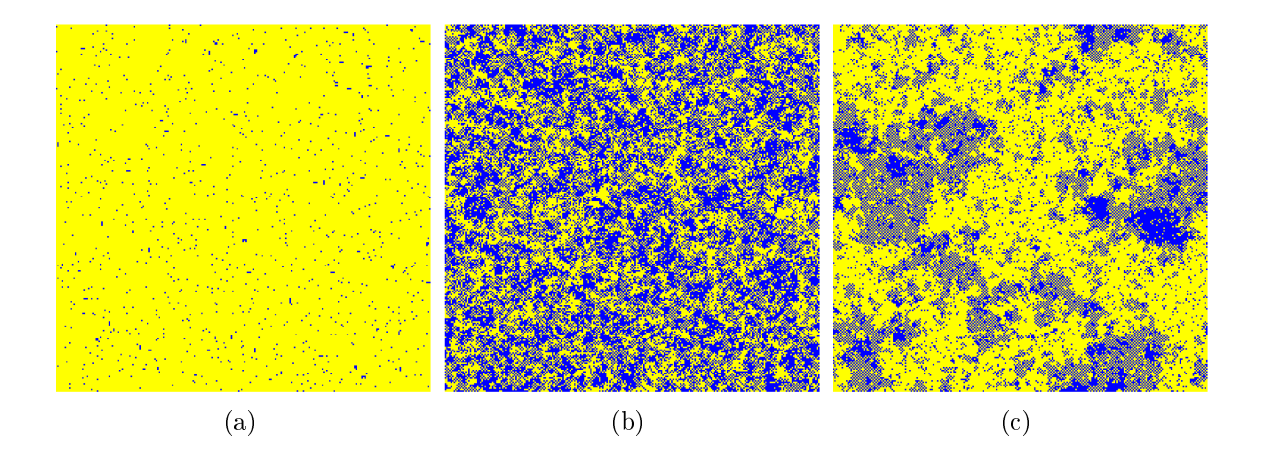


Figure 2.9: Snapshots of the patterns for three different energies. In Figure (a) correspond a case where the system exhibit a paramagnetic behavior (E/N=-1.62), Figure (b) is a the case of a ferromagnetic behavior (E/N=-0.07). Finally, in Figure (c) shows a pattern where the initial energy is close to critical energy (E/N=-1.416). The color map, is the following: yellow represents the boolean variable at +1 and blue means that the boolean variable is at -1.

zation fluctuations that corresponds to the zero-field magnetic susceptibility as a function of energy following the work of Wu et al. [35].

Because all these calculations are done in the canonical ensemble, we shall compare the macroscopic observable in terms of the inverse of the temperature, β . The mean internal energy as a function of β reads

$$\frac{E(\beta)}{N} = -\coth(2\beta) \left(1 + \kappa_1 \frac{2}{\pi} \int_0^{\pi} \frac{dt}{\sqrt{1 - \kappa^2 \sin^2 t}} \right), \tag{2.17}$$

where κ and κ_1 are:

$$\kappa = 2 \frac{\sinh(2\beta)}{\cosh^2(2\beta)} \qquad \kappa_1 = 2 \tanh^2(2\beta) - 1. \tag{2.18}$$

The transition point is characterized by the condition $\sinh(2\beta_c) = 1$, that corresponds to the critical energy $E_c/N = -\sqrt{2}$.

The resulting magnetization because [34]

$$\frac{M(\beta)}{N} = \left(1 - \frac{1}{\sinh^4(2\beta)}\right)^{1/8},\tag{2.19}$$

and, finally, the magnetic fluctuations

$$\Delta M^2 = \left\langle M^2 \right\rangle - \left\langle M \right\rangle^2$$

are related to the magnetic susceptibility via

$$\chi = \beta \left(\left\langle M^2 \right\rangle - \left\langle M \right\rangle^2 \right).$$

On the other hand the magnetic susceptibility has been reported to be [35]

$$\chi_{\pm} = \beta \left(c_{0_{\pm}} \left| 1 - \beta / \beta_c \right|^{-7/4} + c_{1_{\pm}} \left| 1 - \beta / \beta_c \right|^{-3/4} \right) + \dots, \tag{2.20}$$

where the \pm sign correspond to the behavior for $\beta > \beta_c$ or $\beta < \beta_c$. The numerical values for the constants are:

 $c_{0_{+}} = 0.9625817322$ $c_{0_{-}} = 0.0255369719$ $c_{1_{+}} = 0.0749881538$ $c_{1_{-}} = -0.0019894107$

From the numerical results obtained in this section, we have shown clearly the connection of the Q2R model with the Ising model. From this set of equations that shows the behaviors of the Ising model. Moreover, the theoretical curves Magnetization versus Energy (see Fig.2.8(a)), and magnetic susceptibility versus Energy (see Fig.2.8(b)), this verifies that the model is a good example for displays the dynamics between spins, and also the dynamics can develop a phase transition when the energy takes the critical value.

Chapter 3

The Phase Space characterization

3.1 Generalities

The phase space of the Q2R system of N sites possesses 2^{2N} states, which is partitioned in different sub-spaces of constant energy, which themselves are partitioned into a large amount of smaller subspaces of periodic orbits or fixed points. Notice that, because the system is conservative, there are neither attractive nor repulsive limit sets, all orbits are fixed points or cycles.

This feature of the phase space is schematized in Fig. 3.1, where the constant energy subspace shares in principle many cycles and fixed points. An arbitrary initial condition of energy E falls into one of these cycles, and it runs until it comes back to the initial configuration after a time T, which could be exponentially long and it displays a complex behavior.

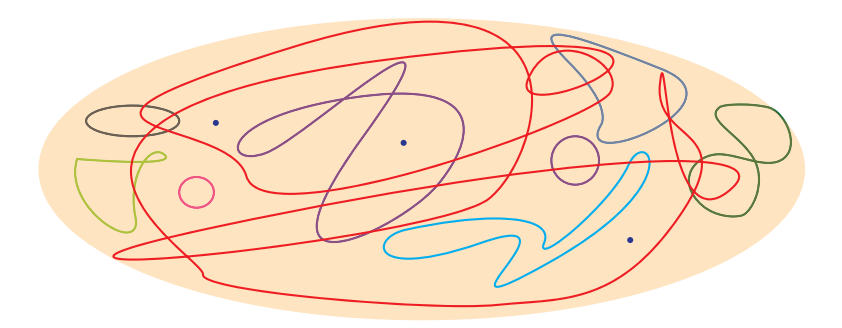


Figure 3.1: Scheme of a sub-space of constant energy composed by a number of cycles and fixed points.

In the following section we shall characterize the phase space of the Q2R automaton.

3.2 Exact phase space calculation for very small lattices

3.2.1 Phase space 2×2

Let us consider, in the first place, the simplest version of a two-dimensional Q2R automata, this is, the periodic of a lattice of 2×2 . As well shall see, the dynamics is extremely simple and then, it is possible to perform manually all calculations.

The phase space is defined by a hypercube of dimension 8, e.g, composed of $2^8 = 256$ vertices which represent the full set possible configurations. As shown in Figure 3.2, the energy takes only five possible values, $E = \{-8, -4, 0, +4, +8\}$. However, the original phase space is not only partitioned by the energy conservation rule, but by a large amount of small cycles with different periods.

This fact suggests that it is possible define unknown invariants that constrain the dynamics that rules in limit cycles. More precisely, for E=8 there are 4 configurations, for an energy E=-4 there are 48 configurations consisting in 12 cycles of period 4, similarly for E=+4 which constant energy set also consists of 12 cycles of 4 period. Finally the case E=0 consists on 152 configurations divided in 36 cycles of 4 period, and 4 cycles of 2 period. The full periodic structure of each set of energy is summarized in Table 3.1.

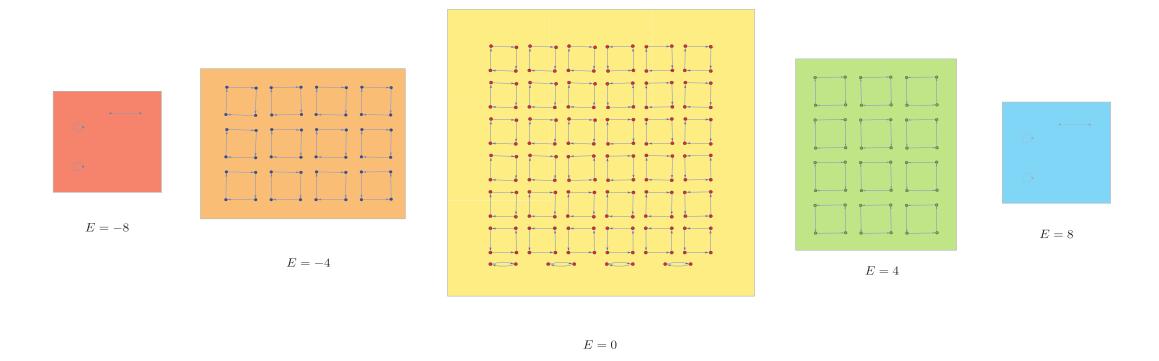


Figure 3.2: Representation of the five subspaces which corresponds to a system $N = 2 \times 2$. Moreover, the five different subspaces of energies $E = \{-8, -4, 0, +4, +8\}$. Each subspace shows a number of periods which depends on the particular energy of such subspace.

3.2.2 Exact Phase Space for the $N = 4 \times 4$ case.

The phase space for $N=4\times 4$ the system exhibits 2^{32} states and a phase space of dimension 32. The full distribution of states for the exact phase space for a $N=4\times 4$ system

			Period				
E	n(E)	1	2	4			
-8	4	2	2	0			
-4	48	0	0	48			
0	152	0	8	144			
4	48	0	0	48			
8	4	2	2	0			

Table 3.1: The distribution of periodic orbits for all energies in the case of Q2R in a 2×2 periodic lattice. The first column indicates the energy E, the second one, n(E), shows the total number of states with an energy E. The following columns indicates the total number of states of period T.

is presented on the next tables.

In the first column of the table 3.2, this present the values of energy. The second column correspond to number of states for energy. On the other hand, from the third to last column these present the periods for each values of energy. Finally, the tables 3.3 and 3.4 shows the continuity of the phase space.

As it can be seen form the data, the Q2R system for 4×4 possesses a number of 29 periods, moreover, this has fixed points for all the energies. However, the cycle longer is T=1080 and only correspond for the energies E=-2 and E=+2. The full data maybe summarized in a probability density of states with a given energy and period: $\rho(E,T)$ that is plotted in Figure 3.3(a). An important point is the symmetry on the phase space, because we have the same quantity of states and periods, for positive and negative energies. On the other hand, in Figure 3.3(b) we have taken some periods, where clearly the phase space, develop a distribution symmetric around of the energies.

Even for small systems one notices that the number and the period of cycles varies from energy to energy. However, the distribution of periods for a given energy presents some robust behaviors that may be studied similarly, but it takes more lengthly processing time because one needs to run the states and wait the complete cycles.

Let be n(T, E) the total number of cycles of period T and energy E, of a system with N sites ruled by Q2R, then one defines the probability density function

$$\rho(E,T) = \frac{T \times n(T,E)}{2^{2N}} \approx e^{-\alpha|E|}.$$
(3.1)

By the ratio of total number of states of period T over the total number of states that satisfies the following normalization rules:

$$\Omega(E) = 2^{2N} \sum_{T=1}^{T_{max}(E)} \rho(E,T)$$
 and $\sum_{E=-2N}^{2N} \sum_{T=1}^{T_{max}(E)} \rho(E,T) = 1$

			Period									
E	n(E)	1	2	3	4	5	6	8	9	10	12	18
-32	4	2	2	0	0	0	0	0	0	0	0	0
-28	128	0	128	0	0	0	0	0	0	0	0	0
-26	256	0	256	0	0	0	0	0	0	0	0	0
-24	2720	32	1344	0	768	0	576	0	0	0	0	0
-22	11008	0	4608	0	1024	0	1536	0	0	3840	0	0
-20	57984	64	9792	0	13568	0	11520	9216	0	0	9216	0
-18	219136	0	19968	0	44032	0	48384	0	0	61440	15360	16128
-16	911088	88	26920	144	140528	0	131952	171776	0	122880	220032	0
-14	3244032	0	35328	0	285696	0	380160	294912	0	168960	777216	274176
-12	11734400	128	51712	384	688128	960	696192	1688576	0	1166400	3240960	516096
-10	38121728	0	66048	0	1323520	0	1362432	2547712	0	65280	8871936	2128896
-8	111191136	32	89152	576	3305024	0	2112000	10482688	0	245760	22628736	4644864
-6	264889088	0	96512	0	4457472	0	2700288	9093120	0	460800	51004416	6773760
- 4	511430528	128	90112	1344	4737280	0	4198080	53696512	4032	368640	96278016	32251968
-2	763062272	0	107520	0	8868864	0	3188736	16793600	0	230400	138407424	6580224
0	885216280	208	136376	0	21223312	0	5621760	103893504	0	2334720	144804096	56254464
2	763062272	0	107520	0	8868864	0	3188736	16793600	0	230400	138407424	6580224
4	511430528	128	90112	1344	4737280	0	4198080	53696512	4032	368640	96278016	32251968
6	264889088	0	96512	0	4457472	0	2700288	9093120	0	460800	51004416	6773760
8	111191136	32	89152	576	3305024	0	2112000	10482688	0	245760	22628736	4644864
10	38121728	0	66048	0	1323520	0	1362432	2547712	0	65280	8871936	2128896
12	11734400	128	51712	384	688128	960	696192	1688576	0	1166400	3240960	516096
14	3244032	0	35328	0	285696	0	380160	294912	0	168960	777216	274176
16	911088	88	26920	144	140528	0	131952	171776	0	122880	220032	0
18	219136	0	19968	0	44032	0	48384	0	0	61440	15360	16128
20	57984	64	9792	0	13568	0	11520	9216	0	0	9216	0
22	11008	0	4608	0	1024	0	1536	0	0	3840	0	0
24	2720	32	1344	0	768	0	576	0	0	0	0	0
26	256	0	256	0	0	0	0	0	0	0	0	0
28	128	0	128	0	0	0	0	0	0	0	0	0
32	4	2	2	0	0	0	0	0	0	0	0	0

Table 3.2: Number distribution of the states as a function of E and T (Part 1), for the case of 4×4 system size.

Here, $\Omega(E)$ is the total number of states, this distribution of states is not known for this system, but it decays exponentially in the energy in the tails.

3.3 The evolution of states in configuration space

3.3.1 Sensitivity to initial conditions

The sensitivity to initial conditions of Q2R has been discussed previously in Ref. [9]. In fact, when starting from two distinct initial conditions, which share the same energy and J, they will evolve along two different paths. As the distance in phase space is bounded, these two cycles will diverge in a non-exponential way. However, the separation growth between them is fast enough so as to be completely analogous with the concept of sensitivity to initial conditions.

		Period									
E	20	24	27	30	36	40	54	60	72		
-32	0	0	0	0	0	0	0	0			
-28	0	0	0	0	0	0	0	0	0		
-26	0	0	0	0	0	0	0	0	0		
-24	0	0	0	0	0	0	0	0	0		
-22	0	0	0	0	0	0	0	0	0		
-20	0	4608	0	0	0	0	0	0	0		
-18	0	0	0	0	0	0	13824	0	0		
-16	7680	73728	0	0	0	15360	0	0	0		
-14	368640	147456	0	276480	0	0	235008	0	0		
-12	614400	1645056	0	737280	0	245760	442368	0	0		
-10	860160	3538944	0	1105920	1548288	4915200	1824768	4423680	0		
-8	2549760	29177856	0	2580480	2064384	2150400	3981312	7925760	0		
-6	13140480	42713088	0	0	22708224	21995520	5806080	9768960	27869184		
-4	2826240	90584064	3456	2580480	39223296	29245440	53523072	18432000	0		
-2	4423680	104472576	0	1382400	89510400	11304960	5640192	24330240	76898304		
0	21427200	107237376	0	1474560	74317824	133048320	99975168	16588800	0		
2	4423680	104472576	0	1382400	89510400	11304960	5640192	24330240	76898304		
4	2826240	90584064	3456	2580480	39223296	29245440	53523072	18432000	0		
6	13140480	42713088	0	0	22708224	21995520	5806080	9768960	27869184		
8	2549760	29177856	0	2580480	2064384	2150400	3981312	7925760	0		
10	860160	3538944	0	1105920	1548288	4915200	1824768	4423680	0		
12	614400	1645056	0	737280	0	245760	442368	0	0		
14	368640	147456	0	276480	0	0	235008	0	0		
16	7680	73728	0	0	0	15360	0	0	0		
18	0	0	0	0	0	0	13824	0	0		
20	0	4608	0	0	0	0	0	0	0		
22	0	0	0	0	0	0	0	0	0		
24	0	0	0	0	0	0	0	0	0		
26	0	0	0	0	0	0	0	0	0		
28	0	0	0	0	0	0	0	0	0		
32	0	0	0	0	0	0	0	0	0		

Table 3.3: Number distribution of the states as a function of E and T (Part 2), for the case of 4×4 system size.

To perform this study we require two close enough initial configurations. A first initial configuration, $\{x,y\}^{t=0}$, is arbitrarily chosen. The second one, is built by swapping a single site \bar{k} in the previous configuration. This site is randomly selected such that the average magnetization due to its neighbors is zero (that is $\sum_{i\in V_{\bar{k}}} x_i = 0$ or $\sum_{i\in V_{\bar{k}}} y_i = 0$). In this way, both initial configurations have the same energy. Finally, running independently both initial configurations, a separation distance between both paths can be measured by the equation.

$$d_H(t) = \sum_{k=1}^{N} (|x_k^t - \bar{x}_k^t| + |y_k^t - \bar{y}_k^t|),$$

with $\{x,y\}^t$ and $\{\bar{x},\bar{y}\}^t$ denoting two different sequences belonging to two different cycles (see Figure 3.4). It can numerically be shown that $d_H(t)$ grows approximately as

					Peri	iod			
E	90	108	120	180	216	270	360	540	1080
-32	0	0	0	0	0	0	0	0	0
-28	0	0	0	0	0	0	0	0	0
-26	0	0	0	0	0	0	0	0	0
-24	0	0	0	0	0	0	0	0	0
-22	0	0	0	0	0	0	0	0	0
-20	0	0	0	0	0	0	0	0	0
-18	0	0	0	0	0	0	0	0	0
-16	0	0	0	0	0	0	0	0	0
-14	0	0	0	0	0	0	0	0	0
-12	0	0	0	0	0	0	0	0	0
-10	0	1327104	2211840	0	0	0	0	0	0
-8	7741440	1769472	1105920	0	0	6635520	0	0	0
- 6	0	19464192	2949120	0	23887872	0	0	0	0
- 4	7741440	33619968	35389440	0	0	6635520	0	0	0
-2	0	76723200	42024960	15482880	65912832	0	30965760	13271040	26542080
0	0	63700992	33177600	0	0	0	0	0	0
2	0	76723200	42024960	15482880	65912832	0	30965760	13271040	26542080
4	7741440	33619968	35389440	0	0	6635520	0	0	0
6	0	19464192	2949120	0	23887872	0	0	0	0
8	7741440	1769472	1105920	0	0	6635520	0	0	0
10	0	1327104	2211840	0	0	0	0	0	0
12	0	0	0	0	0	0	0	0	0
14	0	0	0	0	0	0	0	0	0
16	0	0	0	0	0	0	0	0	0
18	0	0	0	0	0	0	0	0	0
20	0	0	0	0	0	0	0	0	0
22	0	0	0	0	0	0	0	0	0
24	0	0	0	0	0	0	0	0	0
26	0	0	0	0	0	0	0	0	0
28	0	0	0	0	0	0	0	0	0
32	0	0	0	0	0	0	0	0	0

Table 3.4: Number distribution of the states as a function of E and T (Part 3), for the case of 4×4 system size.

 t^2 (see Ref. [9] for details).

3.3.2 Levy flight structure

The Hamming distance is a parameter that can be used in order to understand the dynamics of the states in the hypercube. In the case $N=2\times 2$, Table 3.1 shows the number of states at a specific energy and period, but also, the distance between two consecutive time steps $\{x^t, y^t\}$ and $\{x^{t+1}, y^{t+1}\}$, until a cycle is completed.

$$d_H\left[\{x^t, y^t\}, \{x^{t+1}, y^{t+1}\}\right] = \frac{1}{4N} \sum_k \left(|x_k^{t+1} - x_k^t| + |y_k^{t+1} - y_k^t|\right). \tag{3.2}$$

The evolution of the distance may change respect to the energy and initial configuration. For example, when the energy is E = -4, this exhibit 16 states which evolve at

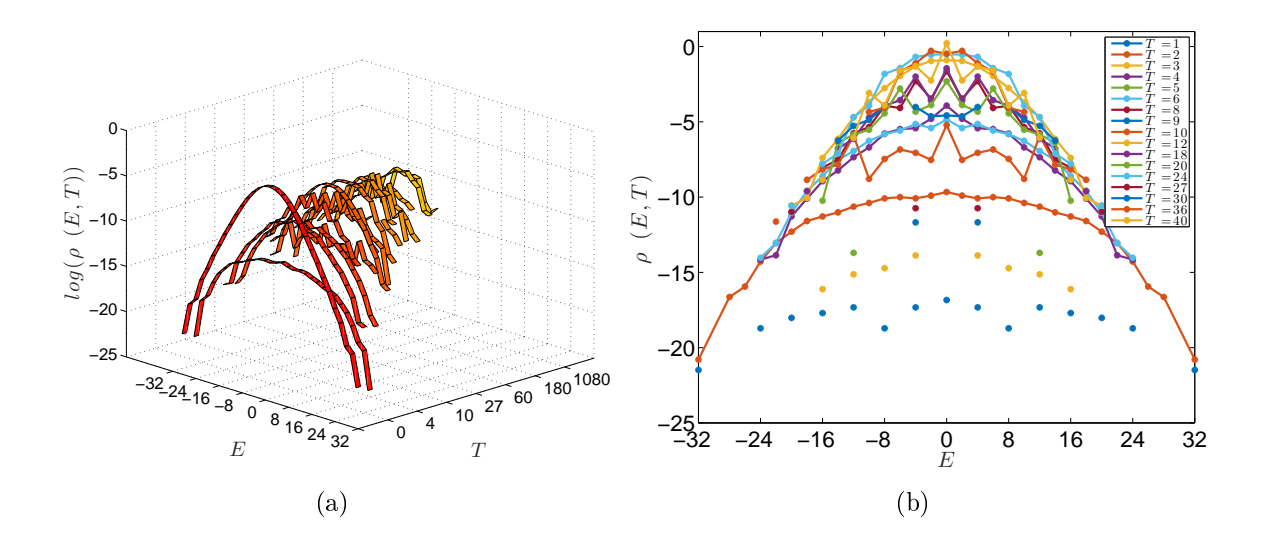


Figure 3.3: Figure (a) logarithm of the probability density function versus the energy E and Period T, here, the plot exhibits all the states for the case 4×4 . In Figure (b) shows some various periods $T = \{1, 2, 3, 4, 5, 6, 8, 10, 12\}$ versus the energy E.

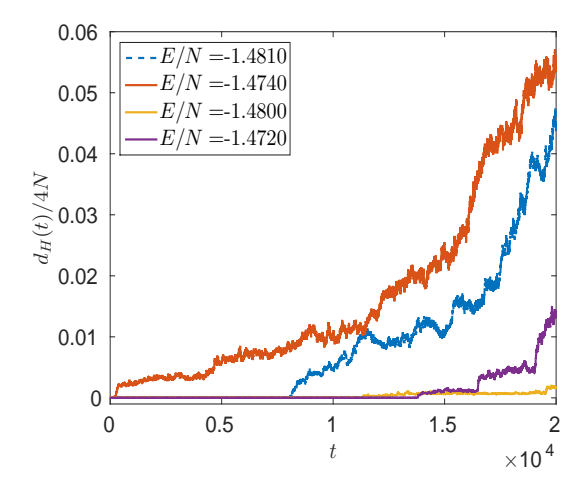


Figure 3.4: These plots manifest the sensibility to the initial condition for a system of size $N = 256 \times 256$. The Hamming distance between the two evolutions x_k^t and $x_k'^t$ in time few initial conditions at the same energy.

a fixed distance $d_H = 4$, similar to random walk like behaviour. However, there are 32 states where its distance changes at each time step, i.e., the states jumps from a state to another making sometimes large jumps and sometimes short jump. This behavior, similar to a Levy flight, indicates a possible anomaly diffusion [36, 37, 38, 39, 40, 41].

3.3.3 Configuration space for a system 256×256

It can be observed that the behavior of almost any initial state may be characterized in configuration space by means of an analogy with a random walk (or a variation of this process), more precisely when we compute the distance among two consecutive steps. Then, from the distance (3.2) is possible determine: if the jump step $d_H(t)$ has a fixed length, we shall say that this corresponds to the case of a random walk [42], thus the state diffuses in the phase space. However, if the step distance, $d_H(t)$ is different from one step to another, then, the behavior will be that of a Lévy flight [43].

We performed a large number of simulations for different energies, in a system of size 256×256 in order to check the behavior of the sampling of the quantity E/N, only for initial configurations of the form $\{x,y\}$ and $\{-x,-y\}$, such that their values are in the range $-2 \le E/N \le 0$.

In figure 3.5(a) one sees the evolution of $d_H(t)$ vs. time. One notices three distinct behaviors: a first region corresponds to the case $E \ll E_c$, here, the evolution of the distance $d_H(t)$ behaves as a random walk, that is, each step possesses almost a fixed length. Figure 3.5(c) quantifies this fact showing that for $E/N \leq -1.54$ the pdf of the distances is well centered around $\langle d_H(t) \rangle \approx 0.025 - 0.07$, in this case its evolution always is respect to the closer nodes in the hypercube. For larger energies $E/N \geq -1.26$ the pdf is peaked and centered at $\langle d_H(t) \rangle \approx 0.5$, for this energy the evolution fluctuates around a quite large mean distance, in this case the states move from a node up to an extremely faraway node in the 2N dimensional hypercube.

Finally, in the third case, that is whenever the energy is close of the critical energy $E \approx E_c(-1.54 \le E/N \le -1.26)$ the pdf of the distances is spread among a wider region $\langle d_H(t) \rangle \approx 0.2 - 0.3$, the motion of the states in the phase space looks similar to a Lévy flight, that is the system may jump from one place to another in the hypercube and the distance maybe either small or large (see figure 3.5(b)).

An important consequence is the amplification of the fluctuations of the distance $d_H(t)$ near $E \approx E_c$. Figure 3.5(c) shows a plot of the standard deviation of the fluctuations of $d_H(t)$ as a function of the energy for the system of size $N = 256 \times 256$. These fluctuations indicate a critical behavior around the critical energy $E_c = -\sqrt{2}$. This amplification of the fluctuations of $d_H(t)$ confirms the previous qualitative behavior in the three mentioned regions. Large fluctuations are consistent with a Lévy flight, however, small fluctuations suggest a random walk-like behavior.

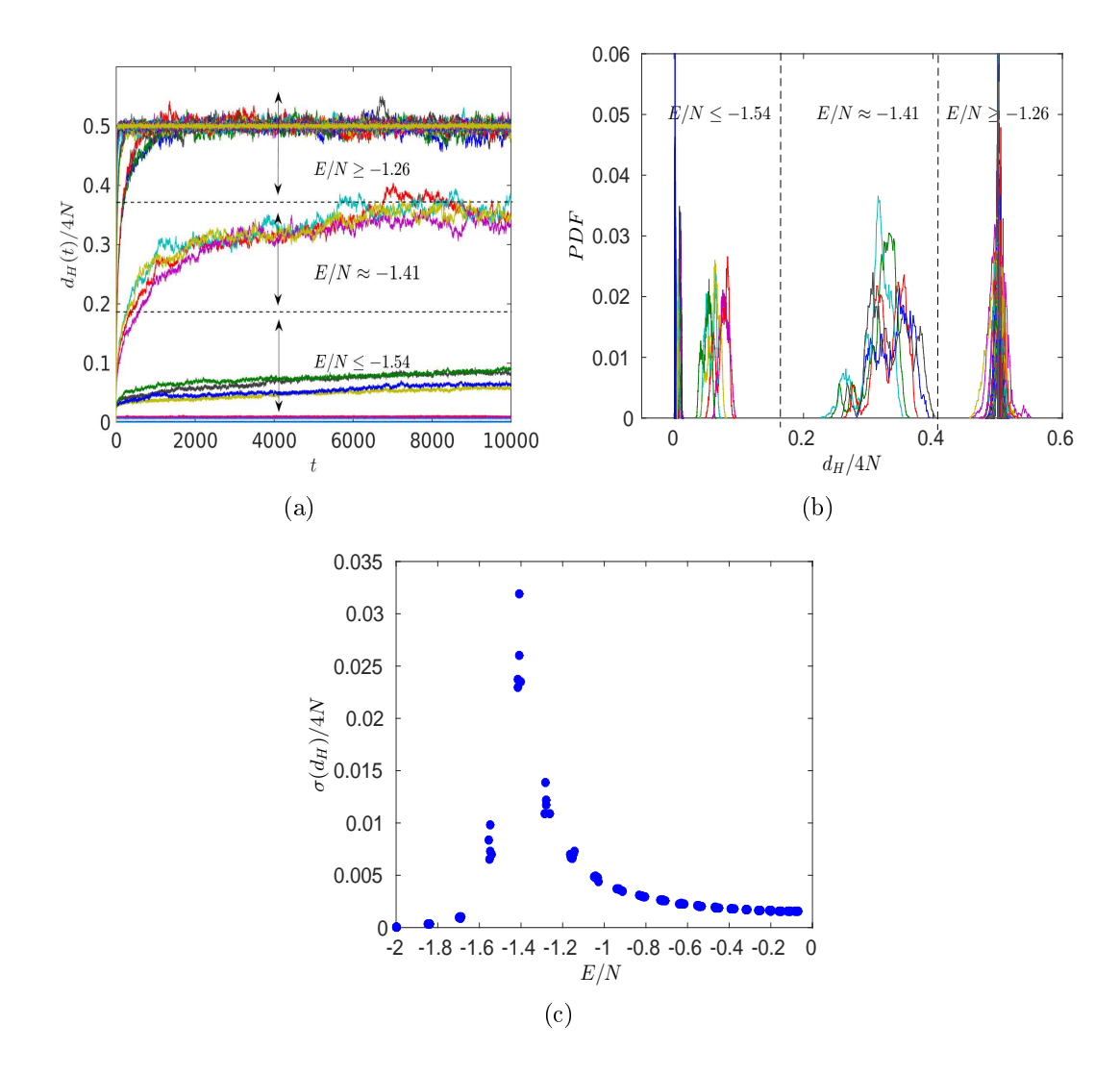


Figure 3.5: (a) Plot of the Hamming distance between two consecutive steps: $d_H(t)$ versus time, for a system of size $N=256\times256$. We can remark the fact that different values of energy, E/N, generate roughly three different regions. (b) The probability density function (PDF), for these three different regimes. (c) the standard deviation of the Hamming distance $\sigma(d_H(t))$ versus the energy.

Chapter 4

Coarse-Graining and Master Equation

4.1 General Scope

Though the Q2R model is quite simple its dynamics is usually very rich as it has been in previous chapter. Moreover, this conservative and reversible system appears to behave as a typical macroscopic system, as the number of degrees of freedom increases, showing, among others, a typical irreversible behavior, sensitivity to initial conditions, a kind of mixing, and it exhibits a phase transition. It is believed that this Q2R is a good representation of an Ising model in thermodynamical equilibrium.

As already said, for a given energy the constant energy set with $\Omega(E)$ states is partitioned in different sub-spaces composed by periodic orbits or fixed points. An arbitrary initial condition of energy E falls into one of these cycles, and it runs until it comes back to the initial configuration after a time T, which could be exponentially long and it displays a complex behavior. More important, the probability that an initial condition exhibits such a complex behavior is finite [44]. Moreover, Q2R manifests sensitivity to initial conditions, that is, if one starts with two distinct, but close, initial conditions, then, they will evolve into very different cycles as time evolves [9]. In some sense, an initial state explores vastly the phase space justifying the grounds of statistical physics.

In conclusion, the overall picture is: although for a finite size system the deterministic automata Q2R possesses periodic dynamics so it is not ergodic, there is a huge number of initial conditions that explore vastly the configuration space (this is particularly remarkable for initial conditions of random structure). Therefore, one expects that a master equation approach may be successful.

4.1.1 General formalism

Given a set of initial conditions with a fixed energy E, the probability distribution $\varrho_t^E(\{x,y\})$ evolves following a Perron-Frobenius like-equation

$$\varrho_{t+1}^E = \mathcal{L}^E \varrho_t^E \tag{4.1}$$

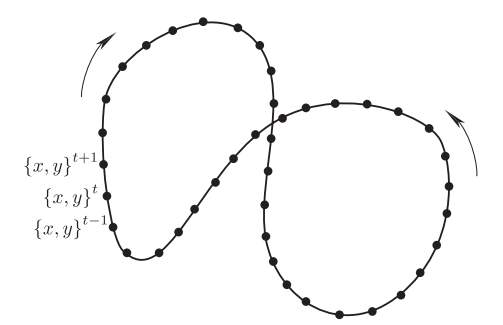


Figure 4.1: Cartoon of a cycle of period T, for which the cycle is composed of T states.

which, in principle, can be computed by using the microscopic evolution rule (2.3). Indeed \mathcal{L}^E is easy to build: if the state $\{x,y\}_i$ at time t evolves into $\{x,y\}_k$, at time t+1, then one sets the (i,k) components to 1, that is $\mathcal{L}^E_{ik} = 1$. Checking all available elements, $\Omega(E)$, for a given energy we can build the huge, $\Omega(E) \times \Omega(E)$, linear operator, \mathcal{L}^E . This matrix possesses a large number of blocks and zeroes revealing the existence of a large number of cycles in the Q2R model (In some sense, \mathcal{L}^E is a kind of adjacency matrix of a graph, the graph being the total number of existing cycles for a given energy).

However, this description is impractical because of the typical magnitude of $\Omega(E)$. Therefore, the full phase space is reduced to a description using gross or macroscopic variables, namely the total magnetization (2.11), instead of microscopic variables.

We proceed with a coarse-graining scheme as in Ref. [12]. Let's define a non invertible projection operator, Π , that maps the original distribution function ϱ_t^E into $\rho_t(M)$

$$\rho_t(M) = \Pi \cdot \varrho_t^E(\{x, y\}) = \sum_{\text{states with } (\sum_k x_k = M)} \varrho_t^E.$$

Formally, ϱ_t^E may be seen as a vector of dimension $\Omega(E)$, and ρ_t as a vector of dimension N+1, indexed by M, hence Π is formally a matrix with N+1 rows and $\Omega(E)$ columns.

Applying the projector operator on the Perron-Frobenius equation (4.1) one gets

$$\rho_t(M) = \Pi \cdot \varrho_t^E = \Pi \cdot \mathcal{L}^E \cdot \varrho_{t-1}^E = \Pi \cdot (\mathcal{L}^E)^t \cdot \varrho_0^E, \tag{4.2}$$

where $\varrho_0^E(\{x,y\})$ is an initial distribution.

As explained in detail in Ref. [12], in general, it is not possible to reduce the original Perron-Frobenius equation into a self-contained master equation.

Following, Nicolis *et al.* [12, 13] we take an initial reduced distribution, $\varrho_0^E(\{x,y\})$, as a combination of step functions in the aforementioned intervals:

$$\varrho_0^E(\{x,y\}) = \sum_M \alpha_M \varphi_M(\{x,y\}). \tag{4.3}$$

In equation (4.3) we have defined

$$\varphi_M(\{x,y\}) = \begin{cases} 1 & \text{if } \sum_k x_k = M \\ 0 & \text{if } \sum_k x_k \neq M \end{cases}.$$

The linear operator φ may be seen as a matrix with N+1 rows and $\Omega(E)$ columns (a state $\{x,y\}$ which belongs to a column vector of dimension $\Omega(E)$ and which maps onto a single magnetization which may take N+1 different values).

This is the central assumption of the coarse-graining approximation. States with the same magnetization are assumed to be uniformly distributed into the original phase space (see the Ansatz (4.3)).

The coefficients α_M may be obtained by inverting (4.3) [12]. The result is

$$\alpha_M = \sum_{\text{states}} \varrho_0^E(\{x,y\}) \varphi_M(\{x,y\}).$$

Therefore, α_M is precisely the M-th component for the coarse-grained distribution $\rho_0(M) = \Pi \rho_0^E$.

Thus, for this special type of initial distributions one has

$$\varrho_0^E(\{x,y\}) = \sum_M \rho_0(M) \varphi_M(\{x,y\}) = \varphi^{\dagger} \cdot \boldsymbol{\rho}_0.$$

Here, in the last equality, we have written explicitly ρ_0 as a N+1 dimensional vector and φ^{\dagger} as a $\Omega(E) \times (N+1)$ matrix. Therefore, the Perron-Frobenius equation (4.2) becomes

$$\boldsymbol{\rho}_t = \Pi \cdot (\mathcal{L}^E)^t \cdot \varphi^\dagger \cdot \boldsymbol{\rho}_0. \tag{4.4}$$

Notice that $\varphi^{\dagger} \cdot \Pi = I$ is the $\Omega(E) \times \Omega(E)$ identity matrix.

Therefore, defining the $(N+1) \times (N+1)$ matrix \mathcal{W} by

$$W = \Pi \cdot \mathcal{L}^E \cdot \varphi^{\dagger}. \tag{4.5}$$

one is able to write the final reduced Perron-Frobenius equation, which will be of the form

$$\boldsymbol{\rho}_{t+1} = \mathcal{W} \cdot \boldsymbol{\rho}_t. \tag{4.6}$$

The linear operator, W, acts only in the subspace of constant E, but is spanned over arbitrary values of magnetization, and at the same time the reduced density ρ is a vector with its components indexed by M.

As the original Perron-Frobenius equation, \mathcal{W} depends explicitly on the Q2R rule through \mathcal{L}^E therefore, in principle, is possible to compute it explicitly. However, in practice, because of the complex and unknown structure of \mathcal{L}^E (in particular because of the existence of a myriad of different periods for a given E) it is not a realistic task, because, the matrix \mathcal{W} could be quite large.

However, the matrix W can be further reduced following a second coarse-graining process. This partition is defined through a finite number of sets of non overlapping intervals: $I_1 = [-N, M_1), I_2 = [M_1, M_2), \dots I_{K-1} = [M_{K-2}, M_{K-1}), I_K = [M_{K-1}, N].$ (The previous case (4.6) corresponds to K = N + 1.)

We can proceed as previously, defining a second non-invertible projection operator, π , which maps the reduced distribution function ρ_t into a discrete and shorter column vector of dimension K: $\mathbf{f}_t = (f_1, f_2, \dots f_K)$. Finally, we obtain a coarse-grained master equation for the probability distribution [12, 13]:

$$\mathbf{f}_{t+1} = \hat{W} \cdot \mathbf{f}_t. \tag{4.7}$$

Here \hat{W} is named the transition probability matrix.

Important features of the master equation (4.7) are:

- 1. The probability vector \mathbf{f}_t should be positive and normalizable. Let $\mathbf{1} = (1, 1, \dots 1)$ be a K-dimensional vector, then we set $\mathbf{1} \cdot \mathbf{f}_t = 1$. More important, because of normalization, $\sum_{i=1}^K w_{ik} = 1$, one has $\hat{W}^{\dagger} \cdot \mathbf{1} = \mathbf{1}$. This implies that the probability is conserved under the evolution $\mathbf{1} \cdot \mathbf{f}_{t+1} = \mathbf{1} \cdot \hat{W} \mathbf{f}_t = \mathbf{1} \cdot \mathbf{f}_t = 1$.
- 2. The Perron-Frobenius equation could be solved exactly, provided is given an initial given distribution \mathbf{f}_0 : $\mathbf{f}_t = \hat{W}^t \mathbf{f}_0$.
- 3. Because of the Frobenius theorem, there exists an eigenvalue which is one, $\lambda_1 = 1$, while other eigenvalues fall inside the unitary circle $|\lambda_i| < 1$ for i > 1. Let \mathbf{f}_{eq} be the Eigenvector associated with the Eigenvalue $\lambda_1 = 1$; this is an invariant vector

$$oldsymbol{f}_{eq} = \hat{W} oldsymbol{f}_{eq}.$$

- 4. In what it follows, we denote by $\chi^{(i)}$ the eigenvectors of \hat{W} corresponding to λ_i . Naturally one has $\chi^{(1)} \equiv f_{eq}$.
- 5. The existence of an equilibrium state: $\lim_{t\to\infty} f_t = f_{eq}$.
- 6. Because all elements in the W-matrix are positive, any non negative initial distribution remains non negative.

4.1.2 Explicit calculation for the transition probability matrix \hat{W}

As already mentioned, to determine empirically the matrices W or \hat{W} we cannot use (4.5). Instead, we shall start with a magnetization sequence $\{\cdots, M_{t-1}, M_t, M_{t+1}, \cdots\}$ obtained from direct numerical simulations. This sequence is always finite but it could be exponentially long (so in practice infinite).

The transition probability matrix \hat{W} may be found from the probability density functions at time t and t+1. The elements of the matrix are given by the following conditional probabilities (Here we use a different notation than Ref. [12]):

$$w_{ik} = P(M_{t+1} \in I_i | M_t \in I_k) = \frac{P(M_{t+1} \in I_i \cap M_t \in I_k)}{P(M_t \in I_k)}.$$

Here M_t belongs to the interval I_k at time t, and M_{t+1} belongs to the interval I_i at t+1. Finally, the matrix \hat{W} does not, depend on time, which is a feature of a Markov process. The coarse-graining method is schematized in Fig. 4.2.

4.1.3 The Chapman-Kolmogorov condition and time reversal symmetry.

The final expression for the probability transition matrix (4.5) found after applying the formalism of Refs. [12, 13] follows directly from equation (4.4) and the Ansatz (4.3), which implies $\varphi^{\dagger} \cdot \Pi = I$. These relations are equivalent to the so-called compatibility condition:

$$\Pi \cdot (\mathcal{L}^E)^t \cdot \varphi^{\dagger} = \mathcal{W}^t.$$

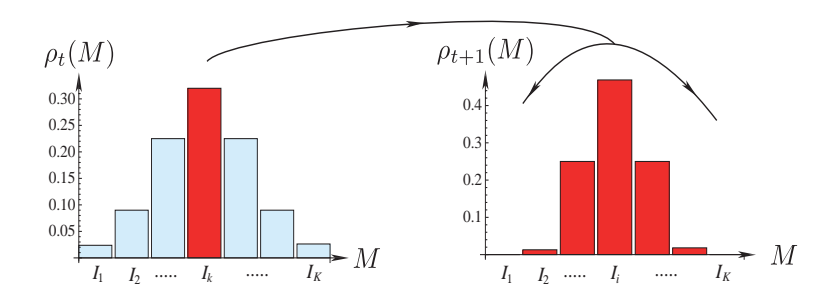


Figure 4.2: The distribution $\rho_t(M)$ at a time t is schematized in the distribution on the left. The fraction inside the interval I_k , is distributed, after the evolution into a new distribution $\rho_{t+1}(M)$ schematized in the diagram on the right. The normalized distribution provides the k-th element of the i-th column: w_{ik} .

This compatibility condition (or Chapman-Kolmogorov condition) arises as a result of the approximations done in Section 4.1.1, however it is not a general property of the dynamics. For instance, by taking a complete cycle (t = T), one readily gets

$$\Pi \cdot (\mathcal{L}^E)^T \cdot \varphi^{\dagger} = I,$$

(with I being the identity matrix) which, evidently, differs from \mathcal{W}^T , because \mathcal{W} represents an irreversible behavior toward equilibrium. Therefore, the compatibility condition is only valid as an approximation for a limited number of time steps which enters into a particular sequence. The same argument holds for the reduced matrix \hat{W} defined through (4.7).

Let us call $\hat{W}^{(\tau)}$ the resulting probability transfer matrix after τ steps, that is, by computing \hat{W} as a consequence of the evolution from t up to $t + \tau$, then, the Chapman-Kolmogorov or compatibility condition for \hat{W} reads

$$\hat{W}^{(\tau)} = \hat{W}^{(\tau_1)} \cdot \hat{W}^{(\tau_2)}, \tag{4.8}$$

where $\tau = \tau_1 + \tau_2$. In particular, for $\tau_1 = \tau_2 = 1$ one should satisfy

$$\hat{W}^{(2)} = \hat{W} \cdot \hat{W} = \hat{W}^2.$$

4.2. SPECIFIC COMPUTATION OF THE TRANSITION PROBABILITY MATRIX IN VARIOUS SITU

Other compatibility conditions are

$$\begin{array}{lll} \hat{W}^{(3)} & = & \hat{W}^{(2)} \cdot \hat{W}, \\ \hat{W}^{(3)} & = & \hat{W} \cdot \hat{W}^{(2)}, \\ \hat{W}^{(4)} & = & \hat{W}^{(2)} \cdot \hat{W}^{(2)}, \\ \hat{W}^{(4)} & = & \hat{W} \cdot \hat{W}^{(2)} \cdot \hat{W}, & \text{etc.} \end{array}$$

$$\hat{W}^{(3)} = \hat{W}^{(2)} \cdot \hat{W},
\hat{W}^{(4)} = \hat{W} \cdot \hat{W}^{(2)} \cdot \hat{W}. \text{ etc.}$$

In section 4.2.3 we shall check in practice how good are these Chapman-Kolmogorov conditions satisfied.

Finally, let us state an important result due to Pomeau [45]. The K-time correlation functions impose some restrictions on the W-matrix.

Because of time reversal symmetry, for all indices $i_1, i_2, \dots i_K = \{1, 2, \dots K\}$, the symmetry relation

$$w_{i_1 i_2} w_{i_2 i_3} \cdots w_{i_{K-1} i_K} w_{i_K i_1} = w_{i_1 i_K} w_{i_K i_{K-1}} \cdots w_{i_3 i_2} w_{i_2 i_1}$$

$$\tag{4.9}$$

must be satisfied.

In what it follows, we apply this coarse graining approach to compute the probability transfer matrix for some particular cases.

4.2 Specific computation of the transition probability matrix in various situations.

In this section we shall apply the coarse graining approach to the Q2R dynamics in the case of a small lattice size. In Ref. [19] we have fairly explored the computation of the transition probability matrix, in particular, in the case of extended systems $(N=256\times256)$. However, in this case the cycles are usually huge, therefore this general approach is not really satisfactory. In this sense, we focus our effort in treating systems of moderate sizes, namely $N=4\times4$, $N=8\times8$, and $N=16\times16$, having all of them tractable cycles.

4.2.1 Robustness of the methodology.

In general for a system of small size, one is able to find some cycles for a given energy. Building a time series for the magnetization $\{M(t)\} = \{M_1, M_2, \dots M_T\}$, then one defines

a partition on the possible values of the magnetization, as explained in a previous Sec. 4.1. In the cases considered here, it is always possible to use the finest possible partition, that is, for the exact available values of the magnetization (something impractical in large systems). In this case the partitions are composed by a set of N+1 (N is assumed to be even) well defined values $M = \{-N, -N+2, -N+4, \cdots, N-2, N\}$. That is for 4×4 the partition has a maximum of 17 elements, for $N = 8 \times 8$ there are 65 elements, and for $N = 16 \times 16$ the partition possesses a maximum of 257 elements.

A first result concerns the equivalence of the probability density function of magnetization obtained via the time series of the magnetization and the equilibrium distribution resulting from the eigenvectors of the transition probability matrix \hat{W} . Hence, the results arising from temporal averages and transition probability matrix into the configuration space are consistent among themselves. This fact ensures a first validation of the method. However, the transition probability matrix provides extra information on a system, among them, the non-equilibrium properties, given by the spectrum of \hat{W} .

Next, we shall describe the methodology for the case of a lattice of size 16×16 for an orbit with E = -292 and period T = 43115258.

The transition probability matrix \hat{W} is constructed following the steps of the previous section 4.1.2. But first, we shall verify that the master equation does not strongly depend on the length of the time series for the magnetization. It is important to remark that we think that this is a crucial step, because it allows us to compare explicitly the dependence of the results on the partial length of the cycles, something which is not possible for larger systems, because in these cases we shall never be able to build the complete period for the time series.

To test the above, we shall use again the finest partition. In this case, the transition matrix is of dimension 257×257 (so we shall not provide them explicitly) and we shall characterize it by its equilibrium distribution, and the full set of eigenvalues of \hat{W} . Fig. 4.3 (a) plots the equilibrium distributions f_{eq} for the total cycle T and f^{T^*} for the partial cycle of length T^* . Similarly, Fig. 4.3 (b) plots the set of 257 eigenvalues, denoted by $\lambda_i^{T^*}$, for the same sequence, $\{M(t)\}$, but for four different lengths of the time series.

Visually it cannot be observed any substantial difference among the different values of T^* . Moreover, Table 4.1 compares quantitatively the mean square difference measuring $Q_1 = ||\mathbf{f}^{T^*} - \mathbf{f}_{eq}||^2/K$ and $Q_2 = \sum_{i=1}^K |\lambda_i - \lambda_i^{T^*}|^2/K$. Here K is the number of partitions. Notice that an important feature of the transition probability matrix is that its eigenvalues are real if the time series satisfies reversibility [45]. We have verified that the coarse-graining approach applied to the full cycle with period T shows this important feature. Namely, the eigenvalues of the \hat{W} matrix are real numbers. However, as we apply

4.2. SPECIFIC COMPUTATION OF THE TRANSITION PROBABILITY MATRIX IN VARIOUS SITU

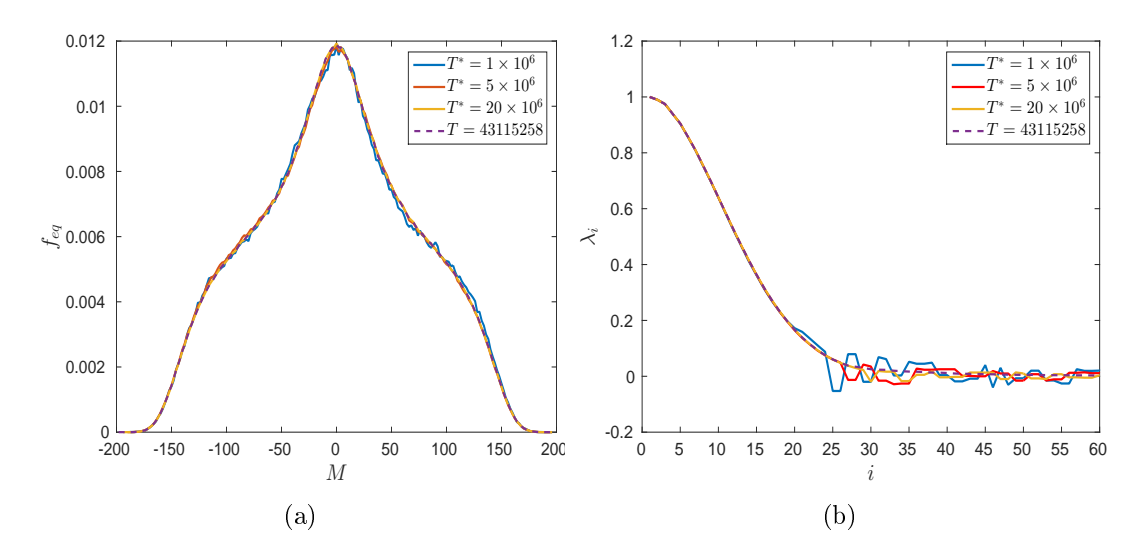


Figure 4.3: (a) Plot of the equilibrium distribution \mathbf{f}_{eq} for the case of a 16×16 system size with E = -292 ($E/N \approx 1.14$) and a cycle of period T = 43115258 (the complete cycle). The computation of \mathbf{f}_{eq} is compared with shorter sequences of the same time series of length $T^* = 10^6$, 5×10^6 , & 20×10^6 . (b) The set of 257 eigenvalues of the \hat{W} -matrix for the same conditions of (b).

T*	Q_1	Q_2
10^{6}	3.95×10^{-5}	0.0038
5×10^{6}	3.91×10^{-5}	0.0020
20×10^{6}	3.84×10^{-5}	0.0002

Table 4.1: Error estimation of the equilibrium distribution and the spectral decomposition of the \hat{W} matrix for different lengths of the time series.

the same approach to a partial sequence of the same cycle of length less than T, some eigenvalues become complex (typically located near the origin in the complex plane). This is important, because in practice for larger size systems, one never closes a cycle, hence only incomplete sequences are available, thus the matrix would not have, in general, pure real eigenvalues. However, we emphasize that the existence of these complex eigenvalues is spurious.

Finally, it is important to compare results for partitions of different size. First, we compute the equilibrium distribution for three different partitions sets. More precisely, for a 8×8 system evolving by Q2R at E=0 in a periodic orbit of T=672018.

Figure 4.4 (a) compares the three different coarse-graining partitions (containing 5, 11

and 34 elements). Despite the evident differences among the coarse and the finer graining partitions, one notices that both partitions exhibit the same accurate behavior of the equilibrium distribution. Moreover, Figure 4.4 (b) compares the second eigenmode $\chi^{(2)}$ without any substantial difference among the partitions.

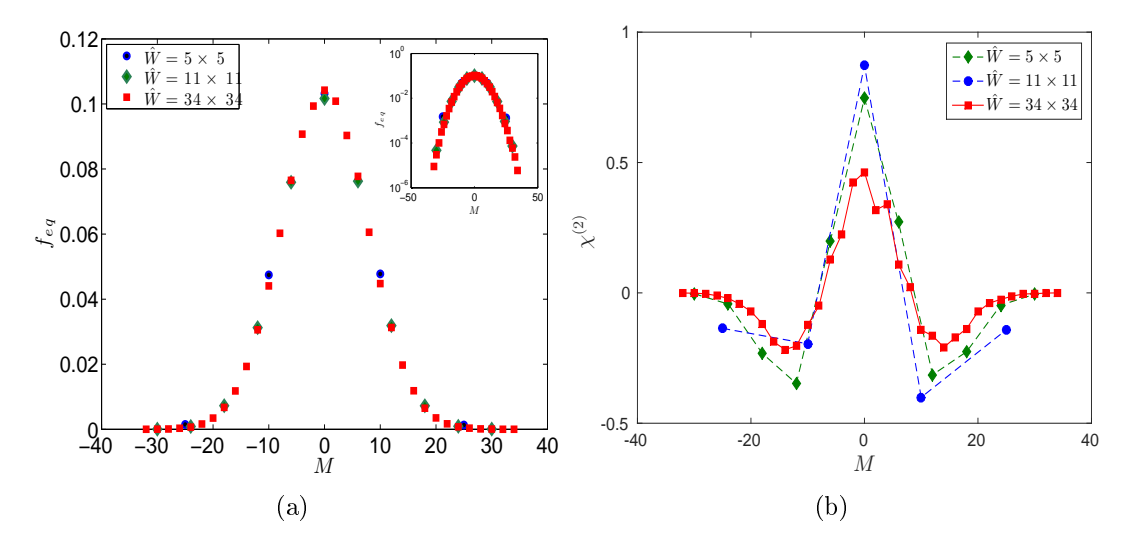


Figure 4.4: (a) Plot of the equilibrium distribution f_{eq} vs M for a 8 × 8 system size with E=0 and a cycle of a period T=672018 for three different partitions of the magnetization values. The plot shows how all distribution functions lies under the same curve. The inset shows the parabolic behavior in magnetization which after a fit reads $\log f_{eq} = -M^2/116$. (b) Plot of the second eigenmode $\chi^{(2)}$ corresponding to the eigenvalue closest to the unit circle. One notices how all partitions produce similar results.

In what follows, we summarize the methodology for cases of size 4×4 , 8×8 and 16×16 . In all cases, the full cycles were considered, and we provide the finest possible partition.

4.2.2 Exact calculation for various lattices.

We have studied in detail the case of a 4×4 periodic lattice, because the phase space possesses $2^{32} \approx 4 \times 10^9$ distinct configurations and the calculations can be completely performed thus showing explicitly the method. It is shown that the coarse graining approach is fully applicable in the 4×4 lattice case. We used different partitions getting a well defined probability transfer matrix \hat{W} .

We shall explore few cycles for larger systems (8 \times 8 and 16 \times 16). The cycles in these cases may be as long as desired for any practical purpose, so that the equilibrium

distribution is calculated with enough precision.

In the case of 8×8 , for various energies and the finest possible coarse graining, as a sake of brevity, we omit explicitly the plots of the first eigenvector, \mathbf{f}_{eq} , as well as the eigenvalues, because they are similar to the 16×16 lattice case.

The case of a 16×16 system size displays the most accurate equilibrium distribution found in the current research. The fluctuations around the distribution are small, and the eigenvalues seems to form a continuous spectrum (the difference among two consecutive eigenvalues is small). We have also explored a wide range of energies. The rank of the matrices (that is for the finest partition) are K = 122 for E = -332; K = 205 for E = -316; K = 197 for E = -292; K = 129 for E = -168; and K = 101 for E = -92.

The equilibrium distribution, as a function of the magnetization, is plotted in Fig. 4.5 (a). Similarly, the spectral decomposition is shown in Fig. 4.5 (b).

In Fig. 4.5 (a) one notices how in the case of larger energies, say E = -92 and E = -168, the equilibrium distribution function is symmetric, under the change $M \to -M$, however as the energy decreases one sees that for the lowest energy, E = -332, it appears a spontaneous symmetry breaking, so that the equilibrium distribution is not anymore an even function. The equilibrium probability may manifest a positive or negative magnetization (switching from one case to the other by changing the initial condition via the transformation $\{x,y\}^{t=0} \to \{-x,-y\}^{t=0}$). Moreover, the energy E = -316 case shows an equilibrium probability density function that manifests bi-stability. Indeed, these bi-modal distributions possess three peaks, one at M = 0 and the two other at $M = \pm M_0 \neq 0$. Finally, the width of the probability density functions increases near the transition energy.

Fig. 4.5 (b) shows the spectral distribution of the probability transfer matrix that defines the master equation. Already for a lattice of size 16×16 one observes how the spectral distribution is almost continuous. One notices that the energies E = -316 and E = -292 possess the largest eigenvalues for a given index i. This means that, probably, the largest eigenvalues occurs near the critical energy.

It is interesting to remark that the non-equilibrium is governed by those eigenvalues close to one. The non-equilibrium features behave as slow modes. In the current, case one has $\mathbf{f}_t = \sum_{i=1}^K \alpha_i \lambda_i^t \mathbf{\chi}^{(i)}$. Defining $\sigma_i = -\log \lambda_i$, one obtains the usual slow mode relaxation. Moreover, the global behavior of the eigenvalues closest to the unity, represents the transport coefficients [19]. Fig. 4.5 (b) indicates that $\lambda_i \approx 1-\gamma i$, something suggesting that the non-equilibrium features are governed by a Fokker-Planck kind of equations. The behavior of the eigenvector agrees also qualitatively with this picture (see [19] for more details).

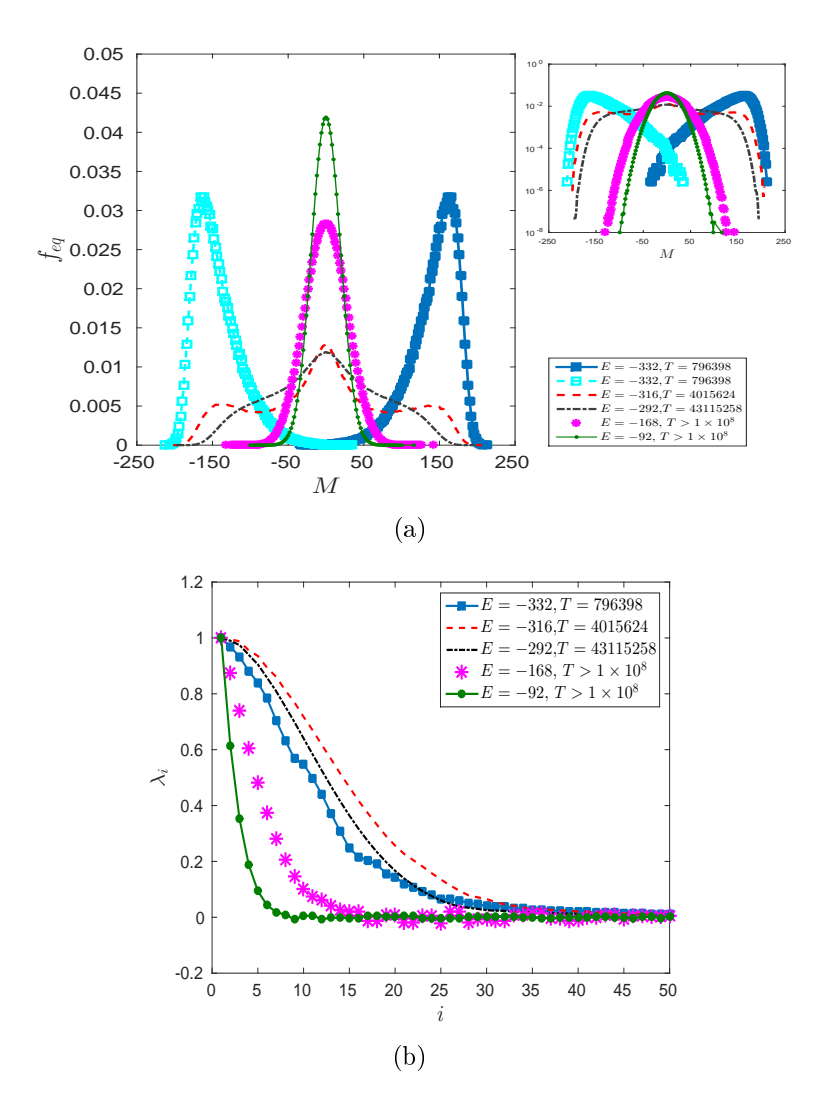


Figure 4.5: (a) Equilibrium distributions, \mathbf{f}_{eq} , for the case of a 16 × 16 system size, and for the energies and periods: E = -332 and T = 796398, E = -316 and T = 4015624, E = -292 and T = 43115258. We also consider E = -168 and E = -92 with periods larger than $T > 10^8$. (b) Eigenvalues of the W-matrix showing the existence of long-wave relaxation properties.

4.2.3 The Chapman-Kolmogorov conditions.

We have checked the Chapman-Kolmogorov relations for the case of Q2R in a 16×16 lattice for the case of E = -292 and a periodic orbit of T = 43115258. We have built five different probability transfer matrices $\hat{W}^{(\tau=1)}, \dots, \hat{W}^{(\tau=5)}$ (See Sec. 4.1.3 for the definition of $\hat{W}^{(\tau)}$).

4.2. SPECIFIC COMPUTATION OF THE TRANSITION PROBABILITY MATRIX IN VARIOUS SITU

First, we compared the matrices $\hat{W}^{(\tau=2)}$ and $\hat{W}^{(\tau=1)} \cdot \hat{W}^{(\tau=1)}$, both of rank 197 × 197, computing the distance among them, e.g., $\hat{W}^{(\tau=2)}$ and $\hat{W}^{(\tau=1)} \cdot \hat{W}^{(\tau=1)}$, via the usual distance (the square indicates the product of a matrix by itself)

$$d = \frac{1}{K^2} \text{Tr}[(\hat{W}^{(\tau=2)} - \hat{W}^{(\tau=1)} \cdot \hat{W}^{(\tau=1)})^2].$$

In the current case, the matrices are similar up to $d = 5.81 \times 10^{-6}$. More quantitatively, we look how good are the eigenvectors of different matrices, namely $\hat{W}^{(\tau=2)}$ and $\hat{W}^{(\tau=1)} \cdot \hat{W}^{(\tau=1)}$. To do that, we computed the ratio among the *n*-th eigenvectors of the aforementioned matrices, that is,

$$q_n = \frac{\chi^{(2)}_n}{\chi^{(1)}_n},$$

where $\chi^{(2)}_{n}$ and $\chi^{(1)}_{n}$ are the *n*-th eigenvector of the matrices $\hat{W}^{(\tau=2)}$ and $\hat{W}^{(\tau=1)}$. This quantity is plotted in Fig. 4.6. One notices that $q_n \approx 1$ almost for all values of magnetization, but it also has an anomalous behavior near the nodal points of the eigenvector $\chi^{(1)}_{n}$. In general the agreement of all this eigenvectors is satisfactory.

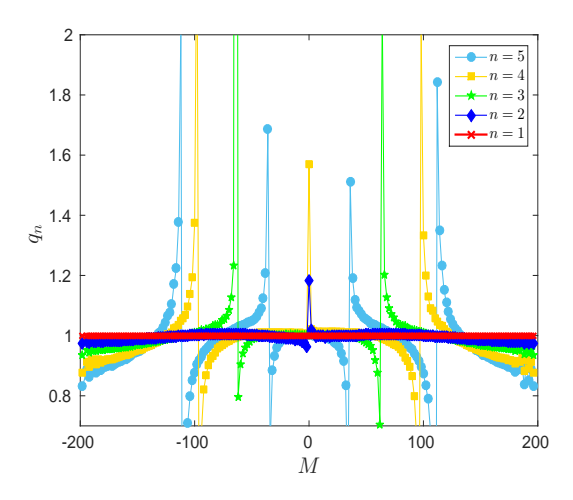


Figure 4.6: Plot of the ratio q_n for five eigenmodes for the case of a 16×16 system.

Next we check, the Chapman-Kolmogorov relations written in Sec. 4.1.3, comparing the spectral properties of both matrices, namely the set of eigenvectors and its eigenvalues.

As it can be seen in Fig. 4.7 (a) the equilibrium distribution f_{eq} matches perfectly for different values of $\tau = \{1, 2, 3, 4, 5\}$. This proves that the equilibrium configuration, f_{eq} , is an invariant of the dynamical system. However, non-equilibrium properties do depend on the sampling time, τ . Indeed, the eigenvalues corresponding to different probability transfer matrices do depend on the choice of the parameter τ . This is not a surprise, because it is expected that the eigenvalues, $\lambda_i^{(\tau)}$, of $\hat{W}^{(\tau)}$ should scale as $\lambda_i^{(\tau)} = \lambda_i^{\tau}$, where

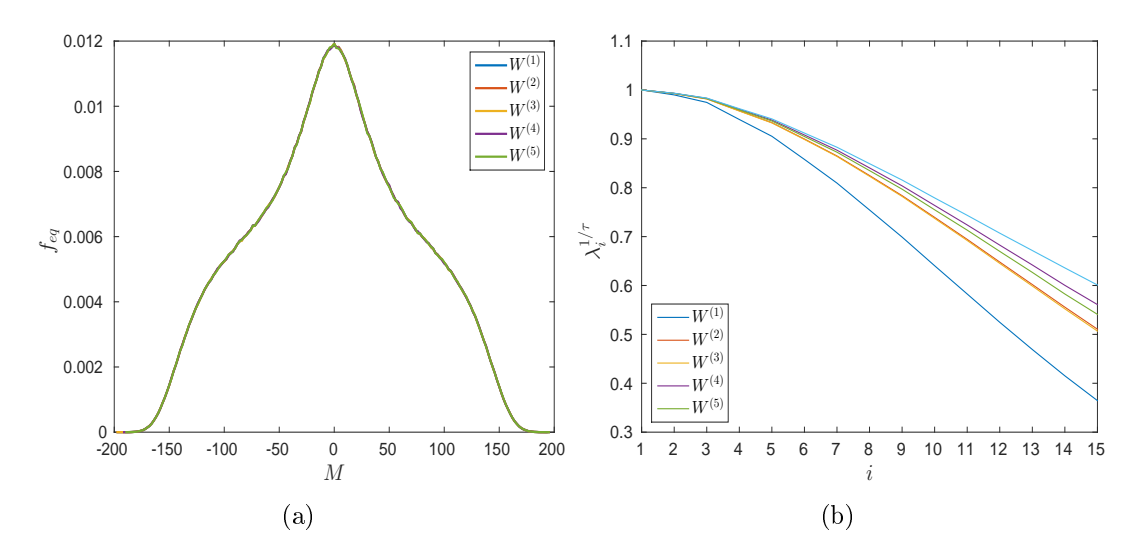


Figure 4.7: (a) Equilibrium distributions, f_{eq} , for the case of a 16×16 system, and for the energy E = -292 and T = 43115258. (b) Eigenvalues of the W-matrix showing the existence of long-wave relaxation properties.

 λ_i are the set of eigenvalues of $\hat{W}^{(\tau=1)}$. This scaling is shown in Fig. 4.7 (b) indicating an anomaly because it does not work for the case $\tau=1$, but the scaling works well for higher τ . This deserves more careful study.

4.3 Slow modes and transport coefficients

The approach to equilibrium follows from the already discussed solution $\mathbf{f}_t = \hat{W}^t \mathbf{f}_0$, which maybe expanded in terms of the eigenvectors of the \hat{W} -matrix, getting $\mathbf{f}_t = \sum_{i=1}^K \alpha_i \lambda_i^t \chi_i$. Therefore, the Eigenvalues near the unity behaves as slow modes. If one defines $\sigma_i = -\log \lambda_i$ one obtain the usual slow mode relaxation:

$$\mathbf{f}_t = \sum_{i=1}^K \alpha_i e^{-\sigma_i t} \mathbf{\chi}_i. \tag{4.10}$$

Moreover, the eigenvalues closest to the unity, represents the transport coefficients, which we shall investigate in the following.

We have consider the cases of a 16×16 system size and a wide range of energies. The rank of the matrices (that is for the finest partition) are K=122 for E=-332; K=197 for E=-292 and K=101 for E=-92. We have showed in Figure 4.3(b) the eigenvalues $|\lambda_i|$, ordered by decreasing absolute value, as a function of its order. As a first sight we have the impression that $\lambda_i \approx 1-\beta i^2$ (for i<15) characteristic of a diffusive mode, however for larger value of i one sees $\lambda_i \approx 1-\gamma i$.

The Eigenmodes corresponding to i = 2, to 4 are also plotted in Figure 4.8, showing the usual behavior of a confined Eigenvalue problem, which does not seem to agree with the diffusive mode.

A possible explanation of the behavior of the eigenvalues, $\lambda_i \approx 1 - \gamma i$, is in agreement with a continuous limit approximation of the Master equation (4.7) leading a Fokker-Planck-type equation:

$$\lim_{\Delta M \to 0} (\mathbf{f}_{t+1} - \mathbf{f}_t) = (\hat{W} - \hat{1}) \mathbf{f}_t \quad \to \quad \frac{\partial \mathcal{P}}{\partial t} = \frac{\partial}{\partial M} \left(\beta \frac{\partial \mathcal{P}}{\partial M} + \gamma M \mathcal{P} \right). \tag{4.11}$$

The slow mode dynamics is provided by the Eigenvalue problem:

$$-\sigma\varphi = \frac{\partial}{\partial M} \left(\beta\varphi' + \gamma M\varphi\right). \tag{4.12}$$

which has a solution

$$\sigma_i = \gamma i$$
 and $\varphi_i = H_i \left(M \sqrt{\frac{\gamma}{2\beta}} \right) e^{-\frac{\gamma M^2}{2\beta}},$

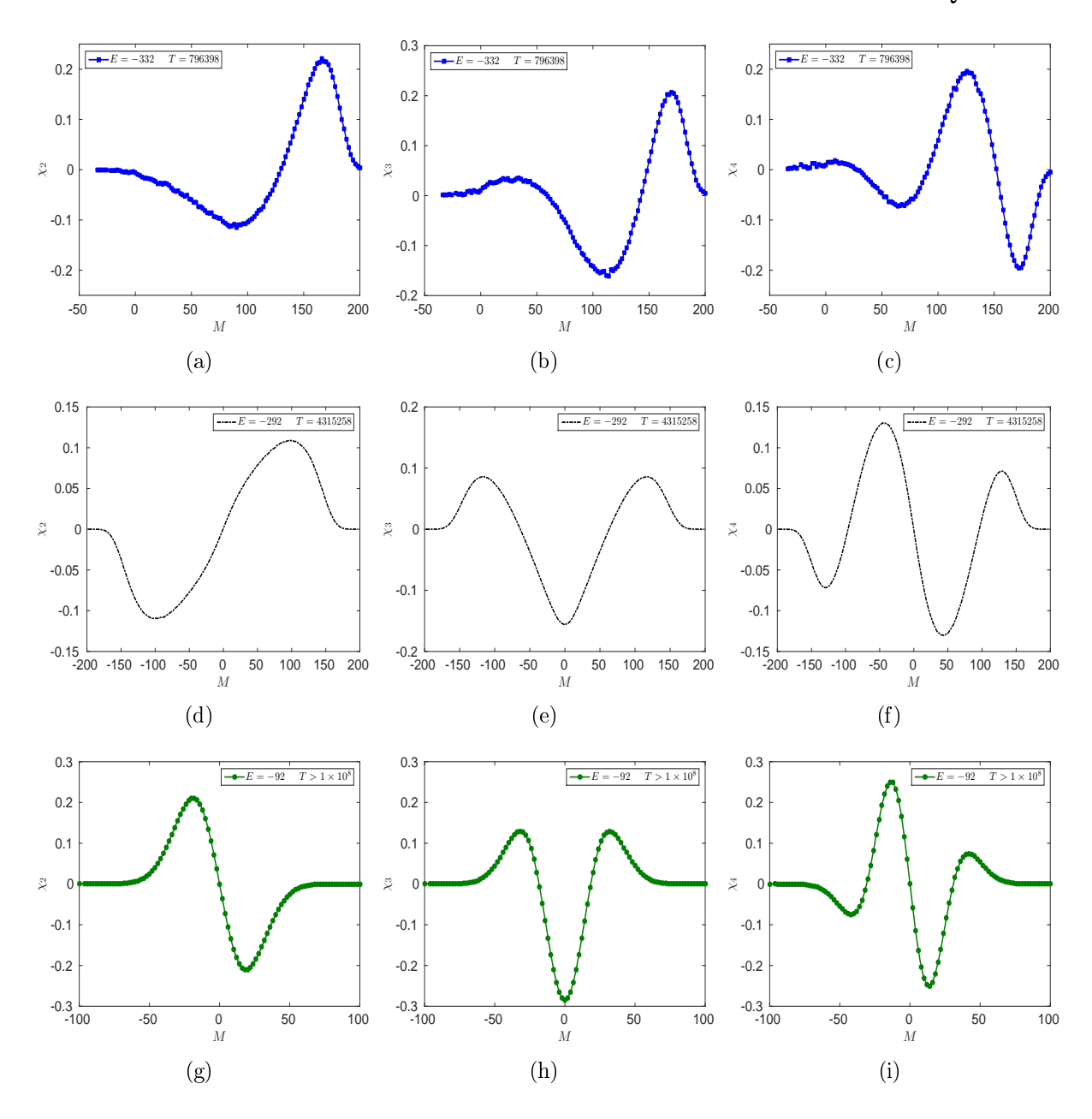


Figure 4.8: Slow modes of the case 16×16 . Here we have presented χ_2 , χ_3 and χ_4 Eigenmodes of the \hat{W} matrices, for the energies E=-332, E=-292 and E=-92 respectively.

where $H_i(x)$ is the Hermite polinomial of degree i which is a nonnegative integer: i = 0, 1, 2... Though, the behavior of the Eigenvalues is not the good one for i < 15, the behavior of the Eigenmodes seems to be the adequate.

4.4. APPENDIX 59

4.3.1 Pomeau's reversal symmetry relation.

According to Pomeau [45], the microscopic time reversal symmetry imposes the symmetry relation (4.9). For a rank K transition probability matrices, it is possible to verify that there are K^K different required conditions (4.9). Therefore, to check this condition is only possible for a moderate ranks K. For the case 4×4 all probability transfer matrices of the Supplementary Information satisfy the Pomeau's reversal symmetry relation.

For larger \hat{W} matrices, say K > 9, we have not checked Pomeau's relation because it involves a cumbersome numerical calculation.

4.4 Appendix

4.4.1 Exact calculation for the 4×4 lattice.

Consider the case of a 4×4 periodic lattice. Though the Q2R dynamics is extremely simple, the calculations are exactly realizable up to end and for all configurations, thus it may explicitly explain the method. The phase space possesses 2^{32} distinct configurations which may be computed directly. The energy takes possible values ranging from $-32 \le E \le 32$. We have characterized few special cases with energies and periods distributed uniformly over the all possible values:

$$(E,T) = (-24,6)(-22,10)(-18,54)(-8,270), (-2,1080)$$
and $(0,120)$

. In all cases below we shall take the finest partitions in which a magnetization belongs into a well defined value from $M = -16, \dots M = 16$. Usually the interval is less than 17 and currently the rank of the matrices ranges from K = 2 up to K = 9.

The eigenvalues and the invariant probability distributions (the corresponding Eigenvectors associated to the unique unitary Eigenvalue) of these matrices are:

$x_{t=0}$	$\left(\begin{array}{cccc} 1 & 1 & 1 & 1 \\ 1 & 1 & 1 & 1 \\ 1 & 1 &$	$ \left(\begin{array}{ccccc} 1 & 1 & 1 & 1 \\ 1 & 1 & 1 & 1 \\ 1 & 1 & 1 & 1 \\ 1 & -1 & 1 & -1 \end{array}\right) $	$ \begin{pmatrix} 1 & 1 & 1 & 1 \\ 1 & 1 & 1 & 1 \\ 1 & 1 & 1 & 1 \\ 1 & -1 & -1 & -1 \end{pmatrix} $	$ \begin{pmatrix} 1 & 1 & 1 & 1 \\ 1 & 1 & 1 & 1 \\ 1 & 1 & 1 & -1 \\ -1 & -1 & -1 & -1 \end{pmatrix} $	$ \left(\begin{array}{ccccc} 1 & 1 & 1 & 1 \\ 1 & 1 & 1 & 1 \\ 1 & 1 & 1 & -1 \\ -1 & 1 & -1 & -1 \end{array}\right) $
$y_{t=0}$	$ \left(\begin{array}{ccccc} 1 & 1 & 1 & 1 \\ 1 & 1 & 1 & 1 \\ 1 & 1 & 1 & 1 \\ 1 & -1 & 1 & -1 \end{array}\right) $	$ \left(\begin{array}{ccccc} 1 & 1 & 1 & 1 \\ 1 & 1 & -1 & 1 \\ 1 & 1 & 1 & -1 \\ 1 & 1 & -1 & 1 \end{array}\right) $	$ \begin{pmatrix} 1 & 1 & 1 & 1 \\ 1 & 1 & -1 & 1 \\ -1 & 1 & 1 & -1 \\ 1 & 1 & -1 & -1 \end{pmatrix} $	$ \begin{pmatrix} 1 & 1 & 1 & 1 \\ 1 & -1 & -1 & -1 \\ 1 & 1 & -1 & -1 \\ 1 & 1 & -1 & -1 \end{pmatrix} $	$ \left(\begin{array}{ccccc} 1 & 1 & 1 & 1 \\ 1 & -1 & -1 & -1 \\ 1 & -1 & -1 & -1 \\ 1 & 1 & -1 & -1 \end{array}\right) $
E	-24	-18	-8 0.5	-2	0
E/N T	-1.5	-1.125 54	-0.5 270	-0.125 1080	0 120
I(M)	[12, 16]	[8, 12]	[2, 10]	[2,6]	[-8, 8]
K	2	3	5	5	4
Ŵ	$\left(\begin{array}{cc} \frac{1}{2} & 1 \\ \frac{1}{2} & 0 \end{array}\right)$	$ \left(\begin{array}{ccc} 0 & \frac{1}{6} & 0 \\ 1 & \frac{1}{2} & 1 \\ 0 & \frac{1}{3} & 0 \end{array}\right) $	$ \begin{pmatrix} 0 & \frac{1}{14} & \frac{1}{17} & 0 & 0 \\ \frac{1}{2} & \frac{15}{14} & \frac{1}{17} & \frac{3}{10} & 0 \\ \frac{1}{2} & \frac{15}{14} & \frac{17}{17} & \frac{3}{10} & 1 \\ 0 & \frac{1}{14} & \frac{17}{17} & \frac{2}{5} & 0 \\ 0 & 0 & \frac{27}{17} & 0 & 0 \end{pmatrix} $	$ \begin{pmatrix} 0 & \frac{1}{26} & \frac{1}{24} & \frac{1}{14} & 0\\ \frac{1}{4} & \frac{26}{26} & \frac{7}{24} & \frac{9}{28} & \frac{1}{2}\\ \frac{1}{4} & \frac{1}{26} & \frac{1}{4} & \frac{2}{27} & \frac{1}{4}\\ \frac{1}{2} & \frac{26}{26} & \frac{1}{3} & \frac{1}{4} & \frac{1}{4}\\ 0 & \frac{2}{13} & \frac{1}{12} & \frac{1}{14} & 0 \end{pmatrix} $	$ \begin{pmatrix} 0 & \frac{1}{20} & \frac{1}{14} & 0 \\ \frac{1}{3} & \frac{3}{3} & \frac{9}{28} & \frac{4}{9} \\ \frac{2}{3} & \frac{19}{20} & \frac{3}{7} & \frac{9}{9} \\ 0 & \frac{1}{5} & \frac{5}{28} & 0 \end{pmatrix} $
$oldsymbol{f}_{eq}$	$\left(\begin{array}{c} 2/3\\1/3\end{array}\right)$	$\left(\begin{array}{c} 1/9\\2/3\\2/9\end{array}\right)$	$\begin{pmatrix} 2/45 \\ 14/45 \\ 17/45 \\ 2/9 \\ 2/45 \end{pmatrix}$	$\begin{pmatrix} 2/45\\ 13/45\\ 4/15\\ 14/45\\ 4/45 \end{pmatrix}$	$\begin{pmatrix} 1/20 \\ 1/3 \\ 7/15 \\ 3/20 \end{pmatrix}$
λ	$\left\{\begin{array}{c}1\\-1/2\end{array}\right\}$	$\left\{\begin{array}{c}1\\-1/2\\0\end{array}\right\}$	$\left\{\begin{array}{c} 1\\ 0.314\\ -0.282\\ 0.183\\ -0.104 \end{array}\right\}$	$ \left\{ \begin{array}{c} 1\\ -0.225\\ -0.137\\0.073\\ -0.019 \end{array}\right\} $	$\left\{ \begin{array}{c} 1\\ -1/4\\ -0.0607\\ 0.0392 \end{array} \right\}$
Reversible	Yes	Yes	Yes	Yes	Yes

Table 4.2: Summary of the coarse-graining procedure for Q2R in a 4×4 system and for a given energy E and period T.

4.4. APPENDIX 61

We notice that the case E=0 is showed up in the finest partition. Actually, in the finest partition this case the probability transfer matrix has a rank K=9. But it has three zero eigenvalues and two complex one. We interpret that the fine coarse graining is not a good partition. This partition must no be an invariant measure as required in Ref.[13]. Why does this happen in the present case?, and it does not happen in other needs to be elucidated.

4.4.2 The Chapmann-Kolmogorov condition

$$W^{(1)} = \begin{pmatrix} \frac{1002561}{1237039} & \frac{234478}{1237039} & 0 & 0 & 0\\ \frac{234478}{5406141} & \frac{362248}{415857} & \frac{462439}{5406141} & 0 & 0\\ 0 & \frac{462439}{8877658} & \frac{7981253}{8877658} & \frac{216983}{4438829} & 0\\ 0 & 0 & \frac{216983}{2549358} & \frac{207913}{728388} & \frac{207913}{5098716}\\ 0 & 0 & 0 & \frac{207913}{029975} & \frac{730162}{029975} \end{pmatrix}$$

$$(4.13)$$

Finally, we emphasize the following remarks:

- 1. Both partitions are symmetric in the sign of M, further we observe that the equilibrium probability are symmetric under the transformation $M \to -M$.
- 2. The equilibrium probability are identically for the cases $E=\pm 4$, recovering a hidden symmetry of the system. However the non-equilibrium behavior is different because the corresponding Eigenvalues have distinct signs. Notice, however, that this "hidden symmetry" is apparently not observed in numerical simulations of the Q2R model (see Fig. 2.8). A more careful inspection of the dynamics indicates that in the cases of the initial conditions R2 and R4 (Fig. 2.8), the magnetization is swapping constantly in time, for instance, if the sequence of values of magnetization for R1 is $\{M_0, M_1, M_2, M_3, \dots\}$, thus, the sequence for R3 would be $\{M_0, -M_1, M_2, -M_3, \dots\}$. Therefore, the temporal average of the magnetization, as computed in Fig. 2.8, would be zero for the cases of R3 and R4. Moreover, taking an average but each every two steps one recovers the Ising bifurcation for positive values of energies. Therefore, the symmetry among positive and negative energies is recovered in the phase diagram.
- 3. It is noticed, that there is qualitative difference for distinct energies: for E=-4 the equilibrium distribution has a maximum for $M \neq 0$, while its maximum is located at M=0 for the case E=0, this is the precursor of the Ising transition, as observed in Fig. 2.8.

Chapter 5

Conclusions

The main goal of this thesis was studies the dynamics of the Q2R cellular automata, using tools of the statistical mechanics. The model possesses different behaviors and features, such as, reversibility, a conservative quantity and a phase transition, whose origin is based from the well-know Ising model.

In the first chapter, we have presented the several features of different models that possess a direct connection with the Ising model, such as, the Glauber-Ising time dependent model, the Q2R cellular automata, the Schelling model for social segregation, the decision-choice model for social sciences and economics and finally the bootstrap percolation model for diseases dissemination. Moreover, the statistical descriptions were: Phase transitions, Bifurcations and Phase Diagrams and most important, the existence of a core principle, e.g., energy minimization which appears to be a robust feature of these models. However, these presents distinct properties. The Glauber Dynamics does not preserve neither the energy or magnetization, however the Q2R dynamics does preserve only the energy but does not preserve the magnetization. The Schelling model does preserve only the magnetization, but if $\theta_k > |V_k|/2$ the system's energy is strictly a decreasing function. Finally, in the infection model, the energy strictly decreases whereas the magnetization is an increasing function of time.

Then, in the second chapter, we have introduced the core of this investigation, the description of the Q2R cellular automata. Where, the numerical simulations in absence of any numerical approximattion showed that the model exhibit ferromagnetic and paramagnetic behaviors respect to the energy. Moreover, the main phenomenon of the model is the phase transition, when one consider a system sizes $N=256\times256$ and a value of energy $E/N\approx-\sqrt{2}$ (called the critical energy). This energy connects the direct relation with the Ising model.

On the other hand, the reversibility that exhibit the cellular automata, turn in, a rich

dynamics characterized by a huge number of invariants which partitions the phase space in terms of the conserved energy and a huge number of periodic cycles. These cycles can be from a fixed point to long orbits, for the case of an 4×4 lattice, the longer cycles was 1080 when the energy can take values $E=\pm 2$. However, using the definition of the Hamming distance, the systems presents two type of behaviors similarly to a random walk, and Lévy flight in the configuration space, typically, this type of behaviors has been observed in the models that take a diffusive dynamics. This can be a good way for study how conservative system can develop a behavior of type diffusive.

Finally, we have closed this investigation with the introduced of a coarse-graining approach, that allowed us to write a coarse-grained master equation, which characterizes equilibrium and non-equilibrium statistical properties of the system. We reviewed the methodology and tested the consistency of results in lattices of different sizes. We found that for well chosen partitions, this coarse graining technique is a powerful tool to reduce the information of the whole system in such a way as to obtain a tractable probability transfer matrix which simplifies the original master equation. A first central property of this matrix, is the existence of an invariant probability distribution which agrees with different coarse-graining procedures. Secondly, we computed the spectral decomposition of the probability transfer matrix characterizing the non-equilibrium properties of the system. Finally, we checked the compatibility conditions, as well as the time reversal symmetry conditions for short time steps. In many situations the methodology is consistent and provides a complete statistical description of the system. However some discrepancies appears which deserves caution. This study provided us with a systematic approach for reducing the number of pertinent macroscopical variables resulting into a manageable master equation.

Bibliography

- [1] W Lenz. Lenz beiträge zum verständnis der magnetischen eigenschaften in festen körpern. *Physikalische Zeitschrift*, 21:613–615, 1920.
- [2] E. Ising. Beitrag zur Theorie des Ferromagnetismus. Z. Phys, 31(253-258):3-4, 1925.
- [3] Fernando Mora, Felipe Urbina, Vasco Cortez, and Sergio Rica. Around the Ising Model, pages 329–345. Springer International Publishing, Cham, 2016.
- [4] Gérard Y. Vichniac. Simulating physics with cellular automata. *Physica D: Nonlinear Phenomena*, 10(1-2):96 116, 1984.
- [5] Y Pomeau. Invariant in cellular automata. Journal of Physics A: Mathematical and General, 17(8):L415, 1984.
- [6] H.J. Herrmann. Fast algorithm for the simulation of ising models. *Journal of Statistical Physics*, 45(1-2):145–151, 1986.
- [7] H J Hermann, H O Carmesin, and D Stauffer. Periods and clusters in ising cellular automata. *Journal of Physics A: Mathematical and General*, 20(14):4939, 1987.
- [8] Shinji Takesue. Relaxation properties of elementary reversible cellular automata. *Physica D: Nonlinear Phenomena*, 45(1–3):278 284, 1990.
- [9] E. Goles and S. Rica. Irreversibility and spontaneous appearance of coherent behavior in reversible systems. *The European Physical Journal D*, 62(1):127–137, 2011.
- [10] K. Huang. Statistical mechanics. Wiley, 1987.
- [11] W. Greiner, L. Neise, and H. Stöcker. *Thermodynamics and statistical mechanics*. Classical theoretical physics. Springer-Verlag, 1995.
- [12] G. Nicolis and C. Nicolis. Master-equation approach to deterministic chaos. *Phys. Rev. A*, 38:427-433, Jul 1988.

66 BIBLIOGRAPHY

[13] G. Nicolis, S. Martínez, and E. Tirapegui. Finite coarse-graining and chapman-kolmogorov equation in conservative dynamical systems. *Chaos, Solitons and Fractals*, 1(1):25 – 37, 1991.

- [14] Roy J. Glauber. Time?dependent statistics of the ising model. *Journal of Mathematical Physics*, 4(2), 1963.
- [15] William A. Brock and Steven N. Durlauf. A formal model of theory choice in science. *Economic Theory*, 14(1):113–130, 1999.
- [16] William A. Brock and Steven N. Durlauf. Chapter 54 interactions-based models. 5:3297 3380, 2001.
- [17] Jean-Philippe Bouchaud. Crises and collective socio-economic phenomena: Simple models and challenges. *Journal of Statistical Physics*, 151(3):567–606, 2013.
- [18] Lars Onsager. Crystal statistics. i. a two-dimensional model with an order-disorder transition. *Phys. Rev.*, 65:117–149, Feb 1944.
- [19] Felipe Urbina, Sergio Rica, and Enrique Tirapegui. Coarse-graining and master equation in a reversible and conservative system. *Discontinuity, Nonlinearity, and Complexity*, page 199, 2015.
- [20] Thomas Schelling. Models of segregation. American Economic Review, 59(2):488–93, 1969.
- [21] Thomas C. Schelling. Dynamic models of segregation. The Journal of Mathematical Sociology, 1(2):143–186, 1971.
- [22] T.C. Schelling. Micromotives and Macrobehavior. W. W. Norton, 2006.
- [23] Nicolás Goles Domic, Eric Goles, and Sergio Rica. Dynamics and complexity of the schelling segregation model. *Phys. Rev. E*, 83:056111, May 2011.
- [24] J Chalupa, P L Leath, and G R Reich. Bootstrap percolation on a bethe lattice. Journal of Physics C: Solid State Physics, 12(1):L31, 1979.
- [25] D. Stauffer and S. Solomon. Ising, schelling and self-organising segregation. *The European Physical Journal B*, 57(4):473–479, 2007.
- [26] Abhinav Singh, Dmitri Vainchtein, and Howard Weiss. Schelling's Segregation Model: Parameters, scaling, and aggregation. *Demographic Research*, 21(12):341–366, 2009.
- [27] L. Gauvin, J. Vannimenus, and J.-P. Nadal. Phase diagram of a schelling segregation model. *The European Physical Journal B*, 70(2):293–304, 2009.

BIBLIOGRAPHY 67

[28] Vasco Cortez, Pablo Medina, Eric Goles, Roberto Zarama, and Sergio Rica. Attractors, statistics and fluctuations of the dynamics of the schelling's model for social segregation. The European Physical Journal B, 88(1):25, 2015.

- [29] JÓZSEF BALOGH, BÉLA BOLLOBÁS, and ROBERT MORRIS. Majority bootstrap percolation on the hypercube. *Combinatorics, Probability and Computing*, 18(1-2):17-51, 003 2009.
- [30] József Balogh and Boris G. Pittel. Bootstrap percolation on the random regular graph. Random Structures and Algorithms, 30(1-2):257–286, 2007.
- [31] Lars Onsager. Crystal statistics. i. a two-dimensional model with an order-disorder transition. *Phys. Rev.*, 65:117–149, Feb 1944.
- [32] Shinji Takesue. Staggered invariants in cellular automata. Complex Systems, 9(2):149–168, 1995.
- [33] N. Goldenfeld. Lectures on Phase Transitions and the Renormalization Group. Frontiers in physics. Addison-Wesley, Advanced Book Program, 1992.
- [34] C. N. Yang. The spontaneous magnetization of a two-dimensional ising model. *Phys. Rev.*, 85:808-816, Mar 1952.
- [35] Tai Tsun Wu, Barry M. McCoy, Craig A. Tracy, and Eytan Barouch. Spin-spin correlation functions for the two-dimensional ising model: Exact theory in the scaling region. *Phys. Rev. B*, 13:316–374, Jan 1976.
- [36] Theo Rhodes and Michael T. Turvey. Human memory retrieval as lévy foraging. Physica A: Statistical Mechanics and its Applications, 385(1):255 – 260, 2007.
- [37] ESA Online Journals The Lévy flight paradigm: random search patterns and mechanisms.
- [38] DAVID W. SIMS, DAVID RIGHTON, and JONATHAN W. PITCHFORD. Minimizing errors in identifying lévy flight behaviour of organisms. *Journal of Animal Ecology*, 76(2):222–229, 2007.
- [39] Marta C. Gonzalez, Cesar A. Hidalgo, and Albert-Laszlo Barabasi. Understanding individual human mobility patterns. *Nature*, 453(7196):779–782, 06 2008.
- [40] Pierre Barthelemy, Jacopo Bertolotti, and Diederik S. Wiersma. A levy flight for light. *Nature*, 453(7194):495–498, 05 2008.
- [41] Andreas Dechant and Eric Lutz. Anomalous spatial diffusion and multifractality in optical lattices. *Phys. Rev. Lett.*, 108:230601, Jun 2012.

68 BIBLIOGRAPHY

- [42] K. Pearson. The Problem of the Random Walk. Nature, 72(1865):294, 1905.
- [43] E V Albano. Diffusion and annihilation reactions of levy flights with bounded long-range hoppings. *Journal of Physics A: Mathematical and General*, 24(14):3351, 1991.
- [44] H J Hermann, H O Carmesin, and D Stauffer. Periods and clusters in ising cellular automata. *Journal of Physics A: Mathematical and General*, 20(14):4939, 1987.
- [45] Pomeau, Y. Symétrie des fluctuations dans le renversement du temps. J. Phys. France, 43(6):859–867, 1982.

Appendix A

Article

Coarse-Graining and Master Equation in a Reversible and Conservative System

Publication details

- Title: Coarse-Graining and Master Equation in a Reversible and Conservative System.
- Authors: Felipe Urbina, Sergio Rica, and Enrique Tirapegui.
- Journal: Discontinuity, Nonlinearity, and Complexity. 4(2), 199 208, (2015).
- DOI: 10.5890/DNC.2015.06.007
- URL: https://lhscientificpublishing.com/journals/dnc-download.aspx/D0I10.5890.

APPENDIX A ARTICLE



Discontinuity, Nonlinearity, and Complexity



https://lhscientificpublishing.com/Journals/DNC-Default.aspx

Coarse-Graining and Master Equation in a Reversible and Conservative System

Felipe Urbina¹, Sergio Rica¹, and Enrique Tirapegui²

¹Facultad de Ingeniería y Ciencias, Universidad Adolfo Ibáñez, Avda. Diagonal las Torres 2640, Peñalolén, Santiago, Chile.

Submission Info

Communicated by Valentin Afraimovich Received 5 January 2015 Accepted 5 March 2015 Available online 1 July 2015

Abstract

A coarse graining process is applied to a Ising like model with a conservative and a reversible dynamics. It is shown that, under some assumptions, this coarse graining leads to a tractable probability transfer matrix of finite size which provides a master equation for a coarse graining probability distribution. Some examples are discussed.

Keywords

Q2R Automata Ising Model Coarse Graining Master equation

©2015 L&H Scientific Publishing, LLC. All rights reserved.

1 Introduction

The long time behavior of conservative and reversible systems with a huge number degrees of freedom usually requires a statistical description which introduces distribution functions of the system. Irreversibility, equilibrium, and more important non-equilibrium properties surge from this probability and its evolution.

In this context, statistical physics starts from a number of, reversible and conservative, ordinary differential equations for Newtonian particles; or, alternatively, with the Liouville description. This cumbersome problem, even for modest number of particles, therefore one reduces (under some assumptions) to a kinetic description which displays the irreversible behavior to equilibrium observed in macroscopic systems. The assumptions for this approach are: i) a macroscopical system does not require a huge number of variable but a limited set of macroscopic observables; ii) Only a coarse grained description of these macroscopic variables has a sense (that is the impractical possibility to measure a quantity with infinite precision), iii) The robust instability of the microscopic motions which is at the basis of the sensibility to the initial conditions and the ergodic hypothesis. iv) A *Stosszahlansatz* which introduces explicitly a broken before-after symmetry of the probability distribution evolution.

About 20 years ago, Nicolis *et al.* [1,2] introduced a systematic corse graining on the macroscopical variables and they were able to derive a master equation, for a reduced probability distribution function of the system. In

Email address: sergio.rica@uai.cl, sergio.rica@gmail.com

ISSN 2164 - 6376, eISSN 2164 - 6414/\$-see front materials © 2015 L&H Scientific Publishing, LLC. All rights reserved. DOI: 10.5890/DNC.2015.06.007

²Departamento de Física, Universidad de Chile, Avda. Blanco Encalada 2002, Santiago, Chile.

[†]Corresponding author.

the present paper, we shall apply this systematic approach to a conservative and explicit reversible cellular automata system. Consequently, we shall consider the Q2R model, introduced by Vichniac in the mid 80s [3], which preserves exactly a kind of energy [4].

The main reason to apply the coarse graining approach to a cellular automata instead to a coupled system of ordinary differential equations, is because a cellular automata is a discrete model with boolean entities as microscopic variables, therefore, there are no round errors neither approximations in the numerical computations, hence, the system is both theoretically and numerically reversible and conservative.

The study of the dynamics and properties of the Q2R model has a long history. In 1986 Herrmann [5] implemented the Q2R algorithm to study the two space dimensional Ising model in a microcanonical description. He studied the global magnetization, obtaining an excellent representation for the magnetization as a function of the initial conserved energy. Later, Takesue [6] focused on the possible realization of statistical mechanics for reversible cellular automata, showing that under certain conditions the system may be described in terms of a canonical description. His studies concerned explicitly all class of rule in the one dimensional case, the Q2R being only a special case. However, the Q2R (90R in his terminology), is the analogue of an ideal gas of particles with speeds +1 or -1, a system that cannot reach equilibrium in practice. It is ergodic only in the thermodynamical equilibrium. More recently, in Ref. [8], one of us (SR) has studied numerically the irreversible behavior and the existence of a spontaneous transition from a non-coherent state to a coherent state in the frame of the reversible cellular automata O2R.

The present article is organized as follows, the Q2R model, as well as its main properties are presented in section 2 We briefly report the numerical studies of Ref. [8] in section 3 The coarse graining in presented in section 4, and some examples are explicitly in next section 5 Finally, the slow modes and transport is discussed in section 6

2 The O2R Model

For simplicity we shall consider a regular two dimensional lattice with $N = L^2 \gg 1$ nodes, each node is only seen by its four closest neighbors (von Neuman neighborhood), finally we use periodic boundary conditions.

Each node k possesses a discrete value x_k that may take values +1 and -1. The Q2R rule considers the following two step rule [3]:

$$x_k^{t+1} = x_k^{t-1} \phi(\sum_{i \in V} x_i^t),$$

where the function ϕ is such a that $\phi(s=0)=-1$ and $\phi(s)=+1$ in all other cases.

This two step rule may be naturally re-written as a one step rule with the aid of an auxiliary dynamical variable [4]:

$$y_k^{t+1} = x_k^t x_k^{t+1} = y_k^t \phi(\sum_{i \in V} x_i^t).$$
 (1)

As shown by Pomeau [4], the following quantity, that we call by an energy

$$E[\{x^t, y^t\}] = -\frac{1}{2} \sum_{\langle i, k \rangle} x_k^t y_i^t,$$
 (2)

is preserved under the dynamics defined by the Q2R rule (1). Moreover, the energy is bounded by $-2N \le E \le 2N$.

Despite the existence of an invariant that is a kind of energy, it does not seem possible to speak about a Hamiltonian discrete dynamics because the variables x^t and y^t and the energy E (2) are discrete variable and quantities [4].

The rule (1) is complemented with an initial condition $x_k^{t=0}$ and $y_k^{t=0}$ that we shall describe more precisely in the next section..

For a finite system size the Q2R automata is always periodic. This period is naturally shorter than (or equal to) the total number of possible configurations with a given energy E (and necessarily shorter than the longest possible period, which is the total number of configurations 2^{2N}). Moreover, it has been shown numerically, that Q2R could have clusters of small periodic motion [7]. However, in practice, for a large enough systems and for random initial conditions, the observation of a periodic dynamics is really improbable. In general, there is a huge number of initial conditions that are "almost" ergodic.

Similarly, one may ask about a "sensibility to the initial conditions". In Ref. [8], it is shown numerically, that if one starts with two distinct, but close, initial conditions, then, they evolve in very different paths as time goes ^a. In some sense, an initial state explores vastly the phase space allowed. This is essentially the fundamental reason why we may use the grounds of statistical physics for studying this problem.

In summary, although for a finite size system the deterministic automata Q2R is not ergodic, there is a huge number of initial conditions that explore vastly the phase space, this is particularly remarkably for initial conditions of random structure, in some sense the dynamic itself realizes a good sampling, so that a statistical description is possible when the initial condition is random. For instance, take a random initial condition with a given fixed energy. It is observed, that if the initial energy is smaller than a critical value, the system becomes spontaneously ordered in average. This transition appears to be of the same class of Ising transition in magnetic models. Therefore, despite the original system being conservative and reversible, for a large set of initial conditions, the system self organizes into an average macroscopic state with a manifest order as we shall see in the next section.

3 "Long-time" dynamics of the Q2R cellular automata [8].

In Ref. [8], we have realized numerical simulations of the Q2R model in 2D and we have explored different system sizes $N = 256 \times 256$ and $N = 512 \times 512$. For the initial condition, we consider the following initial boolean random realization

$$B_k(p) = \begin{cases} +1 & \text{with probability } p \\ -1 & \text{with probability } 1-p \end{cases}, \tag{3}$$

where, the index k represents the independent realizations over the lattice sites.

In Ref. [8] the special choice of initial conditions such that $x_k^{t=0} = y_k^{t=0} = B_k(p)$. This choice is only for convenience because it helps us to identify the initial energy in terms of the energy of ferromagnetic system. Moreover, as stated in [5], this initial condition will be crucial in interpreting the statistical properties of the Q2R dynamics in terms of the Ising model.

Typically, the dynamics shows in time a very random pattern of local magnetization, having patches with magnetization +1 and patches with magnetization -1. Also, zones of zero average magnetization are present, where the spins are in a chessboard-like pattern. The full patterns are difficult to classified and to characterize, therefore we shall characterize them by a global quantity:

$$M(t) = M[\{x^t\}] = \sum_{k} x_k^t,$$
 (4)

which we call the total magnetization of the system. Naturally, M is also bounded $-N \le M \le N$, and the finest grain description has a discrete separation of $\Delta M = 2$.

A simple mean field estimation relates the magnetization and the total energy with of the initial condition (3) with p, via the following relations: M/N = (2p-1), and the mean field energy $E/N = -2(M/N)^2 = -2(2p-1)^2$.

^aThe divergence of these two "trajectories" is not exponential because this distance cannot increase indefinitely in a finite system.

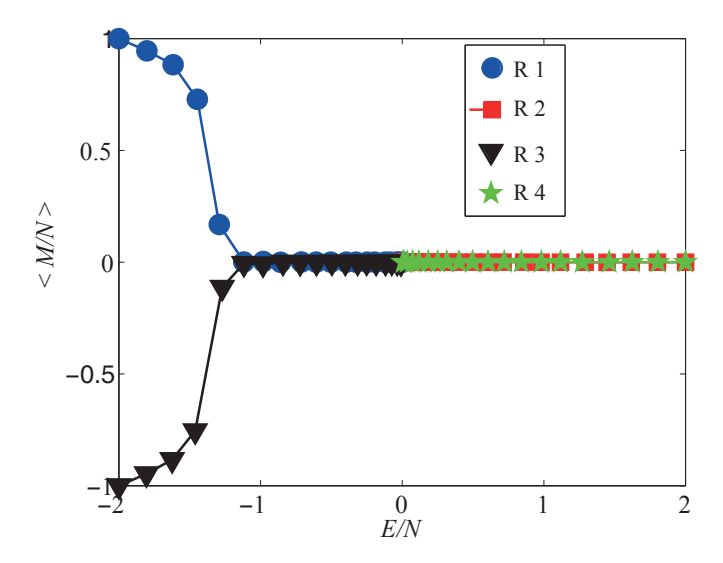


Fig. 1 Magnetization curves as a function of initial energy for a 256 × 256 system size. The points corresponds to different initial conditions. Accordingly with the a boolean random set of values, $B_k(p)$, as described in equation (3), the initial data is: R1 (•): $x_k^{t=0} = y_k^{t=0} = B_k(p)$; R2 (■): $x_k^{t=0} = -y_k^{t=0} = B_k(p)$; R3 (▼): $x_k^{t=0} = y_k^{t=0} = -B_k(p)$; and, R4 (*): $x_k^{t=0} = -y_k^{t=0} = -B_k(p)$.

A detailed characterization of the evolution, as well as, of the fluctuations of the magnetization has been treated in detail in Ref. [8]. Briefly, after a transient the average magnetization depends mainly on the initial energy. If the energy is low, one sees that the average magnetization evolves slowly in time to an "equilibrium" state with an almost constant value plus weak fluctuations. For larger energies, the fluctuations enter to play an important role. One may observe that the system is in an almost stable state, but then suddenly jumps into a metastable state with zero average magnetization, and then jumps into an opposite magnetization state.

The plot of the average magnetization (in time and over the sites) versus the initial energy of the configuration is done in Fig. 1. One sees that the magnetization spontaneously increases below a critical energy per site around $E_c/N = -1.4$, close to the critical energy of the Ising model $E_c/N = -\sqrt{2}$ [9, 10]. Moreover, in Ref. [8] we compare the magnetization as a function of the internal energy of the system showing a close agreement with the numerical values.

4 Coarse graining and master equation for the probability distribution functions

Although the dynamics of the Q2R model cannot be ergodic, in the usual sense, it is quite random and it possesses many aspects of chaotic systems, as sensibility to initial conditions, mixing, etc. providing the initial state is random. Numerical studies shows that the premises of statistical physics are valid, in particular the observables may be computed using the standard methods of statistical physics. In the following we shall introduce statistical tools for the understanding the approach to equilibrium of this system.

Given a phase space D that contains all possible configurations of an state $\{x,y\}$, then $\rho(\{x,y\})$ represents the probability distribution function of the system to be in the state $\{x,y\}$. Naturally, the dimension of D is huge, because it contains 2^{2N} elements, but the distribution function moves in a sub-space, of smaller dimension, of all the configurations with an energy E fixed. The distribution $\rho_t^E(\{x,y\})$ evolves following a Perron-Frobenius type equation

$$\rho_{t+1}^E = \mathcal{L}^E \rho_t^E$$

which, in principle, maybe computed after the microscopic rule of evolution (1).

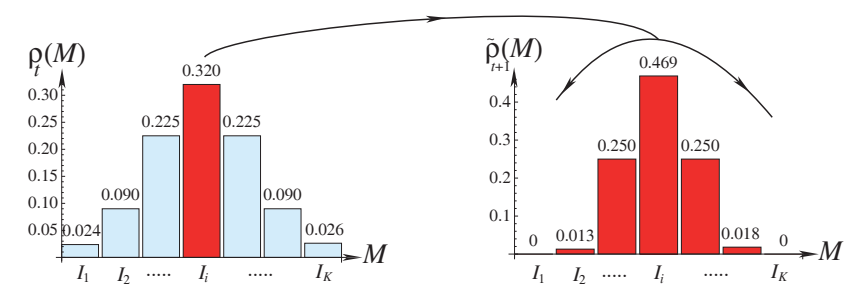


Fig. 2 The distribution $\rho_t(M)$ at a time t is schematised in the left distribution. The fraction inside the interval I_i , is distributed, after the evolution into a new distribute $\tilde{\rho}_{t+1}(M)$ schematised in the left diagram. The normalised distribution provides the k-th element of the i-th column: w_{ik} .

The knowledge of the explicit the reduced Perron-Frobenius operator \mathscr{L}^E is impractical because of the large number of possible values of degrees of freedom. Therefore, usually one restricts the description to a reduced distribution which is only a function of E and M. This reduced probability distribution function reads $\rho_t(M)$, and satisfy a new master equation $\rho_{t+1}(M) = \mathscr{W}\rho_t(M)$, the linear operator \mathscr{W} acts only in the subspace of constant E, but is spanned over arbitrary values of magnetization. As the original Perron-Frobenius equation, \mathscr{W} depends explicitly of the Q2R rule and maybe computed in principle. However, in practice, it is necessary to reduce again the information via a coarse graining partition of the possible values of M. The partition is defined through a set of no overlapping intervals^b: $I_1 = [-N, M_1)$, $I_2 = [M_1, M_2)$, ... $I_{K-1} = [M_{K-2}, M_{K-1})$, $I_K = [M_{K-1}, N]$, and we denote the original distribution function $\rho_t(M)$ by a discrete vector of dimension K, that is: $\rho_t(M) \to f_t = (f_1, f_2, \dots f_K)$. Notice that this probability vector should be normalizable to the unity, let be the vector K-dimensional vector $\mathbf{1} = (1, 1, \dots 1)$, then $\mathbf{1} \cdot f_t = 1$.

Therefore, we construct a corse grained master equation^c

$$\mathbf{f}_{t+1} = \hat{W}\mathbf{f}_t \tag{5}$$

where W is the probability transition matrix defined via the following conditional probability:

$$w_{ik} = P(M_{t+1} \in I_k | M_t \in I_i) = \frac{P(M_{t+1} \in I_k \cap M_t \in I_i)}{P(M_t \in I_i)}$$

being M_t at the interval I_i at the time t, and M_{t+1} would be at the interval I_k at t+1.

Because of normalization, $\sum_{i=1}^{K} w_{ik} = 1$, therefore the left hand product $\mathbf{1} \cdot \hat{W} = \mathbf{1}$. This implies that the probability is conserved $\mathbf{1} \cdot \mathbf{f}_{t+1} = \mathbf{1} \cdot \hat{W} \mathbf{f}_t = \mathbf{1} \cdot \mathbf{f}_t = 1$. Finally, the \hat{W} matrix does not depend on time, which is a characteristic of a Markov process. The coarse graining method is schematized in Fig. 2.

To conclude this section, we shall discuss the equilibrium distributions, the general properties that the W matrix should satisfy, as well as the conditions on the partitions.

The Perron-Frobenius equation maybe solved exactly, provided an initial distribution f_0 and the knowledge of the \hat{W} -matrix, indeed:

$$\mathbf{f}_t = \hat{\mathbf{W}}^t \mathbf{f}_0. \tag{6}$$

The power of the matrix \hat{W}^t maybe computed with the aid of the eigenvalues (λ_i) and eigenvectors (χ_i) of \hat{W}^e . Because of the Frobenius theorem, one eigenvalue, λ_1 , is exactly 1, while others eigenvalues are inside the

^bIf the systems posses more than one observable, one proceeds similarly.

^cIn the present article we use a different notation from the one of Refs. [1,2]. The vectors in Eq. (5) are column matrices, the matrices are denoted as \hat{W} , finally, the usual matrices product operates.

^dThat is the transpose of **1** acting on \hat{W} .

^eWe shall normalize the Eigenvectors as $1 \cdot \chi_i = 1$.

unitary circle $|\lambda_i| < 1$ for i > 1. Let us denote f_{eq} by the Eigenvector associated with the Eigenvalue $\lambda_1 = 1$, this ⁷⁵ is an invariant vector $f_{eq} = \hat{W} f_{eq}$. This vector is, by definition, the equilibrium distribution.

The limit $t \to \infty$ of equation (6), $\mathbf{f}_{\infty} = \lim_{t \to \infty} \hat{W}^t \mathbf{f}_0 = \hat{W}^{eq} \mathbf{f}_0$, is well defined. Indeed, expanding the initial distribution in terms of the eigenvectors^f:

$$\boldsymbol{f}_0 = \sum_{i=1}^K \alpha_i \boldsymbol{\chi}_i,$$

one obtains that

$$oldsymbol{f}_t = \sum_{i=1}^K lpha_i \lambda_i^t oldsymbol{\chi}_i.$$

Therefore, in the limit $t \to \infty$, $\boldsymbol{f}_{eq} = \alpha_1 \boldsymbol{\chi}_1 = \boldsymbol{\chi}_1$.

Moreover, the equilibrium probability transfer matrix, \hat{W}^{eq} , also exists, and it is built with K replicas of the invariant vector \mathbf{f}_{eq} as columns: $\hat{W}^{eq} = (\mathbf{f}_{eq}, \mathbf{f}_{eq}, \dots \mathbf{f}_{eq})$.

One may wonder if one realizes the same process but instead to look at the system at times t and t+1, one looks at time t and t+2 or more generally at t and t+T. Let us call $\hat{W}^{(T)}$ the resulting probability transfer matrix after $T = T_1 + T_2$ iterations, therefore it is easy to show that this matrix should verify the Chapman-Kolmogorov condition, $t = T_1 + T_2$ iterations, therefore it is easy to show that this matrix should verify the Chapman-Kolmogorov condition, $t = T_1 + T_2$ iterations, therefore it is easy to show that this matrix should verify the Chapman-Kolmogorov condition, $t = T_1 + T_2$ iterations, therefore it is easy to show that this matrix should verify the Chapman-Kolmogorov condition.

$$\hat{W}^{(T)} = \hat{W}^{(T_1)} \cdot \hat{W}^{(T_2)}.$$

In particular, for T = 2 one has

$$\hat{W}^{(2)} = \hat{W} \cdot \hat{W} = \hat{W}^2,$$

which is true for conditional probabilities, because of the relation $P(M_{t+2} \in I_k | M_t \in I_i) = \sum_j P(M_{t+2} \in I_k | M_{t+1} \in I_j) P(M_{t+1} \in I_j | M_t \in I_i)$, which is equivalent to the right hand side.

At this respect, there are some open questions:

- Is T=1 the pertinent time scale to define W? One may wonder if the system is Markovian in the shortest time scale, that is one may think that the system possesses a characteristic time scale, such a that beyond this time, the system becomes Markovian.

-Which is the adequate value for T to describe the system with the present approach? A detailed study at this respect deserves more work.

Finally, though in practice the choice of partitions is done in a pure qualitative way, it is crucial to have an idea how the phase space evolves in time under the dynamical system. In Ref. [1], it is considered a Markov partition in which case the boundaries of the intervals I_k are kept invariant by the dynamics. This is easy to precise a in a small degrees of freedom system, because of the existences of fixed points, separatrices and so on. In the present case the qualitative behavior of the phase space is vastly unknown. In some cases a negative magnetization stay negative, in some others it passes to be positive, etc Therefore, a not precise rule maybe extracted.

In the following section we provide some examples of the procedure.

5 Examples

5.1 Exact calculation for the 2×2 lattice.

Consider the case of a 2×2 periodic lattice. Though this is the smallest possible version of the Q2R automata, and the dynamics is extremely simple, the calculations are exactly realizable up to end, therefore it shows explicitly the method. The phase space possesses $2^{2\times4} = 256$ distinct configurations which maybe computed

Frecalling that the initial distribution should be normalizable: $\mathbf{1} \cdot \mathbf{f}_0 = 1$, hence, one has the condition $\sum_{i=1}^K \alpha_i = 1$, however there is a extra free condition and we shall impose $\alpha_1 = 1$.

gActually it is sufficient to verify the case of $T_2 = 1$: $\hat{W}^{(T)} = \hat{W}^{(T-1)} \cdot \hat{W}$.

directly. The energy takes possible values $E = \{-8, -4, 0, 4, 8\}$. Among of them, 4 configurations have an energy E = -8; 48 configurations have an energy E = -4; 152 configurations have a zero energy E = 0; finally, 48 have an energy E = +4 and 4 of them have an energy E = +8.

The magnetization may take values -4, -2, 0, 2, 4, and we shall realize as an example two distinct partitions.

5.1.1 Coarse grained partition

First, let us take a partition of three intervals: $I_1 = [-4, -2]$, $I_2 = [0, 0]$, & $I_3 = [2, 4]$, that is, the partition splits the cases of magnetization, greater, smaller and equal to 0. Let us consider the case of E = 0, that is 152 distinct configurations of the phase space.

Among them, they are distributed with the following magnetizations: 38 with M < 0, 76 with M = 0 and 38 with M > 0. Let us take the 38 configurations with M < 0, after one step of the Q2R algorithm, the 38 initial states end as following: 8 of them remain in the same partition with M < 0, 22 of them pass to M = 0 and 8 of them get a positive magnetization. Therefore the first column of the \hat{W} matrix is (8/38, 22/38, 8/38), naturally their sum is the unity. In a similar way one can build systematically all the other cases^h.

The \hat{W} -matrices read for distinct energies (we shall omit here the cases with $E=\pm 8$ which are not mixing cases):

$$\hat{W}_{E=-4} = \begin{pmatrix} 4/5 \ 1/2 & 0 \\ 1/5 & 0 & 1/5 \\ 0 & 1/2 \ 4/5 \end{pmatrix}, \quad \hat{W}_{E=0} = \begin{pmatrix} 4/19 & 11/38 & 4/19 \\ 11/19 & 8/19 & 11/19 \\ 4/19 & 11/38 & 4/19 \end{pmatrix}, \quad \hat{W}_{E=4} = \begin{pmatrix} 0 & 1/2 \ 4/5 \\ 1/5 & 0 & 1/5 \\ 4/5 \ 1/2 & 0 \end{pmatrix}.$$

As a first sight we observe a symmetry property between the cases $\hat{W}_{E=\pm 4}$. We shall discuss this fact later. The eigenvalues and the invariant probability distributions (the corresponding Eigenvectors associated to the unique unitary Eigenvalue) of these matrices are:

$$\lambda = \begin{cases} \{1, 4/5, -1/5\}, & E = -4 \\ \{1, -3/19, 0\}, & E = 0 \\ \{1, -4/5, -1/5\}, & E = 4 \end{cases} \text{ and } \mathbf{f}_{eq} = \begin{cases} (5/12, 1/6, 5/12), & E = -4 \\ (1/4, 1/2, 1/4), & E = 0 \\ (5/12, 1/6, 5/12), & E = 4 \end{cases}$$
 (7)

5.1.2 Finest grained partition

The finest grained partition consider the exact values of magnetization $M = \{-4, -2, 0, 2, 4\}$, then the 5×5 matrices are:

$$\hat{W}_{E=-4} = \begin{pmatrix} 0 & 1/4 & 0 & 0 & 0 \\ 1 & 1/2 & 1/2 & 0 & 0 \\ 0 & 1/4 & 0 & 1/4 & 0 \\ 0 & 0 & 1/2 & 1/2 & 1 \\ 0 & 0 & 0 & 1/4 & 0 \end{pmatrix}, \quad \hat{W}_{E=0} = \begin{pmatrix} 0 & 0 & 3/38 & 0 & 0 \\ 0 & 1/4 & 4/19 & 1/4 & 0 \\ 1 & 1/2 & 8/19 & 1/2 & 1 \\ 0 & 1/4 & 4/19 & 1/4 & 0 \\ 0 & 0 & 3/38 & 0 & 0 \end{pmatrix}, \quad \hat{W}_{E=4} = \begin{pmatrix} 0 & 0 & 0 & 1/4 & 0 \\ 0 & 0 & 1/2 & 1/2 & 1 \\ 0 & 1/4 & 0 & 1/4 & 0 \\ 1 & 1/2 & 1/2 & 0 & 0 \\ 0 & 1/4 & 0 & 0 & 0 \end{pmatrix}.$$

The corresponding Eigenvalues and invariant probability distributions are:

$$\lambda = \begin{cases} \left\{ 1, \frac{1}{4} \left(1 + \sqrt{5} \right), -\frac{1}{2}, \frac{1}{4} \left(1 - \sqrt{5} \right), 0 \right\}, & E = -4 \\ \left\{ 1, -\frac{1}{76} \left(3 + \sqrt{465} \right), \frac{1}{76} \left(\sqrt{465} - 3 \right), 0, 0 \right\}, & E = 0 \end{cases} \qquad \boldsymbol{f}_{eq} = \begin{cases} \left(1/12, 1/3, 1/6, 1/3, 1/12 \right), & E = -4 \\ \left(3/76, 4/19, 1/2, 4/19, 3/76 \right), & E = 0 \end{cases} \quad \boldsymbol{g}_{eq} = \begin{cases} \left(1/12, 1/3, 1/6, 1/3, 1/12 \right), & E = -4 \\ \left(3/76, 4/19, 1/2, 4/19, 3/76 \right), & E = 0 \end{cases} \quad \boldsymbol{g}_{eq} = \begin{cases} \boldsymbol{g}_{eq} = \boldsymbol{g}_{eq} = \boldsymbol{g}_{eq} \end{cases}$$

^hThe present calculation is recovered in the first column of $\hat{W}_{E=0}$.

Despite the evident differences among the coarse and the fine graining partitions, one notices that both partitions 77 predicts at least qualitatively the same behavior of the equilibrium distribution.

Finally, we emphasize the following remarks:

- 1. Both partitions are symmetric in the sign of M, further we observe that the equilibrium probability are symmetric under the transformation $M \rightarrow -M$.
- 2. The equilibrium probability are identically for the cases $E=\pm 4$, recovering a hidden symmetry of the system. However the non-equilibrium behavior is different because the corresponding Eigenvalues have distinct signs. Notice, however, that this "hidden symmetry" is apparently not observed in numerical simulations of the Q2R model (see Fig. 1). A more careful inspection of the dynamics indicates that in the cases of the initial conditions R2 and R4 (Fig. 1), the magnetization is swapping constantly in time, for instance, if the sequence of values of magnetization for R1 is $\{M_0, M_1, M_2, M_3, ...\}$, thus, the sequence for R3 would be $\{M_0, -M_1, M_2, -M_3, ...\}$. Therefore, the temporal average of the magnetization, as computed in Fig. 1, would be zero for the cases of R3 and R4. Moreover, taking an average but each every two steps one recovers the Ising bifurcation for positive values of energies. Therefore, the symmetry among positive and negative energies is recovered in the phase diagram.
- 3. It is noticed, that there is qualitative difference for distinct energies: for E=-4 the equilibrium distribution has a maximum for $M \neq 0$, while its maximum is located at M=0 for the case E=0, this is the precursor of the Ising transition, as observed in Fig. 1.

5.2 Sampling for a 256×256 system size.

We shall consider now a very large system in a lattice with 256×256 sites, for this case it is not possible to perform all possible configuration to build a probability transfer matrix, therefore we consider a reduced sampling.

In practice for a given p, we use a sample of 10^4 states, but among them, only a fraction of these states have exactly the same energy. Then, these states maybe expanded by a factor two by taking changing $\{x,y\} \rightarrow \{-x,-y\}$. For instance, for an energy E/N=-1.8082 only 4882 states posses the same total energy. In this particular case, one notices that the distributions are well separated in two distinct cases with positive and negative M.

Moreover, the dynamical rule does not allow any transfer of states being at -M into states at +M, hence the system is well separated in phase space. Mixing is possible only between close magnetization regions. It is tempted to write

$$\hat{W} = \begin{pmatrix} 1 & 0 \\ 0 & 1 \end{pmatrix}.$$

But this partition does not consider all the possible values of M because the interval contained M = 0 is empty. One may cure, this singular behavior, adding a small number of configuration with zero magnetization, and using the partition: M > 0, M = 0 and M < 0. But the resulting the \hat{W} matrix should be also close to the identity matrix, therefore any coarse grained distribution f_{eq} is invariant.

For a larger energy, the magnetization mixes among states having negative, positive, and null values of magnetization. Below we reproduces a probability transfer matrix for E/N = -0.0466:

$$\hat{W} = \begin{pmatrix} 1/2 & 2/5 & 0 \\ 1/2 & 11/15 & 1/2 \\ 0 & 2/15 & 1/2 \end{pmatrix}.$$

The corresponding Eigenvalues and invariant probability distributions are:

$$\lambda = \{1, 1/2, 7/30\}, \quad \mathbf{f}_{eq} = (0.174, 0.652, 0.174).$$
 (9)

One may see, that qualitatively the cases of large and low energies display the same qualitative behavior of the previous sections.

6 Slow modes and transport coefficients

The approach to equilibrium follows from the already discussed solution $\mathbf{f}_t = \hat{W}^t \mathbf{f}_0$, which maybe expanded in terms of the eigenvectors of the \hat{W} -matrix, getting $\mathbf{f}_t = \sum_{i=1}^K \alpha_i \lambda_i^t \chi_i$. Therefore, the Eigenvalues near the unity behaves as slow modes. If one defines $\sigma_i = -\log \lambda_i$ one obtain the usual slow mode relaxation: $\mathbf{f}_t = \sum_{i=1}^K \alpha_i e^{-\sigma_i t} \mathbf{\chi}_i$. Moreover, the eigenvalues closest to the unity, represents the transport coefficients, which we shall investigate in the following.

We have consider the case of a 256×256 system size with an energy E/N = -1.445, which is closest to the energy of Ising transition therefore big fluctuations are expected. The magnetization runs over the interval $M \in [32768, 52448]$. We have performed a uniform partition with a $\Delta M = 24$, getting a 820×820 matrix, which we shall not write for obvious reasons. Fig. 3 displays $|\lambda_i|$, ordered by decreasing absolute value, as a function of its order. As a first sight we have the impression that $\lambda_i \approx 1 - \beta i^2$ (for i < 15) characteristic of a diffusive mode, however for larger value of i one sees $\lambda_i \approx 1 - \gamma i$.

The Eigenmodes corresponding to i = 1, to 5 are also plotted showing the usual behavior of a confined Eigenvalue problem, which does not seem to agree with the diffusive mode.

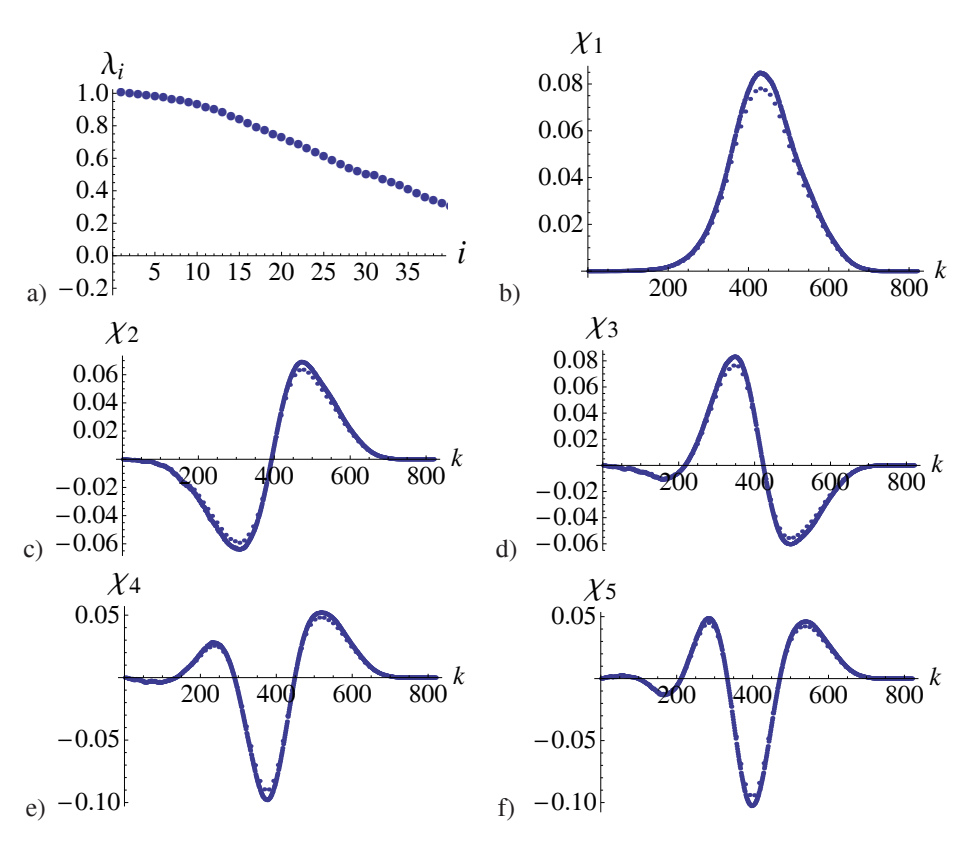


Fig. 3 Slow modes of the case 256×256 for an energy E/N = -1.445 with a uniform partition in M inside the interval $M \in [32768, 52448]$ such a that $\Delta M = 24$ which gives a 820×820 matrix. a) The first 50 Eigenvalues as a function of the index i. b-e) The first 5 Eigenmodes of the \hat{W} matrices. The Eigenmode χ_1 corresponds to the invariant probability vector.

A possible explanation of the behavior of the eigenvalues, $\lambda_i \approx 1 - \gamma i$, is in agreement with a continuous ⁷⁹ limit approximation of the Master equation (5) leading a Fokker-Planck-type equation:

$$\lim_{\Delta M \to 0} (\boldsymbol{f}_{t+1} - \boldsymbol{f}_t) = (\hat{W} - \hat{1})\boldsymbol{f}_t \quad \to \quad \frac{\partial \mathscr{P}}{\partial t} = \frac{\partial}{\partial M} (\beta \frac{\partial \mathscr{P}}{\partial M} + \gamma M \mathscr{P}). \tag{10}$$

The slow mode dynamics is provided by the Eigenvalue problem:

$$-\sigma\varphi = \frac{\partial}{\partial M} \left(\beta\varphi' + \gamma M\varphi\right). \tag{11}$$

which has a solution

$$\sigma_i = \gamma i \quad \text{and} \quad \varphi_i = H_i \left(M \sqrt{\frac{\gamma}{2\beta}} \right) e^{-\frac{\gamma M^2}{2\beta}},$$

where $H_i(x)$ is the Hermite polynomial of degree i which is a nonnegative integer: $i = 0, 1, 2 \dots$ Though, the behavior of the Eigenvalues is not the good one for i < 15, the behavior of the Eigenmodes seems to be the adequate. This exploration deserves a more deep study.

7 Conclusions

Though this article presents an overview of the method, we can see that if the partitions are well done, this coarse graining technique is a powerful tool to reduce the information of whole system in a tractable probability transfer matrix which simplify the original master equation. One central property of this matrix, is the existence of an invariant probability distribution vector (the eigenvector with unitary eigenvalue), which is the coarse grained equilibrium probability distribution of the system. The studied cases agrees, at least qualitatively, with the numerical simulations.

This study may provide the non-equilibrium properties of the system as the slow mode behavior presented in Section 6 A deep study of the present overview seems to be necessary, which is in realization.

F.U. acknowledges support from the Programma de Becas de Doctorado CONICYT and SR and ET acknowledge the FONDECYT grants N 1130709 and 1120329 respectively.

References

- [1] Nicolis, G. and Nicolis, C. (1988). Master-equation approach to deterministic chaos, *Physical Review A* 38, 427–433
- [2] Nicolis, G., Martinez, S. and Tirapegui, E. (1991). Finite coarse-graining and Chapman-Kolmogorov equation in conservative dynamical systems, *Chaos, Solitons and Fractals*, 1, 25–37.
- [3] Vichniac, G. (1984), Simulating Physics with Cellular Automata, *Physica*, **D 10**, 96-116.
- [4] Pomeau, Y. (1984), Invariant in cellular automata, Journal of Physics A: Mathematical and General, 17 L415–L418.
- [5] Herrmann, H. (1986). Fast algorithm for the simulation of Ising models, Journal of Statistical Physics 45, 145–151
- [6] Takesue, S (1987). Reversible Cellular Automata and Statistical Mechanics, *Physical Review Letters* **59**, 2499–4503.
- [7] Herrmann, H.J., Carmesin, H.O. and Stauffer, D. (1987). Periods and clusters in Ising cellular automata, *Journal of Physics A: Mathematical and General*, **20**, 4939–4948.
- [8] Goles, E. and Rica, S. (2011), Irreversibility and spontaneous appearance of coherent behavior in reversible systems, *The European Physical Journal B*, **D 62**, 127–137.
- [9] Onsager, L. (1944). Crystal Statistics. I. A Two-Dimensional Model with an Order-Disorder Transition, *Physical Review* 65, 117–149.
- [10] Yang, C.N. (1952). The Spontaneous Magnetization of a Two-Dimensional Ising Model, *Physical Review* 85, 808–816.

Appendix B

Article

Around the Ising Model

Publication details

- Title: Around the Ising Model.
- Authors: Fernando Mora, Felipe Urbina, Vasco Cortez, and Sergio Rica.
- Journal: Springer International Publishing, Nonlinear Dynamics: Materials, Theory and Experiments, 173, 329 345, (2015).
- DOI: 10.1007/978-3-319-24871-4 25.
- URL: http://dx.doi.org/10.1007/978-3-319-24871-4_25.

Around the Ising Model

Fernando Mora, Felipe Urbina, Vasco Cortez and Sergio Rica

Abstract This chapter discuss several features and connections arising in a class of Ising-based models, namely the Glauber-Ising time dependent model, the Q2R cellular automata, the Schelling model for social segregation, the decision-choice model for social sciences and economics and finally the bootstrap percolation model for diseases dissemination. Although all these models share common elements, like discrete networks and boolean variables, and more important the existence of an Ising-like transition; there is also an important difference given by their particular evolution rules. As a result, the above implies the fact that macroscopic variables like energy and magnetization will show a dependence on the particular model chosen. To summarize, we will discuss and compare the time dynamics for these variables, exploring whether they are conserved, strictly decreasing (or increasing) or fluctuating around a macroscopic equilibrium regime.

1 Introduction

The Ising model, introduced in the early 1920s, by Lenz [1] and Ising [2] as a thermodynamical model for describing ferromagnetic transitions has evolved as one of the most prolific theories in the twenty century opening a huge number of new areas of knowledge (for an historical review see [3]). The importance of the Ising model raises in its universality and robustness, indeed despite its simplicity, this

F. Mora · F. Urbina · V. Cortez · S. Rica (☒)
Facultad de Ingeniería y Ciencias, Universidad Adolfo Ibáñez,
Avda. Diagonal las Torres 2640, Peñalolén, Santiago, Chile
e-mail: sergio.rica@uai.cl

F. Mora

e-mail: femora@alumnos.uai.cl

F. Urbina

e-mail: felipe.urbina@uai.cl

V. Cortez

e-mail: vcortez@alumnos.uai.cl

© Springer International Publishing Switzerland 2016 M. Tlidi and M.G. Clerc (eds.), *Nonlinear Dynamics: Materials, Theory and Experiments*, Springer Proceedings in Physics 173, DOI 10.1007/978-3-319-24871-4_25

F. Mora et al.

model has been the starting point for the emergence of various subfields in physical (and social) sciences, namely, phase transitions, renormalisation group theory, spin-glasses, lattice field theories, etc.

In the current contribution, we shall discuss four distinct applications of Ising-based models with applications to both statistical mechanics as social sciences. The first one is devoted to the Glauber-Ising time dependent model with applications to decision-choice theory in economics and social sciences. In the 60s Glauber [4], introduced an stochastic time dependent rule to mimic the statistical properties of the original Ising problem. Glauber's dynamics has been considered in the context of social sciences by Brock and Durlauf [5, 6], and, more recently, by Bouchaud [7].

The second topic is Q2R automata model introduced in the 80s by Vichniac [8]. The Q2R¹ possess time reversal symmetry, which is at the core of any fundamental theory in physics. Moreover, the temporal evolution of this automata conserves a quantity which is closely related to the energy of the Ising model [9]. We are interested in this model because is a natural starting point for studying the statistical and typical irreversible behavior of reversible systems. As shown in [10], this system evolves in an irreversible manner in time towards an "statistical attractor", moreover the macroscopic observable, the so called global magnetization, depends on the value of the initial energy following a law which is exactly the one obtained theoretically by Onsager [11] and Yang [12], more than 60 years ago. Moreover, in [13] it is shown how this model exhibits the same features of Hamiltonian systems with many degrees of freedom, that is, a sensibility to initial conditions, positive Lyapunov exponents, among others.

The third model that we shall discuss in this article concerns the Schelling model of social segregation, introduced in the early 70s by Thomas C. Schelling [14–16]. This model became one of the paradigm of an individual-based model in social science. Schelling's main contribution is that shows on the formation of a large scale pattern of segregation as a consequence of purely microscopic rules. More recently, it has been shown that the Ising energy, which is a good measure of segregation, acts as a Lyapunov potential of the system is driven, under particular conditions, by a strictly decreasing energy principle [17].

Finally, we shall discuss a model for dissemination's disease known as Bootstrap percolation, first introduced in the late 70s by Chalupa et al. [18]. In this model a healthy individual may be infected if the majority of its neighbors are infected. On the other hand an infected individual never recovers, so it remains infected forever. This model has been used as a model for disease's propagation. One of the most important questions arising is the determination of the critical number of infected individuals to contamine the whole population.

The paper is organized as follows, in Sect. 2, some common features, as well as, the precise rules for each particular model are explicitly described. Next, in Sect. 3 the main dynamical behavior, the salient properties and the phase transitions are shown and explained, for each of them. Finally, we conclude.

¹Q by four, *quatre*, in french, 2 by two steps automata rule as explicitly written below, and R by reversible.

Around the Ising Model

331

2 Ising-Based Models

2.1 Generalities

2.1.1 The Lattice and the Neighborhood

All models discussed below, display similar features, the system consisting of a lattice with $N \gg 1$ nodes, in which each node, k, may take a binary value $S_k(t) = \pm 1$ at a given time. Each node k on the lattice interacts, in general, with all other individuals, with an interaction coefficient J_{ik} (i denotes an arbitrary node). But in particular, a node, k, may interact only with a finite neighborhood denoted by V_k . The number of neighbors for site k, $|V_k|$, is the total number of non zero J_{ik} for each node. In Fig. 1 we show, as an example, four possible lattice configurations.

2.1.2 The "Energy" and the "Magnetization"

We define the macroscopic observables of the system, by analogy with the original Ising model of ferromagnetism, as follows:

$$E[\{S\}] = -\frac{1}{2} \sum_{i,k} J_{ik} S_i(t) S_k(t) , \qquad (1)$$

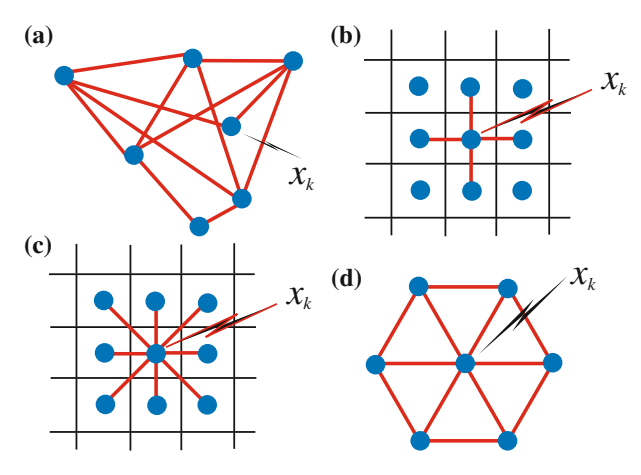


Fig. 1 Examples of lattices and neighborhoods. We illustrate explicitly: \mathbf{a} an arbitrary network with a random number of neighborhoods; and three periodic regular lattices in two space dimensions: \mathbf{b} a square lattice with a von-Neuman neighborhood of 4 individuals (the original lattice of the Ising model with the nearest neighborhood); \mathbf{c} a square lattice with a Moore neighborhood of 8 individuals, and \mathbf{d} a hexagonal lattice with 6 neighborhoods

F. Mora et al.

$$M[\{S\}] = \sum_{k=1}^{N} S_k(t).$$
 (2)

These quantities will be the pertinent observables, and we shall use them to classify the distinct cases that we will be described in the next sections.

2.2 The Time-Dependent Glauber-Ising Model

Glauber [4], in the 60s, introduced a dynamical model for the study of the Ising model. The rule governing Glauber's model is the following:

Let, the local magnetization at the site k and at a time t, be:

$$U_k(t) = B + \sum_i J_{ik} S_i(t), \tag{3}$$

with B being an external magnetic field. Then, the spin's value at the next time step, t+1, will be

$$S_k(t+1) = \operatorname{sgn}(U_k(t)), \tag{4}$$

that is $S_k(t+1) = +1$ if $U_k(t) \ge 0$ and $S_k(t+1) = -1$ if $U_k(t) < 0$. We call (4) the deterministic rule. In probability language, if $U_k(t) \ge 0$, then $S_k(t+1)$ would be +1 with probability 1, and it would be -1 with probability 0. This rule is updated in parallel fashion.

Next, this deterministic rule may be modified by a probabilistic rule, in the following way:

$$S_k(t+1) = \begin{cases} +1 & \text{with probability } p = \frac{1}{1+e^{-\beta U_k(t)}} \\ -1 & \text{with probability } p = \frac{1}{1+e^{\beta U_k(t)}} \end{cases}$$
 (5)

Notice that in the limit $\beta \to \infty$ one recovers the deterministic behavior (4), while in the limit $\beta \to 0$ one reaches a completely random (binomial) dynamics regardless of the value of U, that is $S_k(t+1)$ would be +1 with probability 1/2.

The Glauber rule is indeed a Markov chain which manifests, in a perfect way, the statistical properties of the Ising phase transition for the case of Von-Neuman neighbourhoods, and it also agrees with the mean field approximation for the case of a large number of neighbours. Finally, nowadays the Glauber dynamics is the starting point for numerical simulations of spin glasses systems with random values for the J_{ik} coefficients.

333

2.2.1 Random Decision-Choice Model

Let us consider now a random choice model [5–7] in the context of social sciences. An individual takes a choice based on a combination of decision quantities, namely an individual "decision parameter" f_k , a "global decision" or "public information" parameter F(t) (which could be included in the previous individual decision parameter) and a "social pressure" $\sum_i J_{ik}S_i(t)$.

meter) and a "social pressure" $\sum_i J_{ik} S_i(t)$. Next take, $^2 U_k(t) = f_k + F(t) + \sum_i J_{ik} S_i(t)$, and follow the Glauber deterministic dynamics (4) or more generally the Glauber random dynamics (5).

Due to both, the Ising-like feature as the Glauber Dynamics evolution rule, a phase transition is known to appear. This transition favors the decision into one or another of the two options of the binary variable.

2.3 The Q2R Automata

The Q2R rule considers the following two-step rule which is updated in parallel [8]³:

$$S_k(t+1) = S_k(t-1) \times \begin{cases} +1 & \text{if } \sum_i J_{ik} S_i(t) \neq 0 \\ -1 & \text{if } \sum_i J_{ik} S_i(t) = 0 \end{cases}$$
 (6)

Naturally, it is possible to add, without any difficulty, an external magnetic field B. However, some caution should be taken into account: the model works if $U_k(t) = B + \sum_i J_{ik} S_i(t)$, may vanish, therefore, B and the J_{ik} factors should be integers. For instance in the case of a finite neighborhood, $B + |V_k|$ should be an even number.

The rule (6) is explicitly invariant under a time reversal transformation $t+1 \leftrightarrow t-1$. Moreover, as shown by Pomeau [9], the following quantity, that we may call an energy, despite not being exactly the energy (1)

$$E[\{S(t), S(t-1)\}] = -\frac{1}{2} \sum_{i,k} J_{ik} S_k(t) S_i(t-1), \tag{7}$$

is preserved under the dynamics defined by the Q2R rule (6). Moreover, the energy is bounded by $-2N \le E \le 2N$.

The rule (6) is complemented with an initial condition $S_k(t=0)$ and $S_k(t=1)$ that will be described more precisely in the next section.

²The so called "perceive overall incentive agent function", by Bouchaud [7].

³This two-step rule may be naturally re-written as a one-step rule with the aid of an auxiliary dynamical variable [9].

F. Mora et al.

2.4 Schelling Model for Social Segregation

Schelling model, is also characterized by a binary variable S_k which may take values +1 and -1. We shall say that an individual S_k at the node k is "happy" at his site, if and only if, there are less than θ_k neighbors at an opposite state. θ_k is a tolerance parameter that depends in principle on the node and, it may take all possibles integer values, such that $0 < \theta_k < |V_k|$ (we exclude the cases $\theta_k = 0$ and $\theta_k = |V_k|$ from our analysis). The satisfaction criterion reads⁴

An individual S_k is unhappy at the node k if and only if:

$$\sum_{i \in V_k} S_i = \begin{cases} |V_k| - 2n_k(-1) \le |V_k| - 2\theta_k, & \text{if } S_k = +1\\ 2n_k(-1) - |V_k| \ge 2\theta_k - |V_k|, & \text{if } S_k = -1. \end{cases}$$
(8)

Here $n_k(+1)$ is the number of neighbors of S_k that are in the state +1; and, $n_k(-1)$ the number of neighbors of S_k in the state -1, naturally $n_k(+1) + n_k(-1) = |V_k|$.

Having labeled all different un-happy individuals, one takes randomly two of them in opposite states (one +1, and one -1) and exchanges them. Even when this is not exactly the original Schelling's rule, the present *Schelling's protocol* is a simpler one. In any case, it can be modified in a straightforward way to include for example vacancies [19, 20], different probabilities of exchange [19], multiple states variables [21], etc.

If k and l are these random nodes, then the evolution rules:

$$S_k(t) \to S_k(t+1) = -S_k(t), \quad S_l(t) \to S_l(t+1) = -S_l(t)$$

and for all other nodes $i \neq k \& l$ remain unchanged $S_i(t) \to S_i(t+1) = S_i(t)$.

The protocol is iterated in time forever or until the instant when one state does not have any unhappy individuals to be exchanged.

Notice, that Schelling criteria (8) is deterministic, however the exchange is a random process, therefore two initial configurations will not display the same behavior in detail, but they will evolve to the same statistical attractor [22].

⁴The criteria (8) may be unified in a single criteria [17] (multiplying both sides of the two inequalities by S_k): an individual S_k is unhappy at the node k if , and only if , $S_k \sum_{i \in V_k} S_i \leq |V_k| - 2\theta_k$, which is a kind of energy density instead of the threshold criteria found in Glauber dynamics (4).

Around the Ising Model

335

Schelling's protocol, defined above, has a remarkable property: if $\theta_k > \frac{|V_k|}{2}$ then any exchange $k \leftrightarrow l$, will always decrease the energy

$$E[\{S\}] = -\frac{1}{2} \sum_{k} \sum_{i \in V_k} S_i(t) S_k(t). \tag{9}$$

The energy (9) follows from (1), whenever $J_{ik} = 1$ for neighbors and $J_{ik} = 0$ otherwise

For a proof, we refer to [17]. We shall only add the following remark: if $\theta_k > \frac{|V_k|}{2}$, then the evolution necessarily stops in finite time. This is because the energy (9) is bounded from below by $E_0 = -\frac{1}{2} \sum_{k=1}^N |V_k|$ and because the energy (1) decreases strictly. On the other hand, for $\theta_k < \frac{|V_k|}{2}$, the energy may increase or decrease after an exchange indistinctly.

2.5 Bootstrap Percolation

We shall consider the problem of bootstrap percolation for a given lattice [18]. As in the previous models, each node k interacts with $|V_k|$ neighbors, the neighborhood defined by the set V_k . As before the state, S_k may take values +1 and -1 depending on if it is "infected" or not. At a given "time" the state $S_k(t)$ evolves into $S_k(t+1)$ under the following parallel rule: if a site is not infected, and if the *majority* of its neighbors are infected, then the site becomes infected [23]. On the other hand, if the site is already infected it keeps its infected state.

Summarizing, the evolution rule, which is updated in parallel, may be written in the following general way:

if
$$S_k(t) = -1$$
 and $\sum_k S_k(t) > 0$, then $S_k(t+1) = +1$, (10)

otherwise, if $S_k(t) = 1$ then $S_k(t+1) = 1$.

From the dynamics it follows directly that the energy (9) decreases in time, $E(t+1) \le E(t)$, as well as the magnetization increases in time: $M(t+1) \ge M(t)$. As in the case of the Schelling model, because the energy is a strictly decreasing functional, and because it is bounded from below in a finite network, then the dynamics always stops in finite time.

Finally, let us comment that a problem that has increased in interest in recent times deals with the question of how the total infection depends on the initial configuration which is randomly distributed and such that a site will be at the state $S_k = +1$ with a probability p [24].

F. Mora et al.

Table 1 Recapitulation of the four above mentioned models, and its main conservation properties

Dynamics	Evolution criteria	Energy	Magnetisation
Glauber	$\frac{\operatorname{sgn}(B + \sum_{i} J_{ik} S_i(t))}{\sum_{i} S_i(t)}$	Not conserved	Not conserved
Q2R	$\sum_{i} J_{ik} S_i(t) = 0$	Conserved	Not conserved
Schelling	$sgn(S_k(t)) \sum_{i \in V_k} S_i(t) \le V_k - 2\theta_k$	Not conserved ^a	Conserved
Bootstrap	$\sum_{i \in V_k} S_i(t) > 0$	$\Delta E < 0$	$\Delta M > 0$

^aIf $\theta_k > |V_k|/2$ then $\Delta E < 0$

Naturally, if initially $p \approx 1/2$, then every site has in average the same number of $S_k = +1$ states and $S_k = -1$ in its neighborhood, then the system would percolate almost in one step. However, as p decreases, one can define a probability, P(p), which is the probability that the system would percolate at the end of the evolution process. At the end this probability can be numerically determined.

2.6 Recapitulation

The afore mentioned models have in common a threshold criteria (4), (6), (8), and (10) the subsequent dynamics follows different rules. Therefore one should expect distinct properties.

The Glauber Dynamics does not preserve neither the energy or magnetization, however the Q2R dynamics (Sect. 2.3) does preserve only the energy but does not preserve the magnetization. The Schelling model (Sect. 2.4) does preserve only the magnetization, but if $\theta_k > |V_k|/2$ the system's energy is strictly a decreasing function. Finally, in the infection model of Sect. 2.5, the energy strictly decreases whereas the magnetization is an increasing function of time (Table 1).

3 Ising Patterns, Transitions, and Dynamical Behavior

In this section, we shall roughly describe the essential phenomenology of the Isinglike models and rules described in the previous section, whether they are governed (or not) by the rules of conservation of magnetization energy.

3.1 Glauber and Decision-Choice Model Dynamics

The time dependent Glauber-Ising model shows a very rich phenomenology. As such, the model's behavior has been explored using mean field approximation (the Curie-Weiss law) as well as by direct simulations of the rule (5). Here our macroscopic

Around the Ising Model



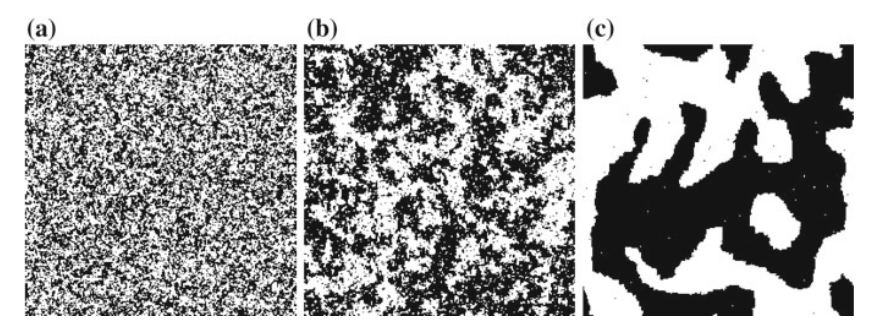


Fig. 2 Snapshots of the patterns for the Glauber-Ising model. The simulation is for a $N=256\times256$ periodic lattice with von Neuman neighborhood. Moreover we take $f_k=0$ and F=0. The parameter of "irrationality" and the magnetization averages are, respectively: **a** corresponds to a paramagnetic phase for $\beta=0.53$ and $\langle M \rangle/N=0.0006$; **b** a critical phase for $\beta=0.82$ and $\langle M \rangle/N=0.02$; and **c** corresponds to a ferromagnetic phase $\beta=1.8$, and $\langle M \rangle/N=0.39$

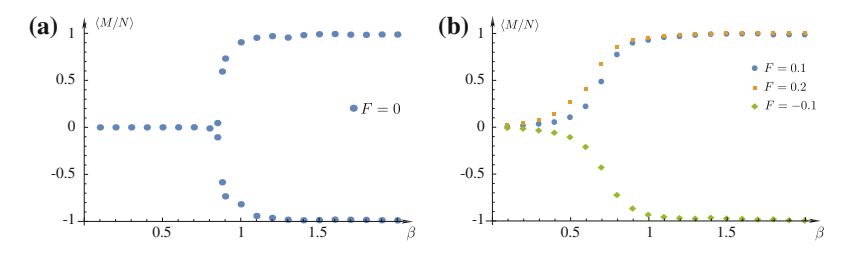


Fig. 3 Average magnetization $\langle M \rangle$ versus β . The average are taken from long time simulations of approximately 20000 time steps. In both cases the random external field is settled to zero $f_k=0$. a Case of F=0; and b Cases of $F=\pm 0.1$ and F=0.2

observable is the total magnetization per site, namely M(t)/N and were M(t) is defined in equation (2). In what it follows, we will only show results for the direct simulation of the Glauber-Ising model (4) and we shall use the terminology of social sciences [7]. In Fig. 2 we show three distinct states characterized by different values of the parameter of "irrationality" β , and a null value for the public information parameter F(t).

In Fig. 3 we show two different figures for the mean magnetization $\langle M \rangle$ /N versus the irrationality parameter β , divided into two groups depending on the non-zero or null value for the public information parameter F(t). Each point, was calculated for a total of approximately 2×10^4 time steps. We can readily observe the appearance of a bifurcation for the case F=0 and β greater than $\beta_c=0.8$.

Therefore, the time dependent Glauber-Ising model displays a transition from a paramagnetic to a ferromagnetic phase for $\beta_c \approx 0.8$ which is in agreement with the critical threshold value of the Ising model, $\beta_c = \log(1 + \sqrt{2}) \approx 0.881...$

⁵In statistical physics, β is the inverse of the thermodynamical temperature, $\beta \sim 1/T$.

F. Mora et al.

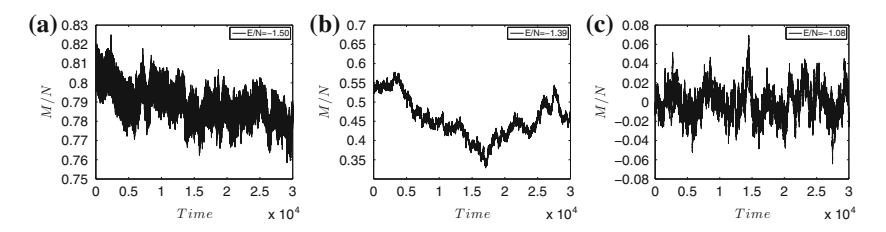


Fig. 4 Three types of magnetization dynamics for a running time of $T = 3 \times 10^4$ time steps, and considering three different values of energy. a Corresponds to an initial energy E/N = -1.50, b corresponds to an initial energy E/N = -1.39 and c corresponds to an initial energy E/N = -1.08. The three figures show the fluctuations in the macroscopic observable M(t)

3.2 Q2R Dynamics

We shall now present the dynamics of the Q2R model for the case of von Neuman vicinity (the coupling interaction $J_{ik} = 1$ for the four closest neighbors), which is the original Q2R cellular automata [8].

The time evolution of magnetization, given an initial energy value E/N, provides a direct observation of the spin's dynamics and fluctuations. In what it follows, we will base our results and analysis taking a periodic grid of size $N=256\times256$.

When the initial energy value is E/N=-1.50, which refers to Fig. 4a, it can be seen that the system's dynamics fluctuates without significative changes in the magnetization's value. This means that the overall set of spins are oriented in a preferred direction. This is known as a ferromagnetic state. If we raise the initial energy value and take E/N=-1.39, which corresponds to Fig. 4b, the dynamics abruptly fluctuates because of the closeness to the critical energy value: E_c/N [10]. Finally, if the initial value of the energy is greater than in the previous cases, e.g. E/N=-1.08, Fig. 4c shows how the dynamics of magnetization decays reaching a zero mean value $\langle M \rangle \approx 0$.

Similarly, Fig. 5 shows some characteristic snapshots of the spin field patterns at a given time for the same energy per site. When the energy value is E/N = -1.50 (see Fig. 5a), it can be seen how the spins are organized with a well defined magnetization, namely $S_k = +1$ or $S_k = -1$. This is a ferromagnetic phase. However, when the initial energy value is E/N = -1.39 (close to the critical energy), as shown in Fig. 5b, the system generates patterns characterized by well defined clusters of states. Finally, for an energy E/N = -1.08 (see Fig. 5c) the system shows an homogeneous state with the spin distributed more or less randomly, which characterizes a paramagnetic phase.

Also it can be shown that the average magnetization $\langle M \rangle$ depends critically on the initial energy, E/N, of the system (Fig. 6).⁶

⁶Q2R is a micro canonical description of the Ising transition, therefore we use the energy in absence of any temperature. In [10] it is shown the excellent agreement among the Q2R bifurcation diagram with the Ising thermodynamical transition.

Around the Ising Model



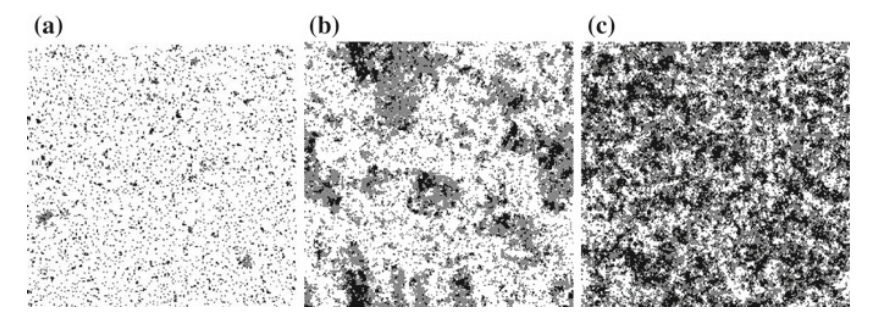
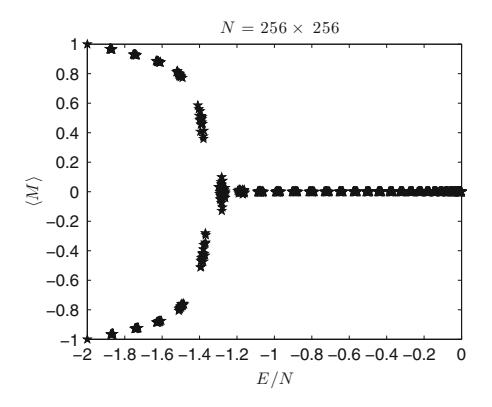


Fig. 5 Snapshots of spin structure at $T=3.5\times 10^4$ considering three initial values. **a** Corresponds to an initial energy E/N=-1.50 and a magnetization M/N=0.79, **b** corresponds to an initial energy E/N=-1.39 (which is close to the transition energy $E/N=-\sqrt{2}$) and M/N=0.455; and **c** corresponds to an initial energy E/N=-1.08 and M/N=0.012

Fig. 6 Phase transition diagram for the average Magnetization $\langle M \rangle$ versus initial energy E/N, for a grid size $N=256\times256$



Finally, we can state three fundamental features from the above phase diagram. First, there exists a zone in which the system stays into a ferromagnetic state when the value of the energy is lower than the critical energy $E < E_c$. Secondly, there is a second order phase transition at $E_c/N = -\sqrt{2}$ and it is formally equivalent to the Ising critical temperature [10]. Third, when the initial energy value is greater than the critical energy $E > E_c$, the system presents a paramagnetic phase, with a magnetization value $\langle M \rangle = 0$.

3.3 Schelling Dynamics

We shall characterize the dynamics of Schelling model for the particular case in which the system is a two dimensional periodic lattice, and each site possess the same neighborhood consisting in the |V| closest individuals. We shall consider also that the parameter θ_k is uniform, that is, $\theta_k = \theta$.

F. Mora et al.

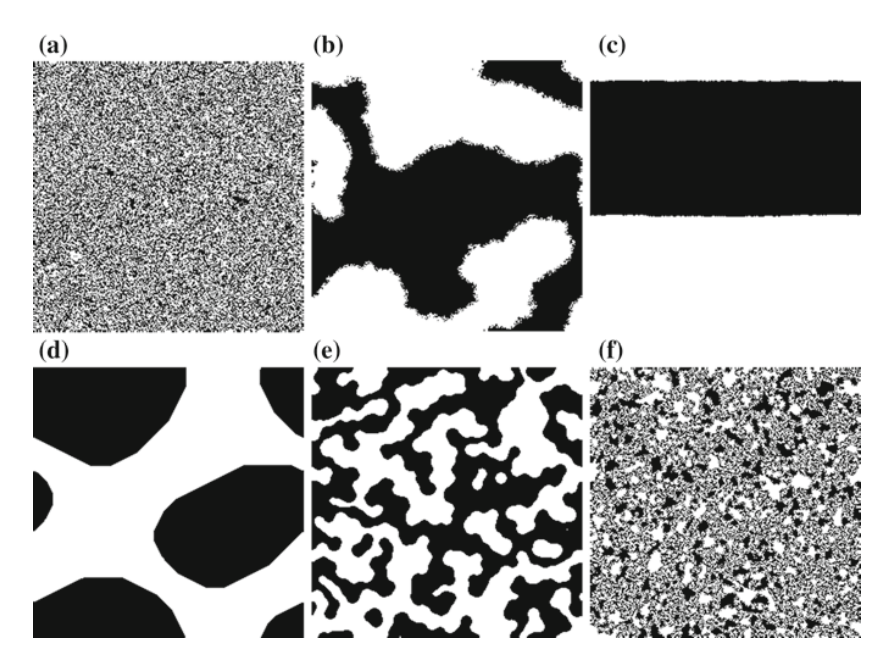


Fig. 7 Schelling's patterns for various satisfaction parameter θ in a square periodic lattice of N=256 nodes. The vicinity is uniform and contains |V|=20 elements. $\mathbf{a} \ \theta=5$; $\mathbf{b} \ \theta=6$; $\mathbf{c} \ \theta=9$; $\mathbf{d} \ \theta=10$ (eventually this case the two spots observed merges into a single one, this coalescence dynamics, however, it happens after a longtime); $\mathbf{e} \ \theta=11$ and $\mathbf{f} \ \theta=15$, are two cases whenever the energy is a strictly decreasing function so the dynamics stops in finite time, in the former case this happens after a time so segregation is possible, however in the later case the dynamics stops shortly after the Schelling algorithm started. For $\theta=15$ we say that this is a frustrated dynamics, because the system cannot reach the ground state energy because the dynamics stops after one of the population is completely happy

Figure 7 displays an example of typical patterns arising in the Schelling's model. As it can be observed, the dynamics depends critically on the value of the tolerance parameter θ , defined above. More precisely, if θ is larger or smaller than $\theta_{c_1} = |V|/4$, $\theta_c = |V|/2$, and $\theta_{c_2} = 3|V|/4$. The initial state was chosen randomly with a binomial distribution, that is $S_k(t=0)$ was +1 with probability 1/2 and -1 with the same probability. Hence, the total magnetization is $M(t=0) \approx 0$, and it is kept fixed during the evolution.

The simulation shown in Fig. 7, corresponds to a Schelling rule with a vicinity of |V|=20 elements. Clearly three different cases can be distinguished, and at least three transition points, namely $\theta_{c_1}=|V|/4$, $\theta_c=|V|/2$, and $\theta_{c_2}=3|V|/4$. For $1<\theta\leq |V|/4$ (see Fig. 7a) one observes a non-segregated pattern, the states $S_k=\pm 1$ are swapping, more or less randomly in the system, without a formation of any kind of large scale structure. In a coarse graining scale, for instance, the scale of the vicinity, the coarse-grained magnetization, namely, $m=\frac{1}{|V|}\sum_{i\in V_k}S_i(t)$ is zero everywhere,

as well as the energy. In this situation, it is tempting to make an analogy with the Ising paramagnetic phase. For $|V|/4 < \theta \le |V|/2$, one observes how a segregation pattern arises (see Fig. 7b, c). More important the coarse-grained magnetization is locally non-zero, and the pattern presents domain walls, which are characteristic of a ferromagnetic phase in the Ising-like terminology. For $|V|/2 < \theta \le 3|V|/4$, one observes also segregation (see Fig. 7e), but the dynamics stops in a finite time. The final state is a quenched disordered phase for which one may conjecture an analogy with a "spin glass" phase, and the appearance of a kind of long-range order. The case $\theta = 3|V|/4$ in (see Fig. 7f) it is interesting because, although the are some islands of segregation, the system also recovers its original heterogeneity, with almost a null coarse-grained magnetization m.

3.4 Bootstrap Percolation

The spin dynamics for the case of Bootstrap percolation of Sect. 2.5 is always characterized by an energy decreasing principle, moreover because a+1 spin never flips to a-1, the magnetization is mandated to increase up to a constant value because of the impossibility to infect more individuals, or simply because the system has been fully percolated by the +1 spin states.

As said in Sect. 2.5, we shall consider a random initial state with a fraction p of the spins at the state $S_k = +1$ (that is, a fraction p of the population would be infected).

It is observed, that for a moderately large value of p, say $p \approx 1/2$, the system becomes unstable very fast, percolating the $S_k = +1$ state everywhere almost instantaneously.

However, as one decreases p, the system presents a well defined scenario. Figure 8 shows the typical evolution of a percolation pattern in time. More precisely, the system nucleates bubbles of infected states ($S_k = +1$) and two scenarios are possible, either these bubbles continues to grow or they stop (compare Fig. 8b, c). In analogy with the instability of a first order phase transition, it should exist a critical radius of nucleation that depends explicitly on p.

This critical radius of nucleation maybe estimated in the limit of large vicinity, in other words, in the range of validity of the mean field approximation. Let be p the fraction of infected sites initially distributed randomly in the system and a the radius of the vicinity ($\pi a^2 = |V|$). We shall add an infection bubble with a radius R (see Fig. 9a). A $S_k = -1$ state in the boundary of the infected circle will become infected if $\sum_k S_k(t) = (2p-1)(\pi r^2 - A(R)) + A(R) > 0$, where A(R) is the surface of the portion of the circle inside the infection bubble (see Fig. 9b). Therefore, the bubble will infect neighbors and will propagate into the system, if

⁷Notice that, as already said, the total magnetization is constant in the Schelling model. Therefore we cannot match the Schelling transitions observed here with the phase transition for the cases of the Glauber-Ising and the Q2R models.

F. Mora et al.

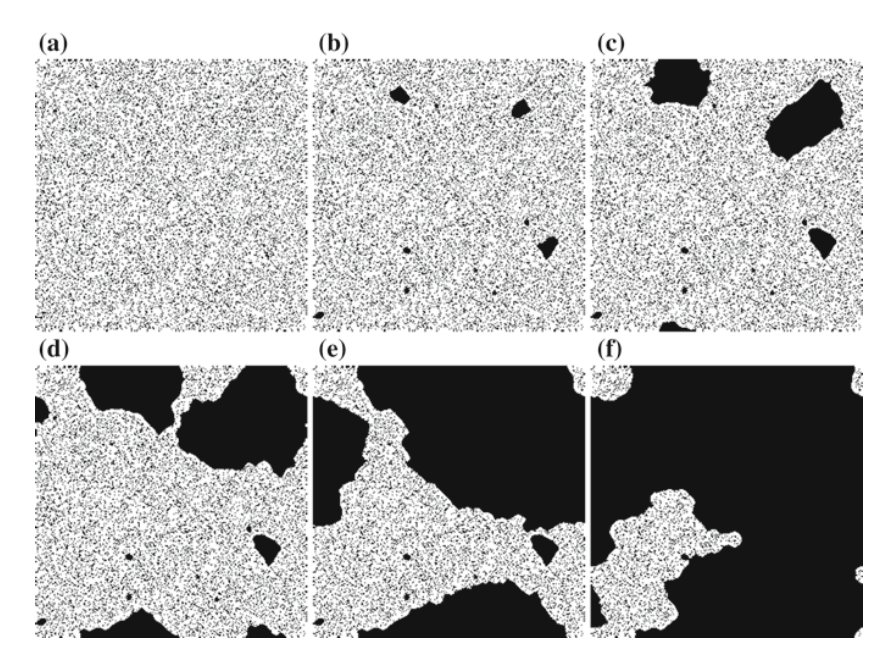
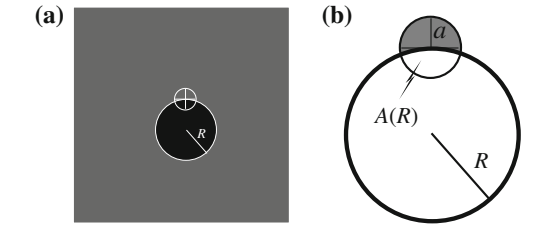


Fig. 8 Bootstrap percolation's patterns at six different time steps. The network is a square periodic lattice of $N=256^2$ sites with a uniform vicinity of |V|=24 sites. **a** Display the initial random state with an initial fraction 0.2 of $S_k=+1$ (that is, a given site is +1 with probability 0.2, and -1 with probability 0.8); In **b** one observes the nucleation of bubbles, which eventually would propagate the +1 state over the random phase; In **c** one observes that some infected bubbles have not reach the critical size and they do not propagate; however, in **d** big bubbles invade the system transforming the interface in a front propagation over the whole system (**e**) and (**f**)

Fig. 9 a Scheme for the mean field estimation of the critical radius of infection. The *gray* region represents the random initial data with a fraction p of +1. **b** Details of the geometry for the calculation of A(R)



$$\frac{A(R)}{\pi a^2} > \frac{1 - 2p}{2(1 - p)}. (11)$$

The surface A(R) follows from a direct geometrical calculation. In the large R/a limit, one gets

$$\frac{A(R)}{\pi a^2} \approx \frac{1}{2} - \frac{a}{3\pi R} + \mathcal{O}(R^{-3}),$$

Around the Ising Model



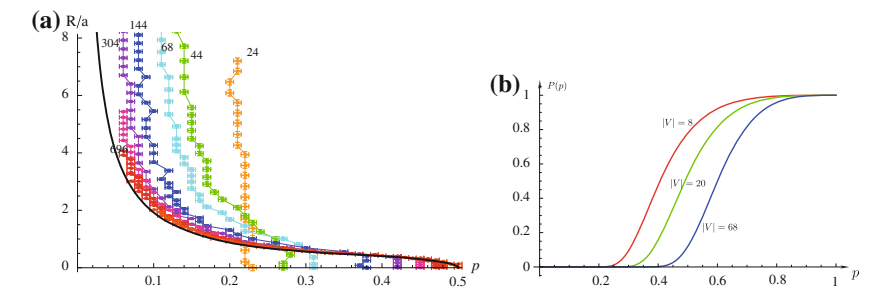


Fig. 10 a Critical radius of nucleation R/a as a function of p. As expected as $p \to 1/2$ the critical radius is zero, while as $p \to 0$ the critical radius diverges. The points correspond to the numerical simulations for different values of the vicinity size: $|V| = \{24, 44, 68, 144, 304, 696\}$ as indicated in the figure. **b** Estimation of the lower bound of the probability P(p) of having a critical nucleation bubble of infected states, for |V| = 8, |V| = 20 and |V| = 68. One notices that this probability takes-off around a precise value of p

therefore, one concludes that the critical radius of nucleation scales as

$$\frac{R_c}{a} \approx \frac{2(1-p)}{3\pi p}.$$

Figure 10 shows a numerical study of the nucleation radius, for various vicinity sizes, |V|, as a function of p. Moreover the figure also presents the mean field estimation by an explicit geometrical calculation of the surface A(R) and using the critical condition (11). One sees that the mean field approach matches perfectly with the data in the large |V| limit.

However, a question remains open: what is the probability to obtain, ab-initio a bubble with a radius larger than R_c ? This probability seems to be very small, because it is proportional to the probability to obtain πR_c^2 sates +1 all together, that is

$$P_{\text{bubble}} \approx p^{\pi R_c^2} = p^{|V|(R_c/a)^2} \sim p^{|V|\frac{4(1-p)^2}{9\pi^2 p^2}},$$

with R_c/a the function of p plotted in Fig. 10. Although, this probability P(p) is quite small, it is a lower bound for the problem of Bootstrap percolation. If, initially, a bubble has a radius greater than $R_c(p)$, then the system percolates, and the nucleation bubble may not initially exist, but it may be built solely by the evolution, this provides a better estimation of the probability P(p) of percolation.

4 Discussion

We have shown how different models amalgamate their underlying behavior under the common principle of the Ising-based models: Phase transitions, Bifurcations and Phase Diagrams and most important, the existence of a core principle, e.g., energy F. Mora et al.

minimization which appears to be a robust feature of these models and which would require a deeper consideration.

It is a remarkable fact, however, how despite a continued interest over the last century, the Ising model continues to fascinate and amaze us, not only on it's original context, but also in some other areas of knowledge were it has been applied. The "paramagnetic-ferromagnetic" transition can be recovered in all models described here, with deeper consequences, for example, in the field of human behavior, specially social sciences. Here we can ask ourselves for example: can the sudden changes of opinion before an election or the choice of a product or racial segregation be related to the basic physics of the Ising model? Even more, the existence of an energy principle, something completely excluded and extraneous to the field of Social Sciences, seems to be the main thread behind, for studying and trying to understand human and social behavior. Certainly, delving deeper on this energy principle would require more attention and research. Finally we conclude by asking, Can we have some hope, in a near future and in the context of Social Science, of being able to develop predictive tools for studying and understanding better the human behavior?

Acknowledgments The authors acknowledge Eric Goles, Pablo Medina, Iván Rapaport, and Enrique Tirapegui for their partial contribution to some aspects of the present paper, as well as Aldo Marcareño, Andrea Repetto, Gonzalo Ruz and Romualdo Tabensky for fruitful discussions and valuable comments on different topics of this work. This work is supported by Núcleo Milenio Modelos de Crisis NS130017 CONICYT (Chile). FU. also thanks CONICYT-Chile under the Doctoral scholarship 21140319 and Fondequip AIC-34.

References

- 1. W. Lenz, Physikalische Zeitschrift 21, 613–615 (1920)
- 2. E. Ising, Beitrag zur Theorie des Ferromagnetismus. Zeitschrift für Physik 31, 253–258 (1925)
- 3. S.G. Brush, History of the Lenz-Ising Model Rev. Mod. Phys. 39, 883 (1967)
- R.J. Glauber, Time-dependent statistics of the Ising model. J. Math. Phys. 4, 294–307 (1963). doi:10.1063/1.1703954
- W.A. Brock, S.N. Durlauf, A formal model of theory choice in science. Econ. Theory 14, 113–130 (1999)
- W.A. Brock, S.N. Durlauf, Interactions-based models, ed. by J.J. Heckman, E. Leader. Handbook of Econometrics, 5, Chapter 54, pp. 3297–3380 (2001)
- J.-P. Bouchaud, Crises and collective socio-economic phenomena: simple models and challenges. J. Stat. Phys. 151, 567–606 (2013)
- 8. G. Vichniac, Simulating physics with cellular automata. Physica D 10, 96–116 (1984)
- 9. Y. Pomeau, Invariant in cellular automata. J. Phys. A: Math. Gen. 17, L415-L418 (1984)
- E. Goles, S. Rica, Irreversibility and spontaneous appearance of coherent behavior in reversible systems. Eur. Phys. J. D 62, 127–137 (2011)
- L. Onsager, Crystal statistics. I. A two-dimensional model with an order-disorder transition. Phys. Rev. 65, 117–149 (1944)
- C.N. Yang, The spontaneous magnetization of a two-dimensional Ising model. Phys. Rev. 85, 808–816 (1952)
- F. Urbina, S. Rica, E. Tirapegui, Coarse-graining and master equation in a reversible and conservative system. Discontin. Nonlinearity Complex. 4(2), 199–208 (2015)
- 14. T.C. Schelling, Models of segregation. Am. Econ. Rev. 59, 488–493 (1969)

Around the Ising Model

345

- 15. T.C. Schelling, Dynamic models of segregation. J. Math. Sociol. 1, 143–186 (1971)
- 16. T.C. Schelling, Micromotives and macrobehavior (W.W. Norton, New York, 2006)
- N. Goles Domic, E. Goles, S. Rica, Dynamics and complexity of the Schelling segregation model. Phys. Rev. E 83, 056111 (2011)
- 18. J. Chalupa, P.L. Leath, G.R. Reich, Bootstrap percolation on a Bethe lattice. J. Phys. C Solid State Phys. 12, L31–L35 (1979)
- D. Stauffer, S. Solomon, Ising, Schelling and self-organising segregation. Eur. Phys. J. B 57, 473 (2007)
- A. Singh, D. Vainchtein, H. Weiss, Schelling's segregation model: parameters, scaling, and aggregation 21, 341–366 (2009)
- 21. L. Gauvin, J. Vannimenus, J.-P. Nadal, Eur. Phys. J. B 70, 293 (2009)
- 22. V. Cortez, P. Medina, E. Goles, R. Zarama, S. Rica, Attractors, statistics and fluctuations of the dynamics of the Schelling's model for social segregation. Eur. Phys. J. B 88, 25 (2015)
- J. Balogh, B. Bollobás, R. Morris, Majority bootstrap percolation on the hypercube. Comb. Probab. Comput. 18, 17–51 (2009)
- J. Balogh, B. Pittel, Bootstrap percolation on the random regular graph. Random Struct. Algorithms 30, 257–286 (2007)

Appendix C

Article

Master equation approach to reversible and conservative discrete systems

Publication details

- Title: Master equation approach to reversible and conservative discrete systems.
- Authors: Felipe Urbina, and Sergio Rica.
- Journal: Physical. Review. E, 94, 062140, (2016).
- DOI: 10.1103/PhysRevE.94.062140
- URL: http://link.aps.org/doi/10.1103/PhysRevE.94.062140.

American Physical Society: Kaleidoscopes, December 2016.

URL: http://journals.aps.org/pre/kaleidoscope/pre/94/6/062140

Master equation approach to reversible and conservative discrete systems

Felipe Urbina and Sergio Rica

Facultad de Ingeniería y Ciencias and UAI Physics Center, Universidad Adolfo Ibáñez, Avenida Diagonal las Torres 2640, Peñalolén, Santiago, Chile (Received 9 August 2016; published 28 December 2016)

A master equation approach is applied to a reversible and conservative cellular automaton model (Q2R). The Q2R model is a dynamical variation of the Ising model for ferromagnetism that possesses quite a rich and complex dynamics. The configuration space is composed of a huge number of cycles with exponentially long periods. Following Nicolis and Nicolis [G. Nicolis and C. Nicolis, Phys. Rev. A 38, 427 (1988)], a coarse-graining approach is applied to the time series of the total magnetization, leading to a master equation that governs the macroscopic irreversible dynamics of the Q2R automata. The methodology is replicated for various lattice sizes. In the case of small systems, we show that the master equation leads to a tractable probability transfer matrix of moderate size, which provides a master equation for a coarse-grained probability distribution. The method is validated and some explicit examples are discussed.

DOI: 10.1103/PhysRevE.94.062140

I. INTRODUCTION

In statistical physics one basically considers a large set of reversible and conservative ordinary differential equations for the description of particle dynamics. The temporal evolution for this cumbersome problem, even for a modest number of particles, requires a statistical description that introduces the concept of a probability distribution function for the phase space of the system. Irreversibility, equilibrium, and, more importantly, nonequilibrium properties emerge from this probability conception of systems (with a large number of degrees of freedom) and its deterministic evolution. Briefly, the methodology reduces (under some assumptions) to a kinetic description that displays an irreversible behavior to equilibrium observed in macroscopic systems. The assumptions for this approach are (i) macroscopically, a system is described by a finite set of observables, (ii) the robust instability of the microscopic motions, which is at the basis of the sensitivity to initial conditions and the ergodic assumption, and (iii) a stosszahlansatz that introduces explicitly a broken before-after symmetry for the evolution of the probability distribution.

Nicolis *et al.* [1,2] introduced a systematic coarse-graining approach for the treatment of the macroscopical variables. As a consequence, this coarse graining breaks naturally the past-future symmetry in time, leading to an irreversible master equation for a reduced probability distribution function of the system. In the current paper we apply this systematic approach to conservative and explicit reversible cellular automata. In particular, we consider the Q2R model, introduced by Vichniac [3], which is a cellular automaton that runs on a two-dimensional grid of finite size and is reversible in a physical sense, that is, not only is the automaton rule invertible, but the backward rule reads exactly the same as the forward one. Moreover, it was shown by Pomeau [4] that the Q2R automaton possesses a conserved energy like quantity.

The main reason to apply the coarse-graining approach to a cellular automaton instead of to a coupled system of ordinary differential equations is because a cellular automaton is a discrete model with Boolean entities as microscopic variables, thus, the system is numerically reversible and conservative. In consequence, Q2R seems to be a good benchmark to test the principles of statistical physics. However, the phase space is

finite, hence the dynamical system only possesses fixed points and periodic orbits; therefore it cannot be ergodic, at least in the usual sense of continuous dynamics. Nevertheless, for large enough systems, the phase space becomes huge and the periodic orbits may be, as we show, exponentially long, thus, in practice, of infinite period. Further, if the initial state is random, the temporal behavior may be quite random and it possesses many properties of chaotic systems, such as sensitivity to initial conditions and mixing. For any purpose, the observation of a short periodic orbit is really improbable for large enough systems with random initial conditions. In general, there is a huge number of initial conditions that are almost ergodic.

By "almost ergodic" we mean that the original Q2R system is formally not ergodic, because it only possesses finite periodic orbits. Although finite, these periodic orbits may be exponentially long, so an arbitrary initial condition explores vastly the phase space, validating the equivalence of ensemble and temporal averages. Indeed, numerical studies confirm that the premises of statistical physics are valid, in particular, observables may be computed using standard methods of statistical physics. We will show that temporal averages of a macroscopic quantity provide the same information as the master equation for the coarse-grained distribution functions.

The study of the dynamics and properties of the Q2R model has had a long history. Soon after the seminal works of Vichniac [3] and Pomeau [4], Herrmann [5] implemented the Q2R algorithm to study the two-dimensional Ising model in the frame of the microcanonical ensemble. He studied the global magnetization, obtaining an excellent representation for the magnetization as a function of the initial conserved energy, displaying a coherent picture for the phase transition of the Ising model. Later, Herrmann et al. [6] studied numerically the probability to reach an infinitely long period for some energies. Moreover, if the energy is large enough, this probability tends to unity [6]. Next Takesue [7] focused on the possible realization of statistical mechanics for reversible cellular automata. His studies concerned explicitly all classes of rules in the one-dimensional case, the Q2R being only a special case. However, the Q2R model (90R in his terminology) is the analog of an ideal gas of particles with speeds +1 or -1, a system that cannot reach equilibrium in practice. However, it is

ergodic only in thermodynamical equilibrium. More recently, in Ref. [8], Goles and Rica studied numerically the irreversible behavior and the existence of a spontaneous transition from a noncoherent state to a coherent state.

The present article is organized as follows. The Q2R model, its main features, and findings are presented in Sec. II, which is subdivided as follows: We briefly report the numerical studies of Ref. [8] in Sec. II A; the phase-space properties, in particular some results on the distribution of periods of the dynamics, are reported in Sec. IIB; the sensitivity to initial conditions is discussed in Sec. IIC; and the scope of the paper is presented in Sec. II D. Section III introduces the notion of a master equation for the statistical description of the dynamics. In Sec. IV we provide some precise examples, where a coarse graining is realized, in order to get an adequate and tractable master equation. We provide an exhaustive validation of the technique and we discuss different coarse graining over the phase space. Finally, we summarize in Sec. V.

II. THE Q2R MODEL

For simplicity, we consider a regular two-dimensional lattice with $N = L^2$ nodes, in which each node is only seen by its four closest neighbors (the von Neumann neighborhood); we use periodic boundary conditions. Each node k possesses a discrete value x_k that may take a value +1 or -1. The Q2R model, introduced by Vichniac [3], is based upon the following two-step rule:

$$x_k^{t+1} = x_k^{t-1} \phi \left(\sum_{i \in V_k} x_i^t \right),$$

where the function ϕ is such that $\phi(s=0)=-1$ and $\phi(s)=$ +1 if $s \neq 0$. In the sum V_k denotes the von Neumann neighbor of the site k. The reversibility follows directly from the inverse relation $x_k^{t-1} = x_k^{t+1}\phi(\sum_{i \in V_k} x_i^t)$, which is the backward rule [notice that $\phi(\sum_{i \in V_k} x_i^t)^2 = 1$ in all cases]. This two-step rule may be naturally rewritten as a one-step

rule by introducing a second dynamical variable [4]

$$y_k^{t+1} = x_k^t, \quad x_k^{t+1} = y_k^t \phi\left(\sum_{i \in V_k} x_i^t\right).$$
 (1)

The rule (1) is complemented with the initial condition $x_k^{t=0}$ and $y_k^{t=0}$.

As shown by Pomeau [4], the energy

$$E[\{x^t, y^t\}] = -\frac{1}{2} \sum_{\langle i, k \rangle} x_k^t y_i^t \tag{2}$$

is conserved, $E[{x^t, y^t}] = E[{x^{t=0}, y^{t=0}}]$, under the dynamics defined by the Q2R rule (1). Moreover, the energy is bounded by $-2N \le E \le 2N$.

Despite the existence of an energylike quantity, it is not possible to speak about a Hamiltonian for a discrete dynamics because the variables x^t and y^t and the energy (2) are discrete quantities [4]. Moreover, supported by the existence of a large number of periodic orbits, it is believed that Q2R possesses a large number of other invariants. An example of additional conserved quantities are the staggered invariants [9]. Indeed, for a square periodic lattice of even size L ($N = L^2$), the full lattice may be divided into two sublattices as follows. We denote by k_x and k_y the indices of the full square. Then we define the W sublattice by all points such that $k_x + k_y$ is an even number, while the B lattice is characterized by the condition $k_x + k_y$ being an odd number. (In other words, these sublattices represent the white and black fields in the chessboard.) Then we define

$$E^{W}[\{x^{t}, y^{t}\}] = -\frac{1}{2} \sum_{k_{x} + k_{y} \text{ even}} x_{k}^{t} \sum_{i \in V_{k}} y_{i}^{t},$$

$$E^{B}[\{x^{t}, y^{t}\}] = -\frac{1}{2} \sum_{k_{x} + k_{y} \text{ odd}} x_{k}^{t} \sum_{i \in V_{k}} y_{i}^{t}.$$

The conserved energy (2) may be rewritten as $E[\{x^t, y^t\}] =$ $E^{W}[\{x^{t}, y^{t}\}] + E^{B}[\{x^{t}, y^{t}\}]$. Further,

$$J[\{x^t, y^t\}] = (-1)^t (E^W[\{x^t, y^t\}] - E^B[\{x^t, y^t\}])$$
 (3)

is also an invariant, i.e., $J[\{x^t, y^t\}] = J[\{x^{t=0}, y^{t=0}\}]$. This extra invariant splits the subspace of constant E into a subset of constant E and constant J. The role of this staggered invariant in the macroscopic behavior will be not be investigated in the present work.

A. Long-time dynamics of the Q2R cellular automata

Numerical simulations of the Q2R model in two space dimensions and for large system sizes, e.g., $N = 256 \times 256$, and random initial conditions show that the dynamics displays a fluctuating spatiotemporal pattern showing regions with states +1 and sectors with states -1, as well as zones with chessboardlike patterns [8]. The full patterns will be characterized by the global magnetization

$$M(t) = M[\{x^t\}] = \sum_{k} x_k^t.$$
 (4)

Naturally, the function M is restricted to the set $\{-N, -N + \}$ $2, \ldots, N-2, N$, therefore there are N+1 possible states of magnetization.

A detailed characterization of the evolution, as well as the fluctuations, for the magnetization has been treated in detail in Ref. [8]. Briefly, after a transient the average magnetization depends mainly on the initial energy. If the energy is low, one sees that the average magnetization evolves slowly in time to an equilibrium state with an almost constant value plus weak fluctuations. For larger energies, the fluctuations play an important role. One may observe that the system is in an almost stable state, but then suddenly jumps into a metastable state with zero average magnetization, and then jumps into an opposite magnetization state [8].

The plot of the temporal average for the global magnetization versus the energy is reported in Fig. 1. One can see that the magnetization spontaneously increases below a critical energy per site around $E_c/N = -1.4$, which is close to the critical energy of the Ising model $E_c/N = -\sqrt{2}$ [10,11]. Moreover, in Refs. [5,8] the magnetization is compared as a function of the internal energy of the system, showing a close agreement with numerical values.

PHYSICAL REVIEW E **94**, 062140 (2016) APPENDIX C. ARTICLE

From the data one has that for 3×3 and 4×4 , $\alpha \approx 0.6$, but this value varies as the lattice size increases. Here one notices a dramatic difference among the cases depending on |E| (greater or smaller than $E_c = \frac{2}{\alpha} \ln 2$). If |E| is greater than $N = 16 \times 16$ E_c the probability to see a long period is exponentially small, but for $|E| < E_c$ this probability reaches unity. Higher lattice sizes confirm this scenario but modify slightly the value of α . This behavior is consistent with the numerical simulations of Ref. [6]. C. Sensitivity to initial conditions

The sensitivity to initial conditions of Q2R has been discussed previously in Ref. [8]. In fact, when starting from two distinct initial conditions, which share the same energy and J, they will evolve along two different paths. As the distance in phase space is bounded, these two cycles will diverge in a nonexponential way. However, the separation growth between them is fast enough so as to be completely analogous with the concept of sensitivity to initial conditions.

To perform this study we require two close enough initial configurations. A first initial configuration $\{x,y\}^{t=0}$ is arbitrarily chosen. The second one is built by swapping a single site \bar{k} in the previous configuration. This site is randomly selected such that the average magnetization due to its neighbors is zero (that is $\sum_{i \in V_i} x_i = 0$ or $\sum_{i \in V_i} y_i = 0$). In this way, both initial configurations have the same energy. Finally, running independently both initial configurations, a separation distance between both paths can be measured by employing the so-called Hamming or Manhattan distance defined as

$$d_{H}(t) = \frac{1}{4N} \sum_{k=1}^{N} (|x_{k}^{t} - \bar{x}_{k}^{t}| + |y_{k}^{t} - \bar{y}_{k}^{t}|),$$

with $\{x,y\}^t$ and $\{\bar{x},\bar{y}\}^t$ denoting two different sequences belonging to two different cycles. It can be shown numerically that $d_H(t)$ grows approximately as t^2 (see Ref. [8] for details).

D. Scope of the paper

Though the Q2R model is quite simple its dynamics is usually very rich, as it has been documented extensively in the literature. Moreover, this conservative and reversible system appears to behave as a typical macroscopic system, as the number of degrees of freedom increases, showing a typical irreversible behavior, sensitivity to initial conditions, a kind of mixing, etc. It is believed that this Q2R is a good representation of an Ising model in thermodynamical equilibrium.

The phase space of the Q2R system of N sites possesses 22N states, which are partitioned in different subspaces of constant energy, which are partitioned into a large number of smaller subspaces of periodic orbits or fixed points. Notice that, because the system is conservative, there are neither attractive nor repulsive limit sets; all orbits are fixed points or cycles.

This feature of the phase space is schematized in Fig. 2(a), where the constant energy subspace shares in principle many cycles and fixed points. An arbitrary initial condition of energy E falls into one of these cycles and runs until it returns to the initial configuration after a time T, which could

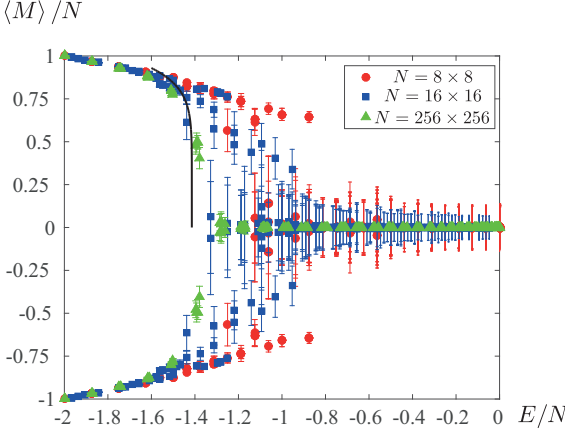


FIG. 1. Magnetization curves as a function of initial energy for three different system sizes $N = 8 \times 8$, $N = 16 \times 16$, and N = 256×256 , as indicated in the legend. Each point corresponds to a different initial condition; in this case we sample different energies. As it can be noticed, there is a finite system dependence on the critical behavior of the system. Indeed, the critical behavior disappears for small system sizes $N = 8 \times 8$ and $N = 16 \times 16$, whereas for large systems the magnetization curve reaches a critical behavior. The continuous line represents the well known statistical mechanics calculation for the Ising model $M/N \approx 2^{5/16} (\sqrt{2} + E/N)^{1/8}$.

We emphasize that the main feature of the Q2R automaton is that it shows a deterministic microcanonical dynamics. Moreover, as shown in Fig. 1, for larger size systems, the results agree with the thermodynamical calculations in an infinite system size [10,11]. On the other hand, other probabilistic evolutions, such as Monte Carlo simulations or Glauber dynamics [12], deal with a spin system in contact with a thermal bath, that is, in canonical equilibrium. However, as expected, both methodologies share the same macroscopic equilibrium.

B. Phase space

The configuration space of all states is defined through all possible values of the state $\{x,y\}$. The resulting space is composed of the 2^{2N} vertices of a 2N-dimensional hypercube. The smallest possible system corresponds to an $N = 2 \times 2$ lattice. In this case there are $2^{2\times 4} = 2^8 = 256$ states and the phase space is a hypercube in dimension 8. However, the dynamics is too simple; it contains cycles of period 4 at most. The phase space for a 4×4 system is the largest possible one that can be studied exactly, case by case. In this case the system possesses $2^{2 \times 16} = 2^{32}$ states and it contains a rich variety of cycles [13]. This case will be studied deeply as a good benchmark for conjectures in larger-dimensional systems.

As an example, from this case, it is observed that the total number of cycles n(T, E) of period T and energy E would be bounded by [14]

$$n(T,E) < \frac{1}{T} 2^{2N} e^{-\alpha |E|} \sim e^{2N \ln 2 - \alpha |E|}.$$

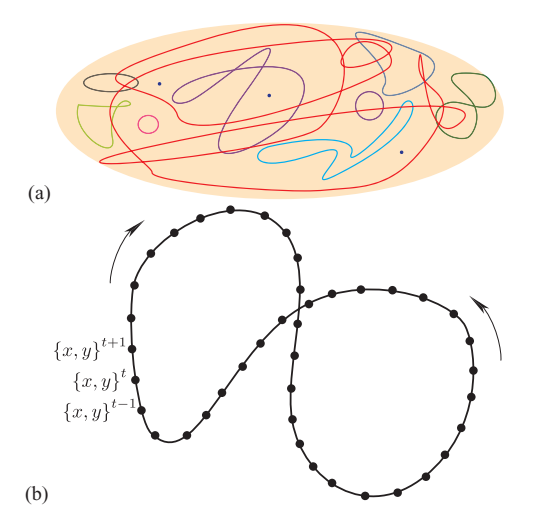


FIG. 2. (a) Scheme for a subspace of constant energy composed of a number of cycles and fixed points. (b) Cartoon of a cycle of period T, for which the cycle is composed of T states.

be exponentially long, and it displays a complex behavior (not chaotic, strictly speaking; see, for instance, [15]). More importantly, the probability that an initial condition exhibits such a complex behavior is finite [6]. Moreover, Q2R manifests sensitivity to initial conditions, that is, if one starts with two distinct, but close, initial conditions, then the conditions will evolve into very different cycles as time runs [8]. In some sense, an initial state explores vastly the phase space, justifying the grounds of statistical physics.

In conclusion, the overall picture is that, although for a finite-size system the deterministic automaton Q2R possesses periodic dynamics so it is not ergodic, there is a huge number of initial conditions that explore vastly the configuration space (this is particularly remarkable for initial conditions of random structure). Therefore, one expects that a master equation approach may be successful.

III. MASTER EQUATION

A. General formalism

Given a set of initial conditions with a fixed energy E, the probability distribution $\varrho_t^E(\{x,y\})$ evolves following a Perron-Frobenius-like equation

$$\varrho_{t+1}^E = \mathcal{L}^E \varrho_t^E, \tag{5}$$

which, in principle, can be computed by using the microscopic evolution rule (1). Indeed, \mathcal{L}^E is easy to build: If the state $\{x,y\}_i$ at time t evolves into $\{x,y\}_k$ at time t+1, then one sets the (i,k) components equal to 1, that is, $\mathcal{L}^E_{ik}=1$. Checking all available elements $\Omega(E)$ for a given energy, we can build the huge, $\Omega(E) \times \Omega(E)$, linear operator \mathcal{L}^E . This matrix possesses a large number of blocks and zeros, revealing the existence of a large number of cycles in the Q2R model (in some sense, \mathcal{L}^E is a kind of adjacency matrix of a graph, the graph being the total number of existing cycles for a given energy). However, this description is impractical because of the typical

magnitude of $\Omega(E)$. Therefore, the full phase space is reduced to a description using gross or macroscopic variables, namely, the total magnetization (4), instead of microscopic variables.

We proceed with a coarse-graining scheme as in Ref. [1]. Let us define a noninvertible projection operator Π that maps the original distribution function ϱ_t^F onto $\varrho_t(M)$,

$$\rho_t(M) = \Pi \cdot \varrho^E_t(\{x,y\}) = \sum_{\text{states with } \sum_k x_k = M} \varrho^E_t.$$

Formally, ϱ_t^E may be seen as a vector of dimension $\Omega(E)$ and ϱ_t as a vector of dimension N+1, indexed by M; hence Π is formally a matrix with N+1 rows and $\Omega(E)$ columns. Applying the projector operator on the Perron-Frobenius equation (5), one gets

$$\rho_t(M) = \Pi \cdot \varrho_t^E = \Pi \cdot \mathcal{L}^E \cdot \varrho_{t-1}^E = \Pi \cdot (\mathcal{L}^E)^t \cdot \varrho_0^E, \quad (6)$$

where $\varrho_0^E(\{x,y\})$ is an initial distribution.

As explained in detail in Ref. [1], in general, it is not possible to reduce the original Perron-Frobenius equation to a self-contained master equation. Following, Nicolis *et al.* [1,2], we take an initial reduced distribution $\varrho_0^E(\{x,y\})$ as a combination of step functions in the aforementioned intervals:

$$\varrho_0^E(\{x,y\}) = \sum_M \alpha_M \varphi_M(\{x,y\}). \tag{7}$$

In Eq. (7) we have defined

$$\varphi_M(\{x,y\}) = \begin{cases} 1 & \text{for } \sum_k x_k = M \\ 0 & \text{for } \sum_k x_k \neq M. \end{cases}$$

The linear operator φ may be seen as a matrix with N+1 rows and $\Omega(E)$ columns (a state $\{x,y\}$ that belongs to a column vector of dimension $\Omega(E)$ and maps onto a single magnetization, which may take N+1 different values). This is the central assumption of the coarse-graining approximation. States with the same magnetization are assumed to be uniformly distributed in the original phase space [see the ansatz (7)]. The coefficients α_M may be obtained by inverting (7) [1]. The result is

$$\alpha_M = \sum_{\text{states}} \varrho_0^E(\{x, y\}) \varphi_M(\{x, y\}).$$

Therefore, α_M is precisely the Mth component for the coarse-grained distribution $\rho_0(M) = \Pi \varrho_0^E$. Thus, for this special type of initial distribution one has

$$\varrho_0^E(\{x,y\}) = \sum_M \rho_0(M)\varphi_M(\{x,y\}) = \varphi^{\dagger} \cdot \boldsymbol{\rho}_0.$$

In the last equality we have written explicitly ρ_0 as an (N+1)-dimensional vector and φ^{\dagger} as an $\Omega(E) \times (N+1)$ matrix. Therefore, the Perron-Frobenius equation (6) becomes

$$\boldsymbol{\rho}_t = \Pi \cdot (\mathcal{L}^E)^t \cdot \boldsymbol{\varphi}^\dagger \cdot \boldsymbol{\rho}_0. \tag{8}$$

Notice that $\varphi^{\dagger} \cdot \Pi = I$ is the $\Omega(E) \times \Omega(E)$ identity matrix. Therefore, defining the $(N+1) \times (N+1)$ matrix \mathcal{W} by

$$W = \Pi \cdot \mathcal{L}^E \cdot \varphi^{\dagger}. \tag{9}$$

one is able to write the final reduced Perron-Frobenius equation, which will be of the form

$$\boldsymbol{\rho}_{t+1} = \mathcal{W} \cdot \boldsymbol{\rho}_t. \tag{10}$$

The linear operator \mathcal{W} acts only in the subspace of constant E, but is spanned over arbitrary values of magnetization, and at the same time the reduced density ρ is a vector with its components indexed by M.

As in the original Perron-Frobenius equation, \mathcal{W} depends explicitly on the Q2R rule through \mathcal{L}^E ; therefore, in principle, it is possible to compute it explicitly. However, in practice, because of the complex and unknown structure of \mathcal{L}^E (in particular because of the existence of a myriad of different periods for a given E), it is not a realistic task because the matrix \mathcal{W} could be quite large.

However, the matrix W can be further reduced following a second coarse-graining process. This partition is defined through a finite number of sets of nonoverlapping intervals $I_1 = [-N, M_1), I_2 = [M_1, M_2), \dots, I_{K-1} = [M_{K-2}, M_{K-1}), I_K = [M_{K-1}, N]$. [The previous case (10) corresponds to K = N + 1.]

We can proceed as previously, defining a second noninvertible projection operator π that maps the reduced distribution function ρ_t into a discrete and shorter column vector of dimension K: $f_t = (f_1, f_2, \dots, f_K)$. Finally, we obtain a coarse-grained master equation for the probability distribution [1,2]

$$f_{t+1} = \hat{W} \cdot f_t. \tag{11}$$

Here \hat{W} is named the transition probability matrix.

The following are important features of the master equation (11).

- (i) The probability vector f_t should be positive and normalizable. Let $\mathbf{1}=(1,1,\dots 1)$ be a K-dimensional vector; then we set $\mathbf{1}\cdot f_t=1$. More importantly, because of normalization $\sum_{i=1}^K w_{ik}=1$, one has $\hat{W}^\dagger \cdot \mathbf{1}=\mathbf{1}$. This implies that the probability is conserved under the evolution $\mathbf{1}\cdot f_{t+1}=\mathbf{1}\cdot \hat{W}f_t=\mathbf{1}\cdot f_t=1$.
- (ii) The Perron-Frobenius equation could be solved exactly provided it is given an initial given distribution f_0 : $f_t = \hat{W}^t f_0$.
- (iii) Because of the Frobenius theorem, there exists an eigenvalue that is one, $\lambda_1=1$, while other eigenvalues fall inside the unitary circle $|\lambda_i|<1$ for i>1. Let $f_{\rm eq}$ be the eigenvector associated with the eigenvalue $\lambda_1=1$; this is an invariant vector $f_{\rm eq}=\hat{W}f_{\rm eq}$.
- (iv) In what it follows we denote by $\chi^{(i)}$ the eigenvectors of \hat{W} corresponding to λ_i . Naturally one has $\chi^{(1)} \equiv f_{eq}$.
 - (v) There exists an equilibrium state $\lim_{t\to\infty} f_t = f_{eq}$.
- (vi) Because all elements in the W matrix are positive, any non-negative initial distribution remains non-negative.

B. Explicit calculation for the transition probability matrix \hat{W}

As already mentioned, to determine empirically the matrix W or \hat{W} , we cannot use (9). Instead, we start with a magnetization sequence $\{\ldots, M_{t-1}, M_t, M_{t+1}, \ldots\}$ obtained from direct numerical simulations. This sequence is always finite, but it could be exponentially long (so in practice infinite).

The transition probability matrix \hat{W} may be found from the probability density functions at times t and t+1. The elements of the matrix are given by the following conditional

PHYSICAL REVIEW E **94**, 062140 (2016) $APPENDIX\ C.\ ARTICLE$

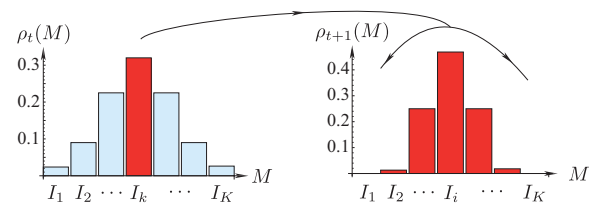


FIG. 3. Distribution $\rho_t(M)$ at a time t schematized in the distribution on the left. The fraction inside the interval I_k is distributed after the evolution into a new distribution $\rho_{t+1}(M)$ schematized in the diagram on the right. The normalized distribution provides the kth element of the ith column: w_{ik} .

probabilities (here we use different notation than in Ref. [1]):

$$w_{ik} = P(M_{t+1} \in I_i | M_t \in I_k) = \frac{P(M_{t+1} \in I_i \cap M_t \in I_k)}{P(M_t \in I_k)}$$

Here M_t belongs to the interval I_k at time t and M_{t+1} belongs to the interval I_i at t+1. Finally, the matrix \hat{W} does not depend on time, which is a feature of a Markov process. The coarse-graining method is schematized in Fig. 3.

C. Chapman-Kolmogorov condition and time-reversal symmetry

The final expression for the probability transition matrix (9) found after applying the formalism of Refs. [1,2] follows directly from Eq. (8) and the ansatz (7), which implies $\varphi^{\dagger} \cdot \Pi = I$. These relations are equivalent to the so-called compatibility condition

$$\Pi \cdot (\mathcal{L}^E)^t \cdot \varphi^{\dagger} = \mathcal{W}^t.$$

This compatibility condition (or Chapman-Kolmogorov condition) arises as a result of the approximations done in Sec. III A, however it is not a general property of the dynamics. For instance, by taking a complete cycle (t=T), one readily gets

$$\Pi \cdot (\mathcal{L}^E)^T \cdot \varphi^{\dagger} = I$$

(with I being the identity matrix), which evidently differs from \mathcal{W}^T because \mathcal{W} represents an irreversible behavior toward equilibrium. Therefore, the compatibility condition is only valid as an approximation for a limited number of time steps that enter to a particular sequence. The same argument holds for the reduced matrix \hat{W} defined through (11).

Let us call $\hat{W}^{(\tau)}$ the resulting probability transfer matrix after τ steps; that is, by computing \hat{W} as a consequence of the evolution from t up to $t+\tau$, the Chapman-Kolmogorov or compatibility condition for \hat{W} reads

$$\hat{W}^{(\tau)} = \hat{W}^{(\tau_1)} \cdot \hat{W}^{(\tau_2)},\tag{12}$$

where $\tau = \tau_1 + \tau_2$. In particular, for $\tau_1 = \tau_2 = 1$ one should satisfy

$$\hat{W}^{(2)} = \hat{W} \cdot \hat{W} = \hat{W}^2$$

Other compatibility conditions are

$$\hat{W}^{(3)} = \hat{W}^{(2)} \cdot \hat{W}, \quad \hat{W}^{(3)} = \hat{W} \cdot \hat{W}^{(2)},$$

$$\hat{W}^{(4)} = \hat{W}^{(2)} \cdot \hat{W}^{(2)}, \quad \hat{W}^{(4)} = \hat{W} \cdot \hat{W}^{(2)} \cdot \hat{W},$$

etc. In Sec. IV C we check in practice how well these Chapman-Kolmogorov conditions are satisfied.

Finally, let us state an important result due to Pomeau [16]. The K-time correlation functions impose some restrictions on the W matrix. Because of time-reversal symmetry, for all indices $i_1, i_2, \ldots, i_K = \{1, 2, \ldots, K\}$ the symmetry relation

$$w_{i_1 i_2} w_{i_2 i_3} \cdots w_{i_{K-1} i_K} w_{i_K i_1} = w_{i_1 i_K} w_{i_K i_{K-1}} \cdots w_{i_3 i_2} w_{i_2 i_1}$$
 (13)

must be satisfied. In what it follows, we apply this coarsegraining approach to compute the probability transfer matrix for some particular cases.

IV. SPECIFIC COMPUTATION OF THE TRANSITION PROBABILITY MATRIX IN VARIOUS SITUATIONS

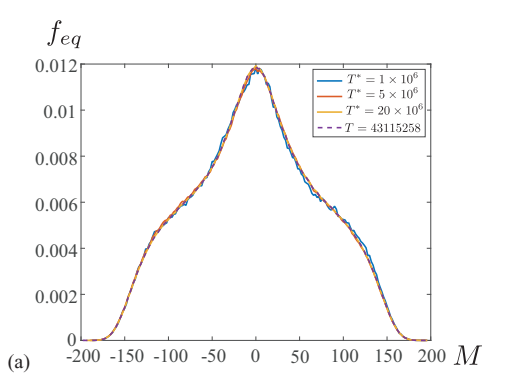
In this section we apply the coarse-graining approach to the Q2R dynamics in the case of a small lattice size. In Ref. [17] we have explored the computation of the transition probability matrix, in particular, in the case of extended systems ($N = 256 \times 256$). However, in this case the cycles are usually huge, therefore this general approach is not really satisfactory. In this sense, we focus our effort on treating systems of moderate sizes, namely, $N = 4 \times 4$, $N = 8 \times 8$, and $N = 16 \times 16$, all of them having tractable cycles.

A. Robustness of the methodology

In general, for a system of small size, one is able to find some cycles for a given energy. Building a time series for the magnetization $\{M(t)\} = \{M_1, M_2, \dots, M_T\}$, one defines a partition of the possible values of the magnetization, as explained in Sec. III. In the cases considered here, it is always possible to use the finest possible partition, that is, for the exact available values of the magnetization (something impractical in large systems). In this case the partitions are composed of a set of N+1 (N is assumed to be even) well defined values $M = \{-N, -N+2, -N+4, \dots, N-2, N\}$. That is, for 4×4 the partition has a maximum of 17 elements, for $N=8\times 8$ there are 65 elements, and for $N=16\times 16$ the partition possesses a maximum of 257 elements.

The first result concerns the equivalence of the probability density function of magnetization obtained via the time series of the magnetization and the equilibrium distribution resulting from the eigenvectors of the transition probability matrix \hat{W} . Hence, the results arising from temporal averages and the transition probability matrix in the configuration space are consistent among themselves. This fact ensures an initial validation of the method. However, the transition probability matrix provides extra information about a system, including the nonequilibrium properties, given by the spectrum of \hat{W} .

Next we describe the methodology for the case of a lattice of size 16×16 for an orbit with E=-292 and period $T=43\,115\,258$. The transition probability matrix \hat{W} is constructed following the steps of Sec. III B. However, first we verify that the master equation does not strongly depend on the length of the time series for the magnetization. It is important to remark that we think that this is a crucial step, because it allows us to compare explicitly the dependence of the results on the partial length of the cycles, something that is not possible for larger



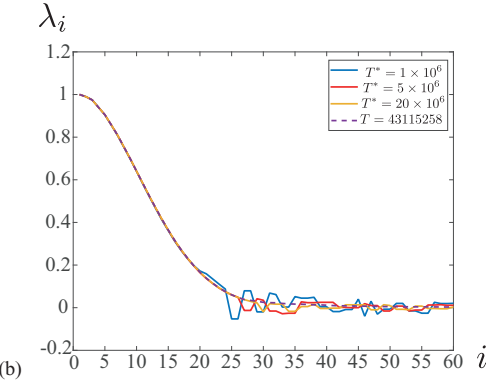


FIG. 4. (a) Plot of the equilibrium distribution $f_{\rm eq}$ for the case of a 16×16 system size with E = -292 ($E/N \approx -1.14$) and a cycle of period T = 43 115 258 (the complete cycle). The computation of $f_{\rm eq}$ is compared with shorter sequences of the same time series of length $T^* = 10^6$, 5×10^6 , 20×10^6 . (b) Set of 257 eigenvalues of the \hat{W} matrix for the same conditions as in (b).

systems, because in these cases we would never be able to build the complete period for the time series.

To test the above, we use again the finest partition. In this case, the transition matrix is of dimension 257×257 (so we will not provide it explicitly) and we characterize it by its equilibrium distribution and the full set of eigenvalues of \hat{W} . Figure 4(a) plots the equilibrium distributions $f_{\rm eq}$ for the total cycle T and f^{T^*} for the partial cycle of length T^* . Similarly, Fig. 4(b) plots the set of 257 eigenvalues, denoted by $\lambda_i^{T^*}$, for the same sequence $\{M(t)\}$, but for four different lengths of the time series. Visually, no substantial difference among the different values of T^* can be observed. Moreover, Table I compares quantitatively the mean square difference measuring $Q_1 = ||f^{T^*} - f_{\rm eq}||^2/K$ and $Q_2 = \sum_{i=1}^K |\lambda_i - \lambda_i^{T^*}|^2/K$. Here K is the number of partitions.

TABLE I. Error estimation of the equilibrium distribution and the spectral decomposition of the \hat{W} matrix for different lengths of the time series.

T*	Q_1	Q_2
106	3.95×10^{-5}	0.0038
5×10^{6}	3.91×10^{-5}	0.0020
20×10^6	3.84×10^{-5}	0.0002

Notice that an important feature of the transition probability matrix is that its eigenvalues are real if the time series satisfies reversibility [16]. We have verified that the coarse-graining approach applied to the full cycle with period T shows this important feature. Namely, the eigenvalues of the \hat{W} matrix are real numbers. However, as we apply the same approach to a partial sequence of the same cycle of length less than T, some eigenvalues become complex (typically located near the origin in the complex plane). This is important because, in practice, for larger-size systems, one never closes a cycle, hence only incomplete sequences are available and thus the matrix would not have, in general, pure real eigenvalues. However, we emphasize that the existence of these complex eigenvalues is spurious.

Finally, it is important to compare results for partitions of different size. First, we compute the equilibrium distribution for three different partitions sets, more precisely, for an 8×8 system evolving by Q2R at E=0 in a periodic orbit of $T=672\,018$. Figure 5(a) compares the three different coarse-graining partitions (containing 5, 11, and 34 elements). Despite the evident differences among the coarse- and the finer-graining partitions, one notices that both partitions exhibit the same accurate behavior of the equilibrium distribution.

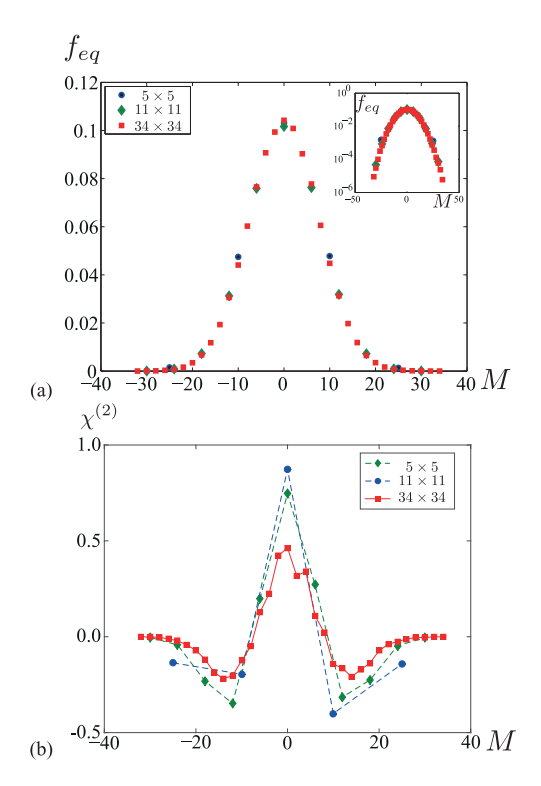


FIG. 5. (a) Plot of the equilibrium distribution $f_{\rm eq}$ vs M for an 8×8 system size with E=0 and a cycle of a period $T=672\,018$ for three different partitions of the magnetization values. The plot shows how all distribution functions lie under the same curve. The inset shows the parabolic behavior in magnetization, which after a fit reads $\ln f_{\rm eq}=-M^2/116$. (b) Plot of the second eigenmode $\chi^{(2)}$ corresponding to the eigenvalue closest to the unit circle. It is noticeable how all partitions produce similar results.

Moreover, Fig. 5(b) compares the second eigenmode $\chi^{(2)}$ without any substantial difference among the partitions.

In what follows, we summarize the methodology for cases of sizes 4×4 , 8×8 , and 16×16 . In all cases, the full cycles are considered and we provide the finest possible partition.

B. Exact calculation for various lattices

We have studied in detail the case of a 4×4 periodic lattice because the phase space possesses $2^{32} \approx 4 \times 10^9$ distinct configurations and the calculations can be completely performed, thus showing explicitly the method. It is shown that the coarse-graining approach is fully applicable in the 4×4 lattice case. We used different partitions, getting a well defined probability transfer matrix \hat{W} . Reference [13] summarizes the calculations and main characteristics for various energies.

Next we explore a few cycles for larger systems (8×8 and 16×16). The cycles in these cases may be as long as desired for any practical purpose so that the equilibrium distribution is calculated with enough precision.

In the case of 8×8 , for various energies and the finest possible coarse graining, for the sake of brevity, we omit explicitly the plots of the first eigenvector $f_{\rm eq}$ as well as the eigenvalues because they are similar to the 16×16 lattice case.

The case of a 16×16 system size displays the most accurate equilibrium distribution found in the current research. The fluctuations around the distribution are small and the eigenvalues seem to form a continuous spectrum (the difference between two consecutive eigenvalues is small). We have also explored a wide range of energies. The rank of the matrices (that is, for the finest partition) is K = 122 for E = -332, K = 205 for E = -316, K = 197 for E = -292, K = 129 for E = -168, and K = 101 for E = -92. The equilibrium distribution, as a function of the magnetization, is plotted in Fig. 6(a). Similarly, the spectral decomposition is shown in Fig. 6(b).

In Fig. 6(a) one notices how in the case of larger energies, say, E = -92 and -168, the equilibrium distribution function is symmetric, under the change $M \rightarrow -M$; however, as the energy decreases one sees that for the lowest energy E = -332 a spontaneous symmetry breaking appears, so the equilibrium distribution is no longer an even function. The equilibrium probability may manifest a positive or negative magnetization (switching from one case to the other by changing the initial condition via the transformation $\{x,y\}^{t=0} \rightarrow \{-x,-y\}^{t=0}$). Moreover, the energy E = -316 case shows an equilibrium probability density function that manifests bi-stability. Indeed, these bimodal distributions possess three peaks, one at M = 0 and the two other at $M = \pm M_0 \neq 0$. Finally, the width of the probability density functions increases near the transition energy.

Figure 6(b) shows the spectral distribution of the probability transfer matrix that defines the master equation. Already for a lattice of size 16×16 one observes how the spectral distribution is almost continuous. One notices that the energies E = -316 and -292 possess the largest eigenvalues for a given index *i*. This means that, probably, the largest eigenvalues occur near the critical energy.

It is interesting to remark that the nonequilibrium is governed by those eigenvalues close to one. The nonequilibrium features behave as slow modes. In the current case one has

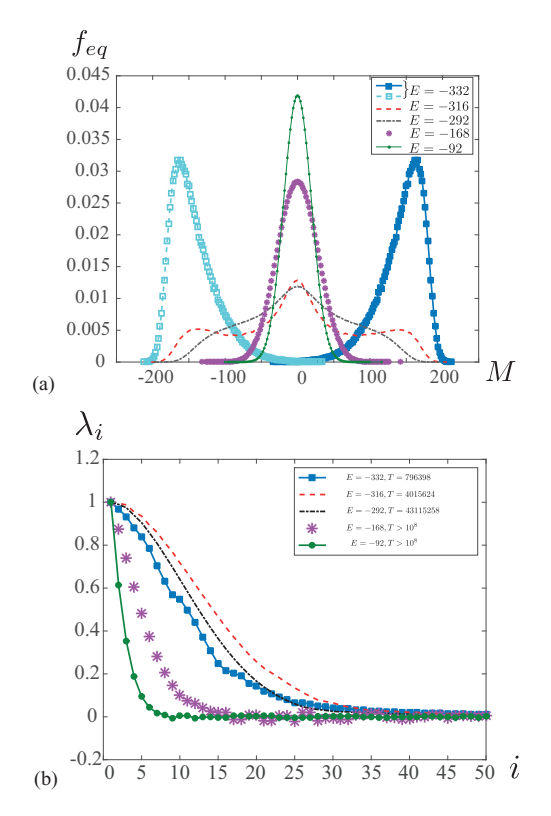


FIG. 6. (a) Equilibrium distributions $f_{\rm eq}$ for the case of a 16×16 system size and for the energies and periods E=-332 and $T=796\,398$, E=-316 and $T=4\,015\,624$, and E=-292 and $T=43\,115\,258$, respectively. We also consider E=-168 and -92 with periods larger than $T>10^8$. (b) Eigenvalues of the W matrix showing the existence of long-wave relaxation properties.

 $f_t = \sum_{i=1}^K \alpha_i \lambda_i^t \chi^{(i)}$. Defining $\sigma_i = -\ln \lambda_i$, one obtains the usual slow mode relaxation. Moreover, the global behavior of the eigenvalues closest to unity represents the transport coefficients [17]. Figure 6(b) indicates that $\lambda_i \approx 1 - \gamma i$, which suggests that the nonequilibrium features are governed by a Fokker-Planck kind of equation. The behavior of the eigenvector agrees also qualitatively with this picture (see [17] for more details).

C. Chapman-Kolmogorov conditions

We have checked the Chapman-Kolmogorov relations for the case of Q2R in a 16×16 lattice for the case of E = -292 and a periodic orbit of $T = 43\,115\,258$. We have built five different probability transfer matrices $\hat{W}^{(\tau=1)},\ldots,\hat{W}^{(\tau=5)}$ (see Sec. III C for the definition of $\hat{W}^{(\tau)}$).

First, we compared the matrices $\hat{W}^{(\tau=2)}$ and $\hat{W}^{(\tau=1)}$. $\hat{W}^{(\tau=1)}$, both of rank 197 × 197, computing the distance between them, e.g., $\hat{W}^{(\tau=2)}$ and $\hat{W}^{(\tau=1)}$. $\hat{W}^{(\tau=1)}$, via the usual distance (the square indicates the product of a matrix by itself)

$$d = \frac{1}{K^2} \text{Tr}[(\hat{W}^{(\tau=2)} - \hat{W}^{(\tau=1)} \cdot \hat{W}^{(\tau=1)})^2].$$

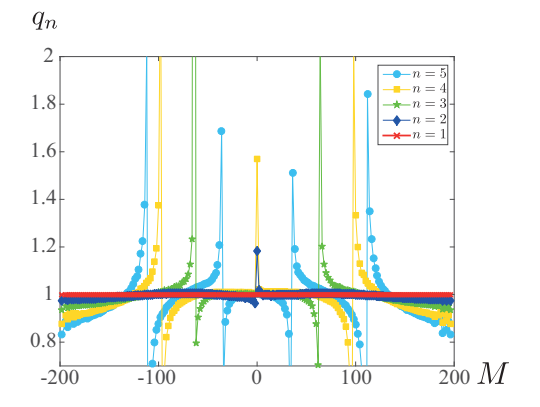


FIG. 7. Plot of the ratio q_n for five eigenmodes for the case of a 16×16 system.

In the current case, the matrices are similar up to $d=5.81\times10^{-6}$. More quantitatively, we look at how good the eigenvectors of different matrices are, namely, $\hat{W}^{(\tau=2)}$ and $\hat{W}^{(\tau=1)} \cdot \hat{W}^{(\tau=1)}$. To do that, we compute the ratio among the nth eigenvectors of the aforementioned matrices, that is,

$$q_n = \frac{\chi_n^{(2)}}{\chi_n^{(1)}},$$

where $\chi_n^{(2)}$ and $\chi_n^{(1)}$ are the *n*th eigenvector of the matrices $\hat{W}^{(\tau=2)}$ and $\hat{W}^{(\tau=1)}$. This quantity is plotted in Fig. 7. One notices that $q_n \approx 1$ almost for all values of magnetization, but it also has an anomalous behavior near the nodal points of the eigenvector $\chi_n^{(1)}$. In general, the agreement of all these eigenvectors is satisfactory.

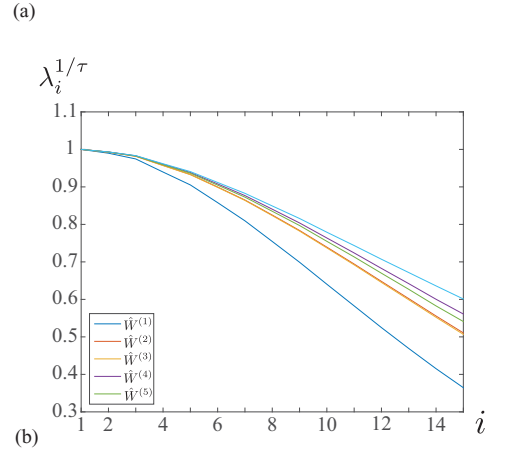
Next we check the Chapman-Kolmogorov relations written in Sec. IIIC, comparing the spectral properties of both matrices, namely, the set of eigenvectors and its eigenvalues. As can be seen in Fig. 8(a), the equilibrium distribution $f_{\rm eq}$ matches perfectly for different values of $\tau = \{1, 2, 3, 4, 5\}$. This proves that the equilibrium configuration $f_{\rm eq}$ is an invariant of the dynamical system. However, nonequilibrium properties do depend on the sampling time τ . Indeed, the eigenvalues corresponding to different probability transfer matrices do depend on the choice of the parameter τ . This is not a surprise, because it is expected that the eigenvalues $\lambda_i^{(\tau)}$ of $\hat{W}^{(\tau)}$ should scale as $\lambda_i^{(\tau)} = \lambda_i^{\tau}$, where λ_i are the set of eigenvalues of $\hat{W}^{(\tau=1)}$. This scaling is shown in Fig. 8(b), indicating an anomaly because it does not work for the case $\tau = 1$, but the scaling works well for higher τ . This deserves more careful study.

D. Pomeau's reversal symmetry relation

According to Pomeau [16], the microscopic time-reversal symmetry imposes the symmetry relation (13). For rank-K transition probability matrices, it is possible to verify that there are K^K different required conditions (13). Therefore, it is only possible to check this condition for a moderate rank K. For the case of 4×4 all probability transfer matrices that we have checked satisfy Pomeau's reversal symmetry relation [13]. For larger \hat{W} matrices, say, K > 9, we have not

PHYSICAL REVIEW E 94, 062140 (2016) APPENDIX C. ARTICLE

 f_{eq} 0.012 0.01 0.008 0.006 0.004 0.002 $\overline{2}$ 00 M100



-100

FIG. 8. (a) Equilibrium distributions $f_{\rm eq}$ for the case of a 16×16 system and for the energy E=-292 and $T=43\,115\,258$. (b) Eigenvalues of the W matrix showing the existence of long-wave relaxation properties.

checked Pomeau's relation because it involves a cumbersome numerical calculation.

V. CONCLUSION

The basic properties of a Q2R cellular automaton, namely, its formal reversibility and the existence of a conserved energy, suggest that Q2R could be a good benchmark to test ideas of statistical mechanics. More importantly, the reversibility is not conditioned by any kind of approximate numerical algorithm. The Q2R model possesses a rich dynamics characterized by a huge number of invariants that partition the phase space in terms of the conserved energy and a huge number of periodic cycles. Although in a system of moderate size the periods are huge [6], for lattices of small size these cycles may be fully characterized.

We introduced a coarse-graining approach that allowed us to write a coarse-grained master equation, which characterizes equilibrium and nonequilibrium statistical properties of the system. We reviewed the methodology and tested the consistency of results in lattices of different sizes. We found that for well chosen partitions, this coarse-graining technique is a powerful tool to reduce the information of the whole system in such a way as to obtain a tractable probability transfer matrix that simplifies the original master equation. One central property of this matrix is the existence of an invariant probability distribution that agrees with different coarse-graining procedures. In addition, we computed the spectral decomposition of the probability transfer matrix characterizing the nonequilibrium properties of the system. Finally, we checked the compatibility conditions, as well as the time-reversal symmetry conditions for short time steps. In many situations the methodology is consistent and provides a complete statistical description of the system. However, some discrepancies appear that deserve caution.

This study provided us with a systematic approach for reducing the number of pertinent macroscopical variables resulting into a manageable master equation.

ACKNOWLEDGMENTS

The authors acknowledge Prof. Enrique Tirapegui for bringing our attention to the coarse-graining methodology for reversible systems and for his participation in the early stages of this work. We also thank Fernando Mora for valuable comments. We would like to acknowledge both anonymous referees for a critical reading of the paper and some valuable remarks that resulted in an improvement of the original manuscript. In particular we are grateful for a remark regarding staggered invariants to which one of the referees drew our attention. F.U. thanks CONICYT (Chile) for financial support through Doctoral Scholarship No. 21140319. S.R. is grateful for a CONICYT Basal-CMM grant. Also, we thank Fondequip AIC-34.

^[1] G. Nicolis and C. Nicolis, Phys. Rev. A 38, 427 (1988).

^[2] G. Nicolis, S. Martinez, and E. Tirapegui, Chaos Soliton. Fract. 1, 25 (1991).

^[3] G. Vichniac, Physica D 10, 96 (1984).

^[4] Y. Pomeau, J. Phys. A: Math. Gen. 17, L415 (1984).

^[5] H. Herrmann, J. Stat. Phys. 45, 145 (1986).

^[6] H. J. Herrmann, H. O. Carmesin, and D. Stauffer, J. Phys. A: Math. Gen. 20, 4939 (1987).

^[7] S. Takesue, Phys. Rev. Lett. **59**, 2499 (1987).

^[8] E. Goles and S. Rica, Eur. Phys. J. D 62, 127 (2011).

^[9] S. Takesue, Complex Systems 9, 149 (1995).

^[10] L. Onsager, Phys. Rev. 65, 117 (1944).

^[11] C. N. Yang, Phys. Rev. 85, 808 (1952).

^[12] R. J. Glauber, J. Math. Phys. 4, 294 (1963).

^[13] F. Urbina, Equilibrium and non-equilibrium in a reversible and conservative cellular automaton, Ph.D. thesis, Universidad Adolfo Ibáñez, 2017.

^[14] F. Urbina, M. Montalva, and S. Rica (unpublished).

^[15] P. Grassberger, J. Stat. Phys. 45, 27 (1986).

^[16] Y. Pomeau, J. Phys. (Paris) 43, 859 (1982).

^[17] F. Urbina, S. Rica, and E. Tirapegui, Discontinuity Nonlinearity Complex. 4, 19 (2015).